

ANALYSIS OF SILO SUPPORTING RING BEAMS AND INTERMEDIATE
RING STIFFENERS

A THESIS SUBMITTED TO
THE GRADUATE SCHOOL OF NATURAL AND APPLIED SCIENCES
OF
MIDDLE EAST TECHNICAL UNIVERSITY

BY

ÖZER ZEYBEK

IN PARTIAL FULFILLMENT OF THE REQUIREMENTS
FOR
THE DEGREE OF DOCTOR OF PHILOSOPHY
IN
CIVIL ENGINEERING

MARCH 2018

Approval of the thesis:

**ANALYSIS OF SILO SUPPORTING RING BEAMS AND INTERMEDIATE
RING STIFFENERS**

submitted by **ÖZER ZEYBEK** in partial fulfillment of the requirements for the degree
of **Doctor of Philosophy in Civil Engineering Department, Middle East Technical
University** by,

Prof. Dr. Halil Kalıpçılar
Dean, Graduate School of **Natural and Applied Sciences**

Prof. Dr. İsmail Özgür Yaman
Head of Department, **Civil Engineering**

Prof. Dr. Cem Topkaya
Supervisor, **Civil Engineering Dept., METU**

Examining Committee Members:

Prof. Dr. Mehmet Utku
Civil Engineering Dept., METU

Prof. Dr. Cem Topkaya
Civil Engineering Dept., METU

Prof. Dr. Özgür Anıl
Civil Engineering Dept., Gazi University

Assoc. Prof. Dr. Eray Baran
Civil Engineering Dept., METU

Asst. Prof. Dr. Burcu Güldür Erkal
Civil Engineering Dept., Hacettepe University

Date: 14.03.2018

I hereby declare that all information in this document has been obtained and presented in accordance with academic rules and ethical conduct. I also declare that, as required by these rules and conduct, I have fully cited and referenced all material and results that are not original to this work.

Name, Last name: ÖZER ZEYBEK

Signature:

ABSTRACT

ANALYSIS OF SILO SUPPORTING RING BEAMS AND INTERMEDIATE RING STIFFENERS

ZEYBEK, Özer

Ph.D., Department of Civil Engineering

Supervisor: Prof. Dr. Cem Topkaya

March 2018, 97 pages

Silos in the form of a cylindrical metal shell are commonly supported by a few discrete columns to permit the contained materials to be directly discharged. The discrete supports produce a circumferential non-uniformity in the axial membrane stresses in the silo shell. One way of reducing the non-uniformity of these stresses is to use a very stiff ring beam which partially or fully redistributes the stresses from the local support into uniform stresses in the shell. Another alternative is to use a combination of a flexible ring beam and an intermediate ring stiffener. A three part analytical and numerical study has been undertaken to address the issues related with silo supporting ring beams and ring stiffeners.

A stiff ring beam is utilized in larger silos to transfer and evenly distribute the discrete forces from the supports into the cylindrical shell wall. A stiffness criterion was developed by Rotter to assess the degree of non-uniformity in axial compressive stresses around the circumference. The stiffness criterion is based on the relative stiffnesses of the ring beam and the cylindrical shell and was verified for loading conditions that produce circumferentially uniform axial stresses around the circumference. The first part of the study has been undertaken to investigate the applicability of the stiffness criterion to cylindrical shells under global shear and

bending. Pursuant to this goal extensive finite element analyses were conducted where different ring beam and cylindrical shell combinations are subjected global shearing and bending actions. The results revealed that the stiffness criterion can be extended to shells under this loading condition. The degree of non-uniformity in axial stresses is quantified and presented as simple formulas that can be readily adopted by design standards.

The ring beam plays an important role in redistributing the majority of the discrete forces from the column supports into a more uniform stress state in the cylindrical wall. The Eurocode EN 1993-4-1 only provides design equations for stress resultants (internal forces) produced in the isolated ring beam under uniform transverse loading. The behavior of a ring beam which interacts with the silo shell is much more complex than that of an isolated ring beam. In traditional design treatments, it is assumed that the discrete support forces are redistributed entirely by the ring beam to provide circumferentially uniform axial membrane stresses in the silo shell. But this assumption is only approximately valid if the ring beam is much stiffer than the silo shell. Since the cylindrical shell is very stiff in its own plane, the ring beam must be remarkably stiff to be stiffer than the shell. The second part of the study has been undertaken to explore the ring beam stress resultants when closed section ring beams of lower stiffness and practical dimensions are used. A finite element parametric study is undertaken to explore the stress resultants and displacements in more flexible ring beams connected to a silo shell.

A combination of a ring beam and an intermediate ring stiffener can be used for large silos to redistribute the stresses from the local support into uniform stresses in the shell. Topkaya and Rotter (2014) has identified the ideal location for the intermediate ring stiffener. The third part of the study explored strength and stiffness requirements for intermediate ring stiffeners placed at or below the ideal location. Pursuant to this goal, the cylindrical shell below the intermediate ring stiffener is analyzed using the membrane theory of shells. The reactions produced by the stiffener on the shell are identified. Furthermore, the displacements imposed by the shell on the

intermediate ring stiffener are obtained. These force and displacement boundary conditions are then applied to the intermediate ring stiffener to derive closed form expressions for the variation of the stress resultants around the circumference to obtain a strength design criterion for the stiffener. A stiffness criterion in the form of a simple algebraic expression is then developed by considering the ratio of the circumferential stiffness of the cylindrical shell to that of the intermediate ring stiffener. These analytical studies are then compared with complementary finite element analyses that are used to identify a suitable value for the stiffness ratio for ring stiffeners placed at different locations.

Keywords: Cylindrical Shells, Closed form solutions, Supports, Stiffening, Silos, Tanks, Global bending, Global shear.

ÖZ

SİLO TAŞIYAN HALKA KİRİŞLERİN VE RİJİTLEŞTİRİCİ HALKA ELEMENLARIN ANALİZİ

ZEYBEK, Özer

Doktora, İnşaat Mühendisliği Bölümü

Tez Yöneticisi: Prof. Dr. Cem Topkaya

Mart 2018, 97 sayfa

Silindirik metal kabuk formunda olan silolar içerdikleri malzemelerin doğrudan boşaltılabilmesine olanak sağlamak için genellikle bir kaç ayrı kolon tarafından mesnetlenirler. Ayrı kolonlar silo kabuğunda oluşan aksenal membran gerilmelerinde silo çevresi boyunca bir düzensizlik meydana getirir. Bu gerilmelerin düzensizliğini azaltmanın bir yolu, kolonlardan gelen gerilmeleri kabuğa homojen olarak kısmen ya da tamamen dağıtacak çok rijit bir halka kirişi kullanmaktır. Başka bir alternatif, esnek bir halka kirişi ve bir ara rijitleştirici halka kombinasyonu kullanmaktır. Silo taşıyan halka kirişler ve halka rijitleştiricileri ile ilgili konuları ele almak üzere üç bölümden oluşan analitik ve sayısal bir çalışma yapılmıştır.

Büyük silolardaki kolonlardan gelen ayrı kuvvetleri silindirik kabuk yüzeyine aktarmak ve eşit bir şekilde dağıtmak için rijit bir halka kirişi kullanılır. Kabuk çevresindeki aksenal basınç gerilmelerinin düzensizlik derecesini belirlemek için Rotter tarafından rijitlik kriteri geliştirilmiştir. Rijitlik kriteri, silindirik kabuk ve halka kirişin göreceli rijitliklerine bağlıdır ve kabuk çevresi boyunca düzgün yayılı aksenal gerilme oluşturacak yük durumu için doğrulanmıştır. Çalışmanın ilk kısmı, rijitlik kriterinin global kesme ve eğilme altındaki silindirik kabuklara uygulanabilirliğini araştırmak için yapılmıştır. Bu amaca uygun olarak, global kesme ve eğilme etkilerine

maruz farklı halka kiriş ve silindirik kabuk kombinasyonlarının kapsamlı sonlu elemanlar analizi gerçekleştirilmiştir. Sonuçlar, rijitlik kriterinin bu yükleme durumları altındaki kabuklar için de kullanılabilirliğini göstermiştir. Eksenel gerilmelerdeki düzensizlik derecesi belirlenmiş ve tasarım standartları tarafından kolaylıkla uyarlanabilir basit formüller olarak sunulmuştur.

Halka kirişi, kolon mesnetlerinden gelen ayırık kuvvetlerin çoğunun silindirik yüzeye daha homojen bir gerilme durumu oluşturacak şekilde dağılmasında önemli bir rol oynar. Eurocode EN 1993-4-1, uniform enine yükleme altındaki tekil halka kirişinde oluşan iç kuvvetler için sadece tasarım denklemleri sunar. Silo kabuğu ile etkileşen bir halka kirişin davranışı, tekil bir halka kirişin davranışından çok daha karmaşıktır. Geleneksel tasarım durumlarında, silo kabuğu çevresi boyunca düzgün eksenel membran gerilmeleri sağlamak için ayırık mesnet kuvvetlerinin tamamen halka kiriş tarafından yeniden dağıtıldığı varsayılmaktadır. Ancak, bu varsayım halka kirişin silo kabuğundan daha rijit olması durumunda geçerlidir. Silindirik kabuk kendi düzleminde çok rijit olduğundan halka kiriş kabuğa oranla daha rijit olmalıdır. Çalışmanın ikinci bölümünde, düşük rijitlik ve pratik boyutlara sahip kapalı kesitli halka kirişlerin kullanıldığı durumlarda halka kirişinde oluşacak iç kuvvetleri elde etmek için bir araştırma yapılmıştır. Silo kabuğuna bağlanan daha esnek halka kirişlerdeki iç kuvvetleri ve yer değiştirmeleri elde etmek için sonlu elemanlar yöntemi ile parametrik bir çalışma yapılmıştır.

Bir halka kiriş ve ara halka rijitleştirici kombinasyonu, büyük silolarda lokal mesnetten kaynaklanan gerilmeleri kabukta uniform bir şekilde dağıtmak için kullanılabilir. Topkaya ve Rotter (2014), ara halka kirişinin ideal konumunu belirlemiştir. Çalışmanın üçüncü bölümü ideal konumda veya bu konumun altında bulunan ara halka rijitleştiricilerin dayanım ve rijitlik gereksinimlerini araştırır. Bu amaca uygun olarak, ara halka rijitleştiricinin altındaki silindirik kabuk membran teorisi kullanılarak analiz edilmiştir. Rijitleştirici tarafından kabuk üzerinde oluşturulan reaksiyonlar belirlenmiştir. Ayrıca, ara halka rijitleştiricisindeki silindirik kabuk tarafından uygulanan yer değiştirmeler elde edilmiştir. Ardından bu kuvvet ve

yer deęiřtirme sınır kořulları, rijitleřtirici dayanım tasarım kriteri elde etmek ve silindirik kabuk çevresi boyunca iç kuvvet deęiřiminin kapalı form ifadelerini türetmek için ara halka rijitleřtiricilere uygulanmıřtır. Sonrasında, basit cebirsel ifade formundaki rijitlik kriteri, silindirik kabuęun çevresel doęrultudaki rijitlięinin ara halka rijitleřtiricinin çevresel doęrultudaki rijitlięine oranı göz önüne alınarak geliştirilmiřtir. Daha sonra, bu analitik çalıřmalar farklı konumlara yerleřtirilen halka rijitleřtiricilerin rijitlik oranının uygun bir deęerini saptamak için kapsamlı sonlu elemanlar analizi ile karřılařtırılmıřtır.

Anahtar Kelimeler: Silindirik kabuk, Kapalı form çözümler, Mesnetler, Rijitleřtirme, Silolar, Tanklar, Global eęilme, Global kesme.

To My Family

ACKNOWLEDGEMENTS

I would like to express my infinite gratitude to my supervisor Prof. Dr. Cem Topkaya for valuable advice, guidance and, infinite patience at each stage of this thesis.

Special thanks go to Professor J. Michael Rotter of University of Edinburgh for his guidance and advices.

I would also like to express my thanks to Prof. Dr. Afşin Sarıtaş, Prof. Dr. Özgür Anıl, Prof. Dr. Mehmet Utku, Assoc. Prof. Dr. Eray Baran and Asst. Prof. Dr. Burcu Güldür Erkal for their valuable advice and constructive comments.

I would also like to thank to Asst. Prof. Dr. Alper Aldemir and Asst. Prof. Dr. Mehmet Bakır Bozkurt for their friendship and support.

I want to thank my laboratory mates, Halil Fırat Özel, M. Ali Özen, Salim Azak, Okan Koçkaya, F. Soner Alicı, Kaan Kaatsız, Utku Albostan and Feyza Albostan for their friendship, support and activities we had.

I would finally to thank my dear wife Yelda for her patience, toleration and boundless support.

TABLE OF CONTENTS

ABSTRACT	v
ÖZ	viii
ACKNOWLEDGEMENTS	xii
TABLE OF CONTENTS	xiii
LIST OF FIGURES	xvi
CHAPTERS	
1. INTRODUCTION	1
1.1. General	1
1.2. Objectives and Scope	8
1.3. Organization of Thesis	9
2. APPLICATION OF RING BEAM STIFFNESS CRITERION FOR DISCRETELY SUPPORTED SHELLS UNDER GLOBAL SHEAR AND BENDING	11
2.1. Ring Beam Stiffness Criterion for Discretely Supported Shells	11
2.2. Derivation of Ring Beam Stiffness Criterion – A Revisit.....	11
2.2.1. Ring Beams Subjected to Fundamental Harmonic of Column Support	13
2.2.2. Cylindrical Shell Subjected to Fundamental Harmonic of Column Support	17
2.2.3. Stiffness Ratio	22
2.3. Numerical Study	24
3. ANALYSIS OF SILO SUPPORTING RING BEAMS RESTING ON DISCRETE SUPPORTS	33
3.1. Algebraic Closed-form Solution of Stress Resultants in the Ring Beam using Vlasov’s Curved Beam Theory	33
3.1.1. Derivation of stress resultants – ring under transverse distributed load (q_x)	34
3.1.2. Derivation of stress resultants – ring under circumferential distributed torque (m_θ)	35

3.1.3. Derivation of stress resultants – ring under concentrated torque at the supports (m_s)	36
3.2. Computational Verification of the Closed Form Solutions	37
3.3. Effect of Ring Beam Stiffness on Ring Beam Stress Resultants and Displacements.....	41
3.3.1. Computational assessment of the ring beam stiffness ratio	42
4. REQUIREMENTS FOR INTERMEDIATE RING STIFFENERS ON DISCRETELY SUPPORTED SHELLS	47
4.1. Behavior of Cylindrical Shells with Intermediate Ring Stiffeners	47
4.2. Stress and displacement transfer into intermediate ring stiffeners	53
4.3. Algebraic Closed-form Solution for the Stress Resultants in the Intermediate Ring Stiffener – Strength Criterion	60
4.3.1. Derivation of stress resultants – In plane behavior	60
4.3.2. Derivation of stress resultants – Out-of-plane behavior.....	62
4.4. Assessment of stress resultants	64
4.5. Computational verification of the Closed-form equations	65
4.5.1. Case1: Intermediate ring at the ideal height.....	66
4.5.2. Case2: Intermediate ring below the ideal height.....	69
4.6. Computational assessment of the dominant harmonic	73
4.6.1. Case1: Intermediate ring at the ideal height.....	73
4.6.2. Case2: Intermediate ring below the ideal height.....	77
4.7. Stiffness Criterion for the Intermediate Ring Stiffener	79
5. SUMMARY AND CONCLUSIONS.....	83
5.1. Summary.....	83
5.2. Conclusions	84
5.2.1. Conclusions about Application of Ring Beam Stiffness Criterion for Discretely Supported Shells under Global Shear and Bending	84
5.2.2. Conclusions about Analysis of Silo Supporting Ring Beams Resting on Discrete Supports.....	85
5.2.3. Conclusions about Requirements for Intermediate Ring Stiffeners on Discretely Supported Shells.....	85

REFERENCES.....	87
CURRICULUM VITAE.....	95

LIST OF FIGURES

FIGURES

Figure 1.1 Alternative support arrangements for discretely supported silos (Rotter (2001)).....	3
Figure 1.2 Axial deformation compatibility between ring beam and shell (Rotter (2001)). a) Traditional design model for column-supported silos. b) Deformation requirement on cylinder imposed by compatibility with beam deformation	6
Figure 1.3 Typical circular planform silo.....	7
Figure 2.1 Fundamental harmonic of column support for 6 supports	12
Figure 2.2 Differential curved beam element and sign conventions.....	14
Figure 2.3 Internal forces and moments for shell element.....	18
Figure 2.4 Relationship between ring beam stiffness ratio and stress amplification ratio for axial line loading	23
Figure 2.5 A typical finite element mesh for the cylindrical shell and ring beam, support conditions and connection of shell and ring.....	25
Figure 2.6 Verification of simple bending theory for silo shells under global bending	27
Figure 2.7 Variation of axial membrane stress along the circumference for cases with different beam geometries and support conditions	28
Figure 2.8 Relationship between ring beam stiffness ratio and stress amplification ratio for global bending (knife edge support).....	29
Figure 2.9 Relationship between ring beam stiffness ratio and stress amplification ratio for global bending (support width to radius ratio of 0.05).....	30
Figure 2.10 Relationship between ring beam stiffness ratio and stress amplification ratio for global bending (support width to radius ratio of 0.10).....	31
Figure 2.11 Relationship between ring beam stiffness ratio and stress amplification ratio for global bending (support width to radius ratio of 0.20).....	31
Figure 2.12 Comparison of responses for different support width-to-radius ratios ...	32

Figure 3.1 Simplified load-carrying mechanism model for the ring beam	34
Figure 3.2 Finite-element modelling for the ring beam and cylindrical shell.....	38
Figure 3.3 Comparison of closed form solution with numerical solutions for the ring beam bending moment (M_r)	40
Figure 3.4 Comparison of closed form solution with numerical solution for the ring beam torsional moment (T_θ).....	40
Figure 3.5 Comparison of closed form solution with numerical solutions for the ring beam transverse displacement (u_x).....	41
Figure 3.6 Assessment of the ring stiffness ratio (ψ) for the bending moment in the radial direction (support moment).....	43
Figure 3.7 Assessment of the ring stiffness ratio (ψ) for the bending moment in the radial direction (span moment)	43
Figure 3.8 Assessment of the ring stiffness ratio (ψ) for the torsional moment	44
Figure 3.9 Assessment of the ring stiffness ratio (ψ) for the transverse displacement	44
Figure 4.1 Typical circular planform silo	48
Figure 4.2 Variation of normalized axial membrane stress throughout the shell	49
Figure 4.3 Normalized axial membrane stress at various levels: Variation around the circumference from the support to midspan: no intermediate ring	51
Figure 4.4 Normalized axial membrane stress at various levels: Variation around the circumference from the support to midspan: intermediate ring 1500 mm above the base ring	51
Figure 4.5 Normalized axial membrane stress at various levels: Variation around the circumference from the support to midspan: intermediate ring 3000 mm above the base ring	52
Figure 4.6 Boundary conditions used in closed-form solution	54
Figure 4.7 Loading, displacements and stress resultants in an element of the cylindrical shell	55
Figure 4.8 Variation of axial stress resultant for various intermediate ring heights with upper to lower shell thickness ratio $g = 0.5$	58
Figure 4.9 Finite-element mesh for the cylindrical shell and I-section ring beam	66

Figure 4.10 Comparison of closed form solution with numerical solution for ring bending moment.....	67
Figure 4.11 Comparison of closed form solution with numerical solution for ring shear force	68
Figure 4.12 Comparison of closed form solution with numerical solution for ring circumferential tension.....	68
Figure 4.13 Comparison of closed form solution with numerical solution for a flexible intermediate ring	70
Figure 4.14 Comparison of closed form solution with numerical solution for a stiff intermediate ring	71
Figure 4.15 Variation of axial displacements throughout the shell.....	72
Figure 4.16 Variation of axial membrane stress resultant at the bottom of the shell.	74
Figure 4.17 Verification of the proposed model for the Fourier coefficient (q_{xn}).....	76
Figure 4.18 Verification of the proposed model for the Fourier coefficient (q_{xn}) (circumferential force).....	78
Figure 4.19 Verification of the proposed model for the Fourier coefficient (q_{xn}) (In-plane bending moment).....	78
Figure 4.20 Boundary conditions used for closed form solution of shell stiffness	80
Figure 4.21 Assessment of an appropriate value for the intermediate ring stiffness ratio χ	82

CHAPTER 1

INTRODUCTION

1.1. General

Silos in the form of cylindrical metal shells can be supported either on the ground or on a few column supports, depending on the requirements of the discharge system. If the stored granular solids are discharged by gravity, a hopper is needed at the base of the cylindrical shell with an access space beneath it to permit discharge into transportation systems. Columns at equal circumferential intervals are invariably used to elevate the silo structure and to provide the necessary access space (Figure 1.1).

There are stringent limitations on the number of column supports that can be used because the presence of many columns does not allow for easy access by transportation systems. Depending on the size of the structure, several different support arrangements (Rotter (2001)) may be chosen, as shown in Figure 1.1. For small silos, terminating columns with rings (Figure 1.1a), engaged columns (Figure 1.1b) or bracket supports (Figure 1.1e) may be suitable. On the other hand, medium and large silos require either columns extending to the eaves (longitudinal stiffeners) (Figure 1.1c) or heavy ring beams (Figure 1.1d) or double rings (Figure 1.1f).

The engaged columns are opted for light silo structures. These columns are attached over a part of the cylindrical silo wall by welding process. Zhao et al. (2006) performed numerical analyses to investigate structural behavior of the steel silos with engaged columns. They demonstrated that the height of the engaged column directly affected the buckling strength of the column-supported cylindrical silos. Doerich et al. (2009) investigated the strength behavior of a cylindrical steel shell that was discretely supported on engaged columns via numerical finite element analyses

considering the effects of geometric imperfection and geometric nonlinearity. The outcome of the study was compatible with the provisions presented in EN 1993-1-6 (2007). Vanlaere et al. (2009) performed different types of numerical analysis including the effect of geometric nonlinearity, plasticity and geometric imperfections in order to investigate stability behavior of steel cylinders with engaged columns. Their results showed that the imperfections caused a main reduction in the failure load of the cylinder. Jansseune et al. (2013) investigated the failure behavior of column-supported cylindrical silos with flexible engaged steel columns using finite element analyses. They showed that the height of the column attached to the silo and its cross-section affected the failure behavior and the failure load of the cylindrical column-supported silos. Jansseune et al. (2016) identified the ideal combination of dimensions of an engaged column to obtain a failure load considering low material in the column. They concluded from numerical finite element analyses that the columns must resist a greater load than the cylindrical silo wall itself.

Smaller (light) silo structures are usually supported on local brackets attached to the outside of the cylindrical shell. The effect of column supports on the stresses produced in tank walls was firstly investigated by Gould and Sen (1974). They assumed that the eccentrically applied column reaction produced a bending moment into the shell wall that was resisted by a couple in the radial direction. A simple algebraic expression for the mechanism of load transfer between the column and the cylindrical shell wall was proposed. The radial forces were distributed linearly over the height of a bracket and uniformly distributed over the column width in their study. Holst et al. (2002) and Gillie et al. (2002) investigated the strength of the shell for the bracket-supported cylindrical silos. They tried to determine ultimate load capacity of the cylindrical steel shell. They conducted numerical analysis to explore nonlinear load-deformation behavior of the bracket-supported cylindrical silo structures. Gillie and Holst (2003) performed finite element analyses considering the effects of bracket width, bracket height and geometric imperfections. They showed that the strength of bracket supported silos was dependent on the bracket width. They also tried to predict the collapse strength of silos with equidistant support brackets of typical dimensions.

Doerich and Rotter (2008) investigated elastic-plastic strength of an imperfect cylindrical shell attached to a bracket that was restrained by the column. Their study was conducted in a manner consistent with the framework of the European Standard for Shell Structures EN 1993-1-6 (2006), which requires that the two reference strengths of the shell that are the plastic collapse resistance and the linear bifurcation resistance.

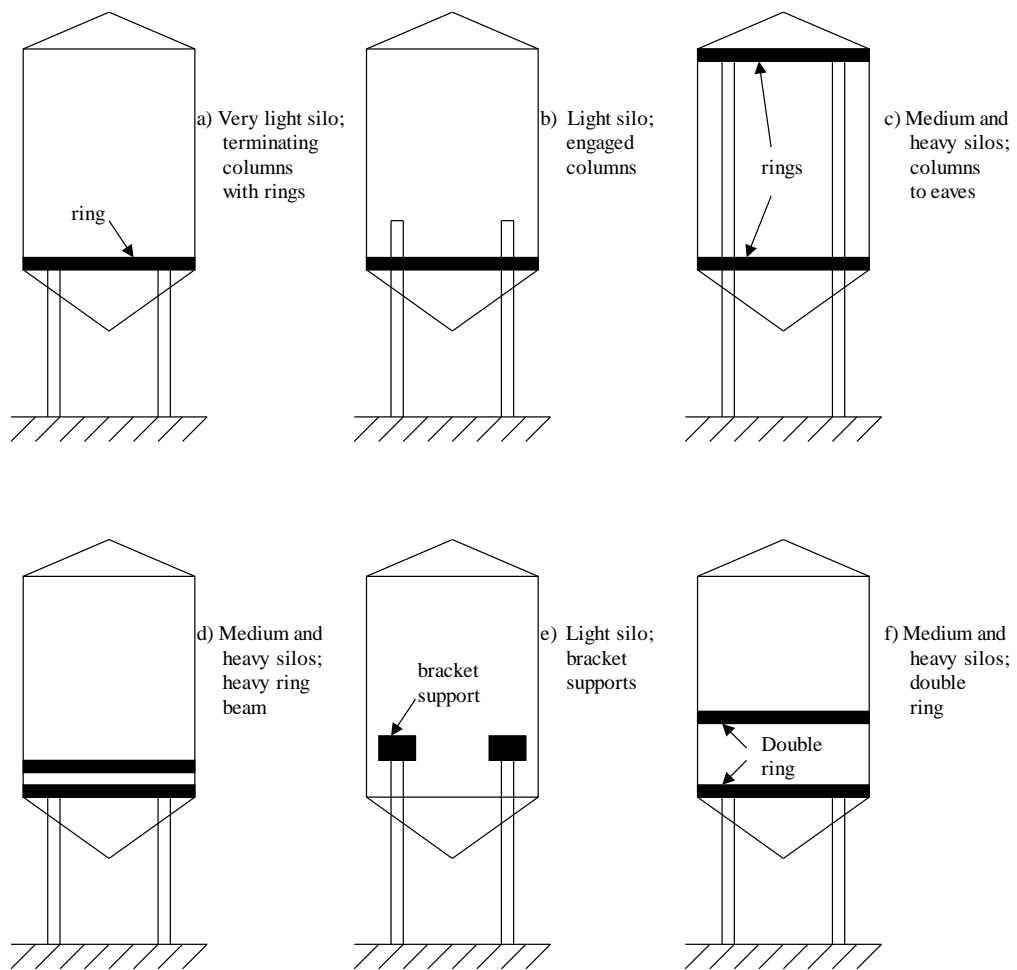


Figure 1.1 Alternative support arrangements for discretely supported silos (Rotter (2001))

Longitudinal stiffeners (stringers) are placed on the outside of the cylindrical wall with either a partial length or whole length for the medium and large silos. Ellinas et

al. (1981) investigated the buckling behavior of axially loaded stringer stiffened cylinders. They tried to predict lower bounds of the imperfection sensitive elastic overall buckling. They showed that buckling of stringer stiffened cylinders was substantially dependent on geometry of cylindrical shell and the stiffener. Samuelson (1982) provided simplified design rules for the design of circular cylindrical shells with longitudinal stiffeners under axial compression. The proposed conservative method was dependent on assumptions in regard to boundary conditions, initial imperfections and load eccentricities. Vanlaere et al. (2005) investigated strengthening effect of the longitudinal stiffeners. The influence of the dimensions of the stiffeners on the buckling stress and the failure pattern were identified using finite element analysis. Vanlaere et al. (2006) utilized two longitudinal flat-bar stiffeners with partial length above each support to eliminate failure due to local instability of the cylindrical shell. They performed the experiments on scale models to validate numerical simulations of the cylinders. They also tried to develop design rules for stringer stiffened cylindrical shells on local supports. Vanlaere et al. (2009) performed finite element analyses to show effectiveness of the flat rectangular plate longitudinal stiffeners that were treated as flexurally and axially rigid. Their study indicated that geometrical nonlinearity, plasticity and geometric imperfections were major effects on the failure load of the stringer stiffened cylinders on local supports. Jansseune et al. (2015) investigated the influence of the dimensions of partial height U-shaped longitudinal stiffeners on the failure behavior of a thin-walled silo using finite element analyses. They showed that the height of the longitudinal stiffener had a beneficial influence, since the stiffener would distribute the stresses better in circumferential direction when elastic buckling occurred in the unstiffened region above the terminations of the stiffeners.

The presence of discrete supports results in a high stresses adjacent to the column terminations, which trigger failure by local instability of the cylinder. This support condition produces also a circumferential non-uniformity in the axial membrane stresses in the silo shell. To eliminate this failure case wall thickness of the bottom course of the cylinder can be increased (Guggenberger et al. (2004)). However,

unnecessary material is used in this solution. One way of reducing the non-uniformity of these stresses is to use a very stiff ring beam which partially or fully redistributes the stresses from the local support into uniform stresses in the shell. Another alternative is to use a combination of a flexible ring beam and an intermediate ring stiffener.

Previous studies of discretely supported cylinders (Kildegaard (1969), Gould and Sen (1974), Gould et al. (1976), Gould et al. (1998), Rotter (1987), Rotter (1987), Rotter (1990), Teng and Rotter (1992), Guggenberger et al. (2000), Guggenberger et al. (2004), Jansseune et al. (2012), Jansseune et al. (2013), Jansseune et al. (2016), Doerich et al. (2009)) and those on ring beams above columns (Rotter (1984), Rotter (1985)) have shown the great complexity of the behavior.

Since the design of the cylindrical shell is governed by considerations of buckling under axial compression, a much thinner wall can be provided if the axial membrane stress distribution is circumferentially uniform. Classical design treatments (Wozniak (1979), Trahair (1983), Gaylord and Gaylord (1984), Safarian and Harris (1985)) adopted this assumption so that the criterion for buckling under axial compression above the ring is that for uniform compression. As illustrated in Figure 1.2a, the tradition is for each component to be treated separately under the action of uniform loading around the circumference (e.g. Pippard and Baker (1957), EN 1993-4-1 (2007)). But the underlying assumption can only be valid if the ring beam properly fulfills its critical function in redistributing the discrete support loads into a relatively uniform state of stress. The extent to which this redistribution of the support forces can be achieved is directly related to the stiffness of the ring beam relative to the stiffness of the cylindrical shell (Figure 1.2). Since the cylindrical shell is very stiff in its own plane, the ring beam that is subject to flexure and twisting must be remarkably stiff to be stiffer than the shell. An approximate criterion to determine the appropriate ring beam stiffness was first identified by Rotter (1985) and was further developed and verified by Topkaya and Rotter (2011). The criterion developed by these authors is very demanding and usually leads to very big ring beams for typical geometries.

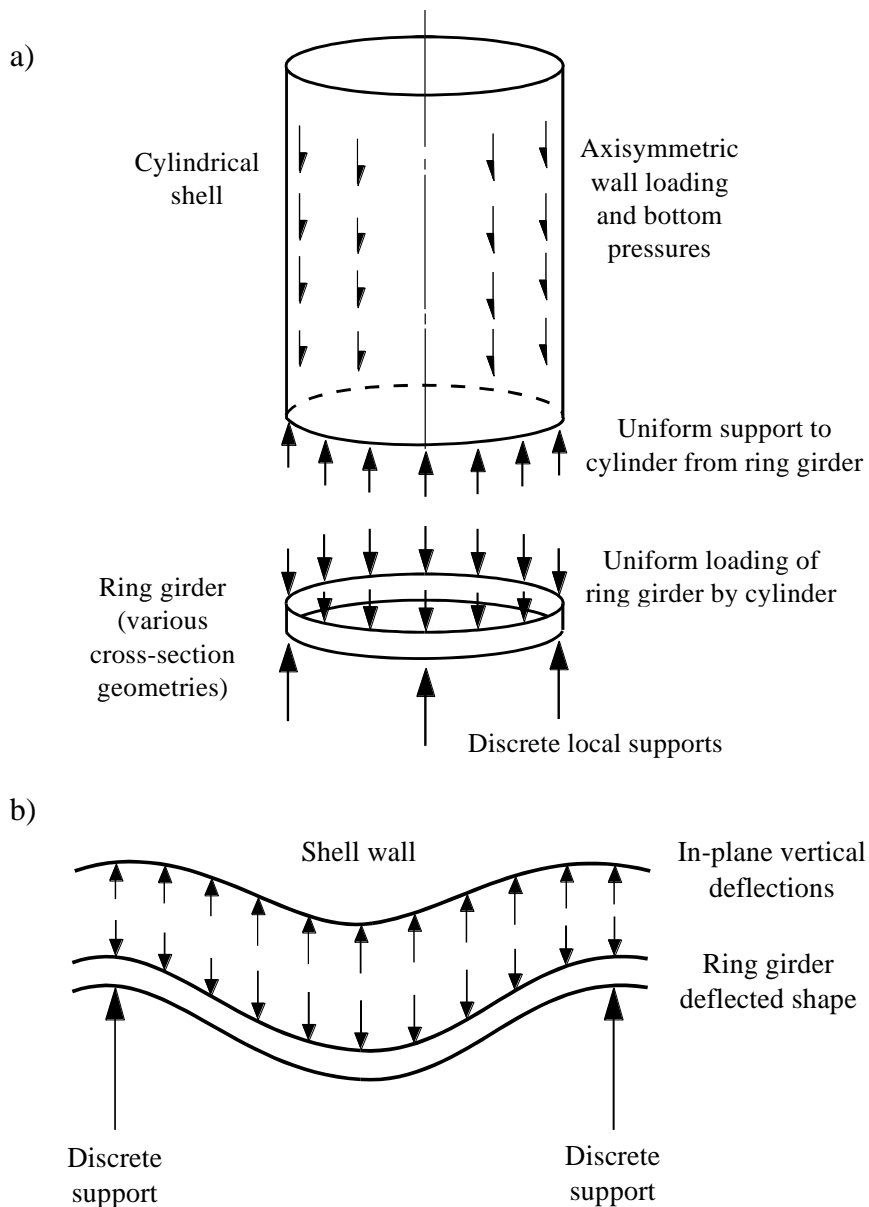


Figure 1.2 Axial deformation compatibility between ring beam and shell (Rotter (2001)). a) Traditional design model for column-supported silos. b) Deformation requirement on cylinder imposed by compatibility with beam deformation

One alternative method of achieving uniform axial membrane stresses is to use an intermediate ring stiffener as shown in Figure 1.3. Greiner (1983, 1984), Öry et al. (1984) and Öry and Reimerdes (1987) showed that an intermediate ring stiffener can be very effective in reducing the circumferential non-uniformity of axial stresses in the

shell. Studies conducted by these researchers identified the variation of the axial membrane stress distributions up the height of the shell. It was shown that an intermediate ring stiffener can cause a dramatic decrease in the peak axial membrane stress, producing a more uniform stress state above the intermediate ring. Recently Topkaya and Rotter (2014) showed that there is an *ideal location* for an intermediate ring stiffener, such that the axial membrane stress above this ring is circumferentially completely uniform. The ideal location (H_I) shown in Figure 1.3 was determined analytically and is expressed in terms of basic geometric variables.

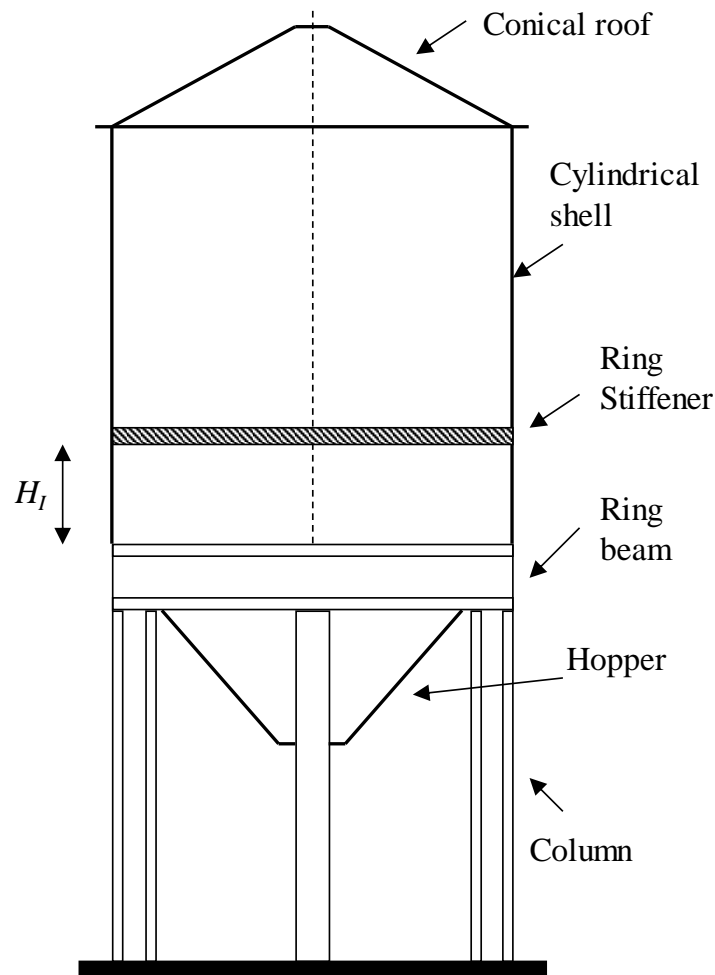


Figure 1.3 Typical circular planform silo

The intermediate ring stiffener is expected to have sufficient strength and stiffness to fulfill its function properly. The key requirement for this intermediate ring stiffener is to prevent or significantly control the circumferential displacements of the cylindrical shell at that level. If the ring stiffener has inadequate stiffness then the circumferential uniformity of the axial stresses above it is not achieved. Furthermore, there is an interaction between the cylindrical shell and the ring stiffener which causes stress resultants to develop in the ring. These stress resultants could potentially cause failure of the ring stiffener either by yielding or by instability.

1.2. Objectives and Scope

The presence of discrete supports results in a non-uniformity of meridional stresses around the circumference. One way of reducing the non-uniformity of these stresses is to use a very stiff ring beam which partially or fully redistributes the stresses from the local support into uniform stresses in the shell. Another alternative is to use a combination of a flexible ring beam and an intermediate ring stiffener. A three part analytical and numerical study has been conducted to address the issues related with silo supporting ring beams and ring stiffeners.

The aim of the first study is to extend the stiffness criterion developed by Rotter (1985) to loading cases that produce global bending of the silo shell. Pursuant to this goal the stiffness criterion is revisited. The underlying assumption behind its development is extended to cover global shear and bending effects. The applicability of the stiffness criterion is checked via extensive finite element analysis.

The second study explores the extent to which a practical silo shell causes these stress resultants to be reduced when the ring beam has only practical stiffness. Pursuant to this goal the stress resultants produced in the ring beam were re-derived using Vlasov's curved beam differential equations (Vlasov (1961), Heins (1975)). The advantage of using Vlasov's equations is that the transverse displacements can also be obtained from the differential relationships. A finite element parametric study was

undertaken to explore the effect of ring beam flexibility on stress resultants and displacements for cases where the ring beam interacts with the silo shell. The effects of the ring beam stiffness ratio on the stress resultants were explored.

The third study explores the strength and stiffness requirements for intermediate stiffeners placed at ideal location or below this location, where the force transfer and displacement boundary conditions differ from those for a ring at the ideal location. A general shell and ring combination is studied using the membrane theory of shells to identify the membrane shear forces induced in the shell by the ring. These forces are then considered as loads applied to the intermediate ring stiffener. Vlasov's curved beam theory (Vlasov (1961)) is used to derive closed form expressions for the variation of the stress resultants around the circumference to obtain a suitable strength design criterion for the stiffener. A stiffness criterion is then developed by considering the ratio of the circumferential stiffness of the cylindrical shell to that of the intermediate ring stiffener. The circumferential displacements of the ring and the shell are found for the loading condition previously obtained to determine the required strength. A simple algebraic expression is developed for this intermediate ring stiffness criterion. These analytical studies are then compared with complementary finite element analyses that are used to identify a suitable value for the intermediate ring stiffness ratio for practical design.

1.3. Organization of Thesis

This thesis consists of four chapters which follow the introduction. The brief contents of these chapters can be summarized as follows:

In Chapter 2, the effectiveness of a ring beam in an elevated silo structure in redistributing the discrete forces from column supports is investigated. A criterion that can be used in design to determine the adequacy of a ring for the purpose of minimizing the non-uniformity of vertical stresses in the shell was proposed by Rotter (1985). The applicability of the stiffness criterion proposed by Rotter (1985) to a silo shell resting

on a discretely supported ring beam and subjected to global shear and bending was studied herein. A total of 4320 three dimensional finite element analyses were conducted to evaluate the stiffness ratio.

In Chapter 3, design equations for ring beams used to support cylindrical shells are developed and re-derived. Closed form design equations obtained from Vlasov's curved beam theory were compared with numerical results. A complementary finite element parametric study was also conducted to investigate variation of the values of stress resultants and displacements caused by the connection of the ring to the stiff shell. These variations were plotted as a function of stiffness ratio developed by Rotter (1985).

In Chapter 4, the effectiveness of an intermediate ring stiffener in reducing the non-uniformity of axial membrane stresses in the silo shell is investigated. A design criteria for the strength and stiffness of intermediate ring stiffeners used in cylindrical silo shells resting on discretely supported ring beams is developed via extensive finite element analysis.

Finally, Chapter 5 summarizes the conclusion from all studies performed as a part of this research program and recommendations.

CHAPTER 2

APPLICATION OF RING BEAM STIFFNESS CRITERION FOR DISCRETELY SUPPORTED SHELLS UNDER GLOBAL SHEAR AND BENDING

2.1. Ring Beam Stiffness Criterion for Discretely Supported Shells

Studies on ring beam silo shell interaction mostly focused on the loading case that produces uniform axial line load on the cylindrical shell. This condition represents forces produced on the shell wall due to the frictional resistance between the wall and the stored granular material. On the other hand, lateral loads should also be considered in the design of silos. These actions can be produced due to wind or earthquakes. Similar to axial loading the design against lateral loads which produce global shear and bending on the silo shell is greatly simplified if the simple bending theory can be utilized. This assumption greatly relies on the ability of the ring beam in redistributing the support forces.

The aim of this study is to extend the stiffness criterion developed by Rotter (1985) to loading cases that produce global bending of the silo shell. Pursuant to this goal the stiffness criterion is revisited. The underlying assumption behind its development is extended to cover global shear and bending effects. The applicability of the stiffness criterion is checked via extensive finite element analysis.

2.2. Derivation of Ring Beam Stiffness Criterion – A Revisit

In the algebraic analysis of shells under non-symmetrical loads, it is normal practice to transform the loading into a harmonic series (Timoshenko and Woinowsky-Kreiger, (1959), Novozhilov (1959), Kraus (1967), Flügge (1973)). A harmonic

treatment is only feasible under geometrically linear conditions where the harmonics are decoupled. In the case of the local forces from discrete supports, the dominant harmonic term is the fundamental (Flügge (1973), Rotter (1987)), which corresponds to the number of supports around the circumference (Figure 2.1). The key features of the required stiffness for the ring beam are therefore captured if only the fundamental harmonic is used. The idea here is that considering the fundamental harmonic should be sufficient to cover load cases that can be transformed into a harmonic series. In the both axial line loading and global shear and bending cases local forces from discrete supports are produced which can be considered as non-symmetrical loads. Therefore, it is logical to use the same stiffness criterion to study the effects of axial line loading and global bending. As mentioned before the stiffness criterion was first devised by Rotter (1985). Later the criterion was re-derived and its application to axial line loading was demonstrated by Topkaya and Rotter (2011). The derivation of the stiffness criterion is presented again in this study to provide a background on its development.

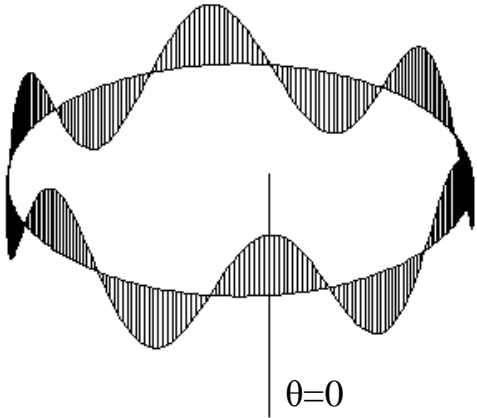


Figure 2.1 Fundamental harmonic of column support for 6 supports

The criterion is based on developing a relationship to describe the relative stiffnesses of the cylindrical shell and the ring beam. For this purpose, the ring beam and the cylindrical shell were treated separately and a compatibility requirement then imposed to determine the extent to which the redistribution of the column forces would be shared between the ring and shell. It was assumed that the fundamental harmonic

of column support given in Equation 2.1 is sufficient to evaluate the key features of the behavior of a discretely supported cylindrical shell.

$$q_x = q_{xm} \cos n\theta \quad (2.1)$$

where q_x = external distributed axial line load; q_{xm} = Fourier coefficient for the n^{th} harmonic of axial line load; n = number of uniformly spaced column supports; and θ = circumferential coordinate. Based on this assumption, closed-form expressions were derived for the stiffnesses of the cylindrical shell and the ring beam.

2.2.1. Ring Beams Subjected to Fundamental Harmonic of Column Support

The Vlasov's curved beam differential equations (Vlasov (1961), Heins (1975)) were used to study the response of the ring beam. In general, the behavior of a curved beam is governed by a series of differential equations. The equilibrium equations were first derived for the curved beam element shown in Figure 2.2, where three orthogonal internal forces and three internal moments develop at each cross-section. The six basic equilibrium equations can be expressed as follows:

$$\frac{1}{R} \left[\frac{\partial Q_r}{\partial \theta} + Q_\theta \right] + q_r = 0 \quad (2.2)$$

$$\frac{1}{R} \frac{\partial Q_x}{\partial \theta} + q_x = 0 \quad (2.3)$$

$$\frac{1}{R} \left[\frac{\partial Q_\theta}{\partial \theta} - Q_r \right] + q_\theta = 0 \quad (2.4)$$

$$\frac{1}{R} \left[\frac{\partial M_r}{\partial \theta} + T_\theta \right] - Q_x + m_r = 0 \quad (2.5)$$

$$\frac{1}{R} \frac{\partial M_x}{\partial \theta} + m_x + Q_r = 0 \quad (2.6)$$

$$\frac{1}{R} \left[\frac{\partial T_\theta}{\partial \theta} - M_r \right] + m_\theta = 0 \quad (2.7)$$

where M_r = bending moment in the ring about a radial axis; M_x = bending moment in the ring about a transverse axis; T_θ = torsional moment in the ring; R = radius of the ring beam centroid; q_x, q_θ, q_r = distributed line loads per unit length in the transverse, circumferential and radial directions respectively; m_x, m_θ, m_r = distributed applied torques per unit circumference about the transverse, circumferential and radial directions respectively; Q_θ = circumferential force in the ring; Q_x, Q_r = shear forces in the ring in transverse and radial directions respectively.

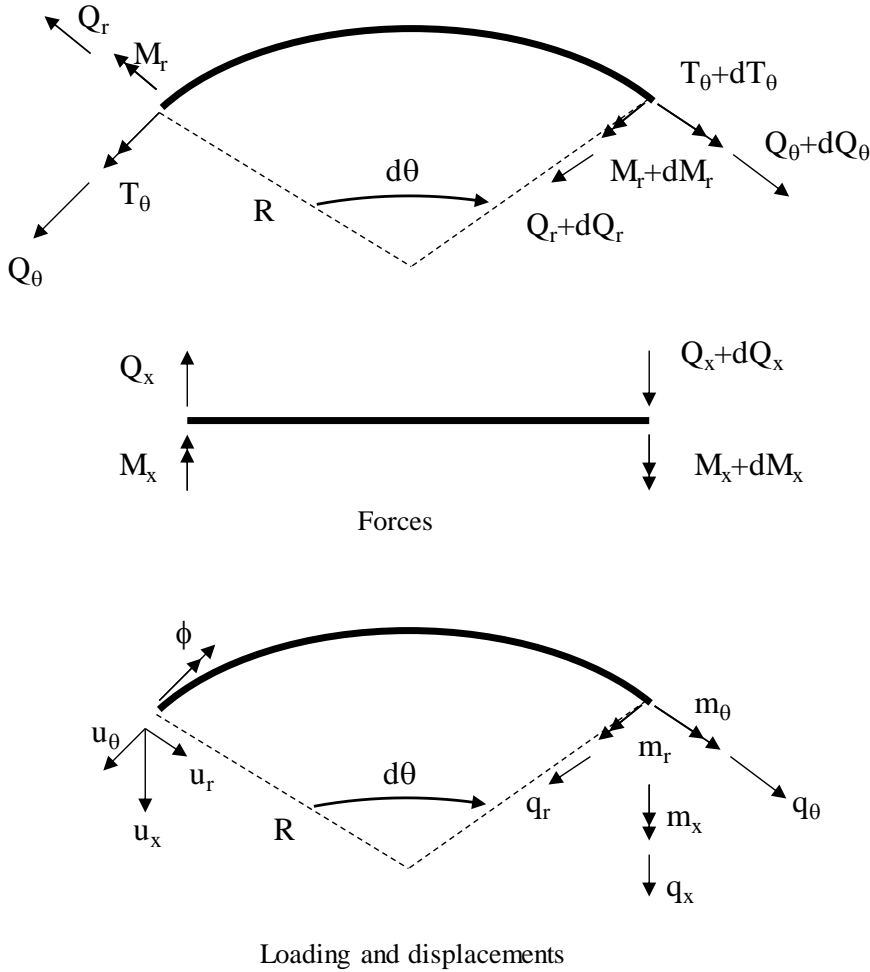


Figure 2.2 Differential curved beam element and sign conventions

The six basic equilibrium equations can be reduced to three differential relationships. One differential equation concerns bending of the ring in its own plane

and can be uncoupled from the other two. The two coupled differential equations of equilibrium can be expressed as:

$$\frac{1}{R^2} \left[\frac{\partial^2 M_r}{\partial \theta^2} + \frac{\partial T_\theta}{\partial \theta} \right] = -q_x \quad (2.8)$$

$$\frac{1}{R} \left[\frac{\partial T_\theta}{\partial \theta} - M_r \right] = -m_\theta \quad (2.9)$$

To determine the transverse displacements, the global force-deformation relationships for a curved beam can be written as (Heins (1975)):

$$Q_\theta = \frac{EA}{R} \left(\frac{\partial u_\theta}{\partial \theta} - u_r \right) \quad (2.10)$$

$$M_x = \frac{EI_x}{R^2} \left(\frac{\partial^2 u_r}{\partial \theta^2} + u_r \right) \quad (2.11)$$

$$M_r = \frac{-EI_r}{R} \left(\frac{1}{R} \frac{\partial^2 u_x}{\partial \theta^2} - \phi \right) \quad (2.12)$$

$$T_\theta = \frac{GJ}{R} \left[\frac{\partial \phi}{\partial \theta} + \frac{1}{R} \frac{\partial u_x}{\partial \theta} \right] - \frac{EC_w}{R^3} \left[\frac{\partial^3 \phi}{\partial \theta^3} + \frac{1}{R} \frac{\partial^3 u_x}{\partial \theta^3} \right] \quad (2.13)$$

where E = modulus of elasticity; A = cross sectional area of the curved beam; G = shear modulus; ϕ = angle of twist about the circumferential axis; u_x , u_θ , u_r = displacements in the vertical (transverse), circumferential and radial directions respectively; I_r , I_x = second moment of area of the ring stiffener about the radial and vertical axes respectively; J = uniform torsion constant; C_w = warping constant for an open section. The first term (in the square brackets) in Equation 2.13 represents the response under St Venant torsion, while the second term represents warping.

The transverse displacements of the ring beam arise from the transverse distributed force q_x which is here applied to the ring by the cylindrical shell. For a

concentrically loaded ring beam cross-section with the transverse forces passing through the shear center, no additional distributed torques are created.

The bending moment and torsional moment variations around the circumference must be derived before the displacements can be deduced. For the loading case represented by Equation 2.1 and without other loading terms (i.e. $q_r = q_\theta = m_r = m_\theta = m_x = 0$), Equations 2.8 and 2.9 can be solved simultaneously to obtain:

$$M_r(\theta) = \frac{R^2 q_{xn}}{(n^2 - 1)} \cos n\theta \quad (2.14)$$

$$T_r(\theta) = \frac{R^2 q_{xn}}{n(n^2 - 1)} \sin n\theta \quad (2.15)$$

The resulting bending moment and torsional moment variations can be directly inserted into Equations 2.12 and 2.13 and solved simultaneously to find the vertical displacements as:

$$u_x(\theta) = u_{xn} \cos n\theta = \frac{R^4 q_{xn}}{(n^2 - 1)^2} \left[\frac{1}{n^2 K_T} + \frac{1}{EI_r} \right] \cos n\theta \quad (2.16)$$

where

$$K_T = GJ + n^2 \frac{EC_w}{R^2} \quad (2.17)$$

The stiffness of the ring can then be expressed as:

$$K_{ring} = \frac{q_x}{u_x} = \frac{(n^2 - 1)^2 EI_r}{R^4} \frac{1}{f_r} \quad (2.18)$$

where

$$f_r = \left[1 + \frac{EI_r}{n^2 K_T} \right] \quad (2.19)$$

It should be noted that the vertical displacements of the ring arise due to bending and twisting of the ring. Therefore, the stiffness of the ring as calculated by Equations 2.18 and 2.19 is influenced by the bending and torsional rigidity of the ring.

2.2.2. Cylindrical Shell Subjected to Fundamental Harmonic of Column Support

Following the description of Calladine (1983), the dominant structural effects in a discretely supported shell are circumferential bending and axial stretching. Under these conditions, the shell can be approximately modeled by ignoring all axial bending and twisting of the wall, together with circumferential stretching effects. These assumptions lead to the semi-membrane theory of shells.

The semi-membrane theory of shells for unsymmetrical loading of cylindrical shells was proposed by Vlasov (1964). This approximate theory is based on three assumptions; (i) the bending (M_x), and twisting ($M_{x\theta}$) moments at sections normal to the shell generator are insignificant and can be neglected, (ii) the circumferential strain (ϵ_θ) and the shear strain ($\gamma_{x\theta}$) on the middle surface are neglected, (iii) Poisson's ratio is zero ($\nu=0$). A detailed summary of the semi-membrane theory for cylindrical shells was presented by Ventsel and Krauthammer (2001). Considering the cylindrical shell element shown in Figure 2.3, the equilibrium equations may be found as:

$$\begin{aligned} R \frac{\partial N_x}{\partial x} + \frac{\partial N_{x\theta}}{\partial \theta} + p_x R &= 0 \\ \frac{\partial N_\theta}{\partial \theta} + R \frac{\partial N_{x\theta}}{\partial x} - \frac{1}{R} \frac{\partial M_\theta}{\partial \theta} + p_\theta R &= 0 \\ \frac{1}{R} \frac{\partial^2 M_\theta}{\partial \theta^2} + N_\theta + p_r R &= 0 \end{aligned} \quad (2.20)$$

where N_x = axial membrane stress resultant; N_θ = circumferential membrane stress resultant; $N_{x\theta}$ = membrane shear stress resultant; M_θ = circumferential bending moment; p_x, p_θ, p_r = external distributed pressures in the axial, circumferential and radial directions, respectively.

The membrane forces $N_{x\theta}$ and N_θ can be eliminated in Equation 2.20 to derive a single differential equation that relates N_x to M_θ as:

$$\frac{\partial^2 N_x}{\partial x^2} + \frac{1}{R^3} \Omega(M_\theta) = -\frac{\partial p_x}{\partial x} + \frac{1}{R} \frac{\partial p_\theta}{\partial \theta} - \frac{1}{R} \frac{\partial^2 p_r}{\partial \theta^2} \quad (2.21)$$

where the operator Ω , is called Vlasov's operator:

$$\Omega(\dots) = \frac{\partial^4(\dots)}{\partial \theta^4} + \frac{\partial^2(\dots)}{\partial \theta^2} \quad (2.22)$$

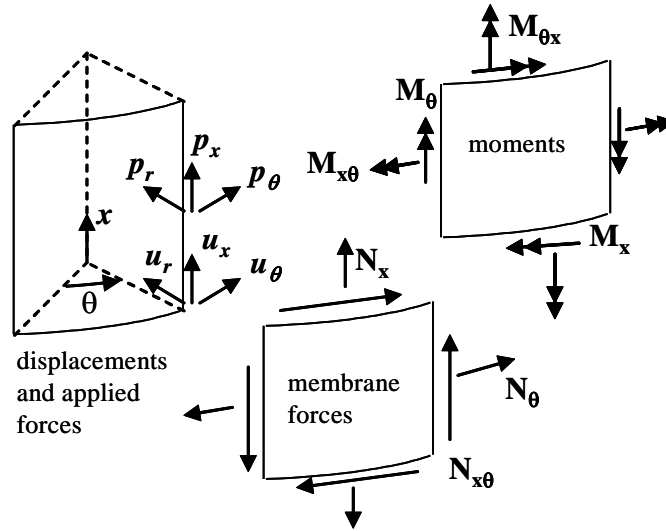


Figure 2.3 Internal forces and moments for shell element

Taking into account the assumptions of the semi-membrane theory ($\varepsilon_\theta = \gamma_{x\theta} = \kappa_x = 0$), the kinematic relationships can be expressed as:

$$\varepsilon_x = \frac{\partial u_x}{\partial x} \quad \varepsilon_\theta = \frac{1}{R} \frac{\partial u_\theta}{\partial \theta} - \frac{u_r}{R} = 0 \quad \gamma_{x\theta} = \frac{\partial u_\theta}{\partial x} + \frac{1}{R} \frac{\partial u_x}{\partial \theta} = 0 \quad (2.23)$$

$$\kappa_x = 0 \quad \kappa_\theta = -\frac{1}{R^2} \left(\frac{\partial u_\theta}{\partial \theta} + \frac{\partial^2 u_r}{\partial \theta^2} \right) \quad \kappa_{x\theta} = -\frac{1}{R} \left(\frac{\partial u_\theta}{\partial x} + \frac{\partial^2 u_r}{\partial x \partial \theta} \right) = 0 \quad (2.24)$$

where u_x, u_θ, u_r = displacements in the axial, circumferential, and radial directions, respectively; $\varepsilon_x, \varepsilon_\theta$ = strain components in the axial and circumferential directions, respectively; $\gamma_{x\theta}$ = shear strain component; κ_x, κ_θ = bending curvatures in the directions of axial and circumferential coordinate lines, respectively; $\kappa_{x\theta}$ = twist of a differential element of the middle surface due to the shell bending.

Based on the assumptions adopted, the constitutive equations can be represented in the form:

$$N_x = Et \frac{\partial u_x}{\partial x} \quad M_\theta = D \kappa_\theta \quad \text{where} \quad D = \frac{Et^3}{12} \quad (2.25)$$

where t = thickness of the cylindrical shell; D = bending rigidity of the cylindrical shell.

Following Ventsel and Krauthammer (2001), the governing differential equation of the semi-membrane theory can be derived in terms of a displacement function (Φ) which is introduced as:

$$u_x = -\frac{\partial \Phi}{\partial x} \quad u_\theta = \frac{1}{R} \frac{\partial \Phi}{\partial \theta} \quad u_r = \frac{1}{R} \frac{\partial^2 \Phi}{\partial \theta^2} \quad (2.26)$$

The constitutive equations in terms of the displacement function, Φ , take the form:

$$N_x = -Et \frac{\partial^2 \Phi}{\partial x^2} \quad M_\theta = -\frac{Et^3}{12R^3} \left(\frac{\partial^2 \Phi}{\partial \theta^2} + \frac{\partial^4 \Phi}{\partial \theta^4} \right) \quad (2.27)$$

The governing partial differential equation of the semi-membrane theory of cylindrical shells is then obtained by substituting Equation 2.27 into Equation 2.21:

$$Et \frac{\partial^4 \Phi}{\partial x^4} + \frac{D}{R^6} \left(\frac{\partial^8 \Phi}{\partial \theta^8} + 2 \frac{\partial^6 \Phi}{\partial \theta^6} + \frac{\partial^4 \Phi}{\partial \theta^4} \right) = \frac{\partial p_x}{\partial x} - \frac{1}{R} \frac{\partial p_\theta}{\partial \theta} + \frac{1}{R} \frac{\partial^2 p_r}{\partial \theta^2} \quad (2.28)$$

The above differential equation must be solved to obtain the axial displacements of the cylindrical shell under the action of the fundamental harmonic of the column support. The particular solution vanishes when $p_x = p_\theta = p_r = 0$. The displacement function can be assumed to take the form:

$$\Phi = \xi(x) \cos n\theta \quad (2.29)$$

which permits compatibility with the ring beam deformations of Equation 2.16. The governing ordinary differential equation then takes the form:

$$\left[\frac{d^4 \xi(x)}{dx^4} + \frac{D}{EtR^6} n^4 (n^2 - 1)^2 \xi(x) \right] \cos n\theta = 0 \quad (2.30)$$

For a specific harmonic n , the solution has the form:

$$\xi(x) = e^{\pi(x/\mu)} \left[C_1 \sin \frac{\pi x}{\mu} + C_2 \cos \frac{\pi x}{\mu} \right] + e^{-\pi(x/\mu)} \left[C_3 \sin \frac{\pi x}{\mu} + C_4 \cos \frac{\pi x}{\mu} \right] \quad (2.31)$$

where $C_1, C_2, C_3, C_4 =$ constants to be determined to satisfy the boundary conditions.

The parameter μ is the long wave bending half wavelength (Calladine (1983)), expressed as:

$$\mu = \frac{\pi}{n} \sqrt[4]{\frac{4EtR^6}{D(n^2-1)^2}} = \frac{2\pi^4\sqrt{3}}{n\sqrt{(n^2-1)}} \sqrt{\frac{R}{t}} R \approx \frac{8.27}{n\sqrt{(n^2-1)}} \sqrt{\frac{R}{t}} R \quad (2.32)$$

The constants (C_1, C_2, C_3, C_4) can be determined by applying the boundary conditions. The circumferential displacements at the bottom and top of the shell are zero due to the restraints provided by attached shells at these locations. An axial line loading described by Equation 2.1 is applied at the bottom of the shell while the top of the shell is free from any axial loading. These boundary conditions can be expressed as:

$$u_\theta(x=0) = 0 \quad u_\theta(x=H) = 0 \quad N_x(x=0) = -q_x \quad N_x(x=H) = 0 \quad (2.33)$$

where H = the height of the cylindrical shell.

The resulting displacements at the level ($x = 0$) where the harmonic traction is applied can be found as:

$$u_x(x=0) = \frac{q_{xn}\mu}{2\pi Et} f_s \cos n\theta \quad (2.34)$$

where

$$f_s = \frac{F^2 - 2Fs' - 1}{F^2 - 2Fc' + 1} \quad F = e^\eta \quad s' = \sin \eta \quad c' = \cos \eta \quad (2.35)$$

in which $\eta = 2\pi H / \mu$.

Finally, the stiffness of the cylindrical shell (K_{shell}) can be represented as:

$$K_{shell} = \frac{q_{xn}}{u_x(x=0)} = \frac{2\pi Et}{\mu f_s} = n\sqrt{(n^2-1)} \frac{E}{\sqrt[4]{3}} \left(\frac{t}{R}\right)^{3/2} \frac{1}{f_s} \quad (2.36)$$

2.2.3. Stiffness Ratio

The expressions developed for the stiffnesses of cylindrical shell and ring beam can be combined to obtain the ratio of their stiffnesses ψ , which describes the stiffness required to maintain displacement compatibility. The stiffness ratio corresponds to the extent to which the shell is required to carry non-symmetrical stresses due to the supports:

$$\psi = \frac{K_{shell}}{K_{ring}} = 0.760 \frac{(Rt)^2}{I_r} \sqrt{\frac{R}{t}} \sqrt{\frac{n^2}{(n^2-1)^3}} \cdot \frac{f_r}{f_s} = \frac{1}{10.9} \frac{\mu Rt^2}{I_r} \left(\frac{n^2}{n^2-1}\right) \cdot \frac{f_r}{f_s} \quad (2.37)$$

This ratio is intended to give a strong indication of the effectiveness of the ring in the role assigned to it. If the ring is stiff compared with the shell, it should achieve the goal of redistributing the discrete forces from the supports and providing relatively uniform support to the shell. This corresponds to a low value of the stiffness ratio ψ . By contrast, where the ring beam is not very stiff, and high values of ψ are found, it is likely that the ring beam will fail to redistribute the discrete forces, the shell will be subject to high local meridional membrane stresses above the support, and there is considerable potential for buckling failures in this location (Teng and Rotter (1992), Guggenberger et al. (2000), Guggenberger et al. (2004)).

The applicability of the stiffness ratio to the case with axial line loading was studied by Topkaya and Rotter (2011) through finite element analysis. Different combinations of ring beams and silo shells were considered. The silo shell was loaded with a uniform axial load at the top and the peak value of axial membrane stress above the ring beam was calculated using linear finite element analysis. Its value relative to

the uniform applied load is termed the “stress amplification ratio ζ ”. A plot of the stress amplification ratio as a function of the stiffness ratio is given in Figure 2.4.

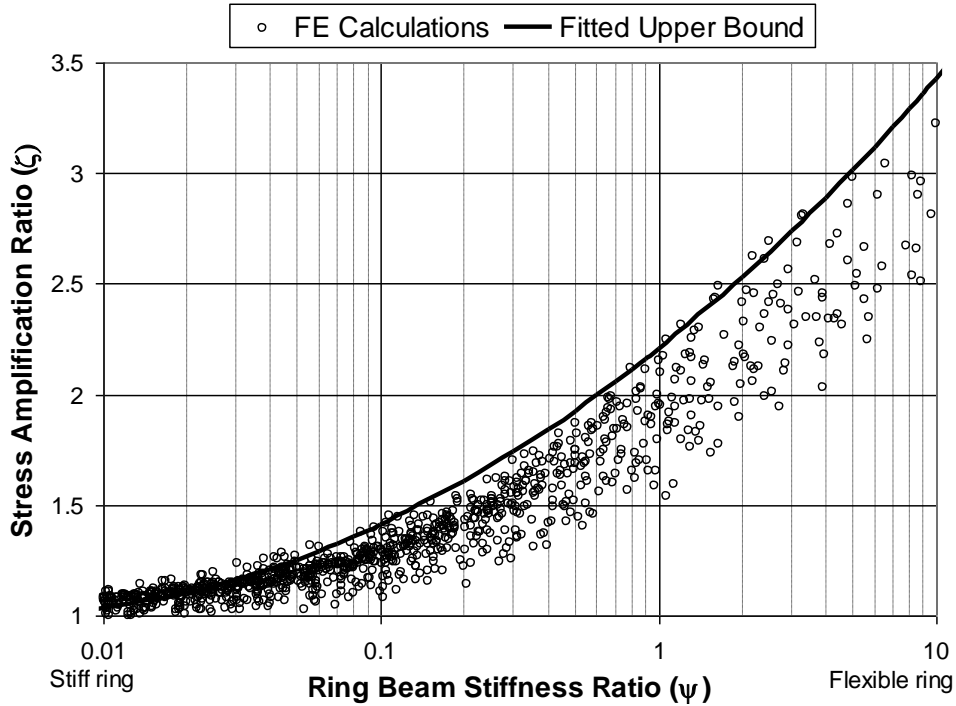


Figure 2.4 Relationship between ring beam stiffness ratio and stress amplification ratio for axial line loading

The following upper bound was developed to quantify the response.

$$\zeta = 1 + 0.21 \left(3 + \log \left(\frac{\psi}{4} \right) \right)^2 \quad (2.38)$$

Axial compression buckles are relatively short in the axial direction (Timoshenko and Gere (1961), Calladine (1983), Rotter (2004)), so axial non-uniformity has little effect on the buckling strength. However, circumferentially non-uniform stresses lead to very different buckling conditions (Greiner and Guggenberger (1998), Guggenberger et al. (2000), Guggenberger et al. (2004), Rotter et al. (2011)), so it is vital to determine both the peak values and the rate of decay away from the peak

(Rotter (1986), EN 1993-4-1 (2007), ECCS (2008)). The presence of discrete supports produces circumferentially non-uniform stresses for shells under axial compression or shear and bending. Where a single ring beam is used, Equation 2.38 can be used to determine the peak value under axial compression due to the non-uniformity of stresses caused by discrete supports. Sonat et al. (2015) developed a methodology for buckling assessment of silo shells resting on discretely supported ring beams. The methodology requires the peak value of stress above the support and this value can be readily found using Equation 2.38.

2.3. Numerical Study

A parametric study was conducted using linear analysis of three dimensional finite element structures to evaluate the applicability of the stiffness ratio to silo shells under global shear and bending. The commercial finite element program, ANSYS (2010), was used to perform the numerical analyses. To cover a wide range of behaviors, cylindrical shells and ring beams with many geometries were studied.

Four-node shell elements (shell63) were employed to model the cylindrical shell. The ring beam was modeled using two-node beam elements (beam 4). A representative finite element mesh of the silo shell and ring beam is given in Figure 2.5. At the bottom, the nodes shared by the cylindrical shell and the ring beam were restrained against displacement in the radial direction only. The radial restraint simulates the restraint provided by the hopper which is attached to the bottom of the shell. Because the ring beam is stiff in the circumferential direction, it provides a natural restraint against circumferential displacements. Nodes lying within the width of the support on the base of the ring beam were restrained against vertical movement u_x . Four support conditions were considered. The first one represents a knife edge support where vertical movement of only one node is restrained at each support (Figure 2.5). In the past, a support width-to-radius ratio of 0.2 was considered by Teng and Rotter (1992). Support width-to-radius ratios of 0.05, 0.10, and 0.20 were considered to cover a range of support conditions (Figure 2.5). The connected shell which is a

circular plate at the top was modeled explicitly by 20 mm thick three-node and four node shell elements as shown in Figure 2.5. A concentrated load of 2000 kN in the horizontal direction was applied at the center of the circular plate. The concentrated load was oriented to produce maximum amount of non-uniformity in axial membrane stresses as shown in Figure 2.5. For all analyses, the modulus of elasticity was taken as 200 GPa and Poisson's ratio as 0.30.

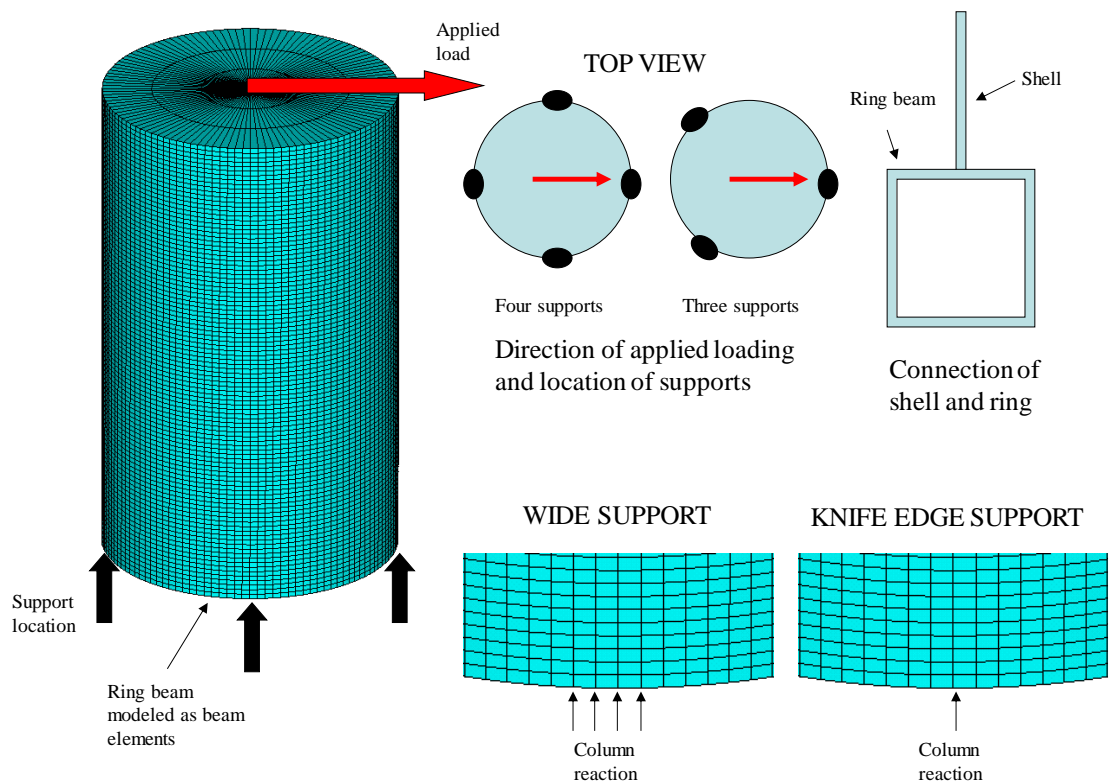


Figure 2.5 A typical finite element mesh for the cylindrical shell and ring beam, support conditions and connection of shell and ring

The ability of the ring beam in redistributing the axial membrane stresses was explored first. In the absence of a ring beam the stresses due to global shear and bending can be calculated using simple bending theory. In other words the following formula can be used to determine the maximum axial membrane stress in a ground

supported silo shell under global bending actions which can be used as a reference (σ_{ref}).

$$\sigma_{ref} = \frac{Mc}{I} = \frac{M}{\pi R^2 t} \quad (2.39)$$

where M = bending moment at the base of the silo; c = maximum distance from the centroid of the cylindrical shell cross-section to the point of interest ($c = R$); I = second moment of area of the cylindrical shell cross-section.

The accuracy of Equation 2.39 was assessed by analyzing a ground supported silo with $R = 3000$ mm, $H = 10000$ mm, and $t = 6$ mm using the finite element modeling details presented earlier. Comparison of the axial membrane stress variations around the circumference given in Figure 2.6 indicates that using simple bending theory provides an accurate representation of the stresses obtained using a more detailed numerical analysis. In other words the reference stress (σ_{ref}) can be used to represent the maximum axial membrane stress for a silo shell under global shear and bending in the absence of a ring beam.

For the parametric study, the finite element models described earlier were adopted, with different geometries defined as radius $R = 3000$ and 4000 mm, thickness $t = 6, 8,$ and 10 mm, shell heights $H = 10000, 15000, 20000$ mm, and number of supports $n = 3$ and 4 . A total of 36 combinations were adopted for the shell geometries with 30 different square hollow section beam geometries. The hollow section ring beams had wall heights of 300, 400, 500, 600, 700, 800 mm and wall thicknesses of 30, 40, 50, 60, and 70 mm. Different cross-section dimensions provide variations in the cross-section properties. A total of 1080 cases were analyzed for each of the support conditions using the finite element method resulting in a total of 4320 analyses.

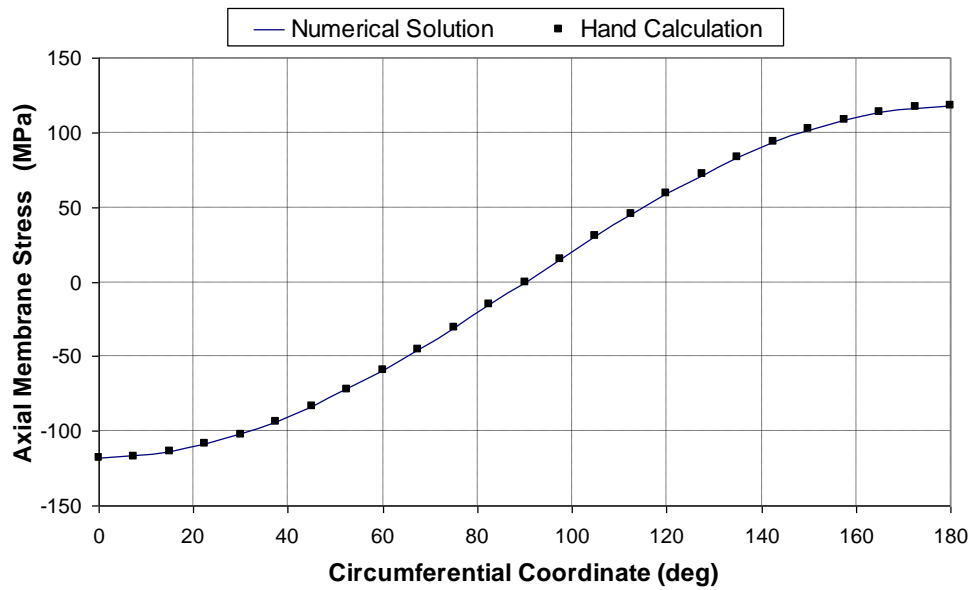


Figure 2.6 Verification of simple bending theory for silo shells under global bending

The finite element analyses were chiefly used to explore the variation of the axial membrane stress at the base of the cylindrical shell over the support. This gives a measure of the uniformity of support provided by the ring beam. Where the ring beam is very effective in distributing the discrete forces from the supports (e.g. $\psi = 0.01$), the stress levels in the shell over the support should be equal to the reference stress (σ_{ref}) obtained from Equation 2.39. Where the ring is ineffective (e.g. $\psi = 10$), the stress above the support is very much greater than the reference stress (σ_{ref}). Typical variations of axial membrane stress are shown in Figure 2.7 for a cylindrical shell of radius 3000 mm, height 10000 mm, thickness 6 mm, and resting on 4 supports. In this figure the stress variation for a ground supported silo shell is provided as a reference where the maximum stress is reached over the support ($\theta = 0^\circ$) with a value equal to 118 MPa. Two different ring beam geometries were considered. The first one has a wall height of 800 mm and a wall thickness of 50 mm and represents a sizeable ring beam geometry ($\psi = 0.05$). In this case the maximum axial membrane stress is calculated as 123 MPa at $\theta = 6^\circ$ which results in an increase of 4.2%. The second beam has a wall height of 300 mm and a wall thickness of 50 mm and represents a relatively

flexible beam ($\psi = 1.29$). For this case the maximum axial membrane stress is calculated as 218 MPa at $\theta=6^\circ$ which results in an increase of 84.7%. The aforementioned cases were analyzed for the support width to radius ratio of 0.2. The locations where the support width terminates are indicated by dashed solid vertical lines in Figure 2.7. The analysis results show that the stresses are smoothed over the support and the maximums are reported at locations where the support width terminates. For comparison purposes the results for the flexible beam case with a knife edge support is also reported in Figure 2.7. In this case the smoothing action of the support is not present and the maximum axial membrane stress is calculated as 321 MPa at $\theta=0^\circ$ which results in an increase of 172.0%. These observations strengthen the assertion that the stiffness of the ring beam plays a very important role in the redistribution of support forces.

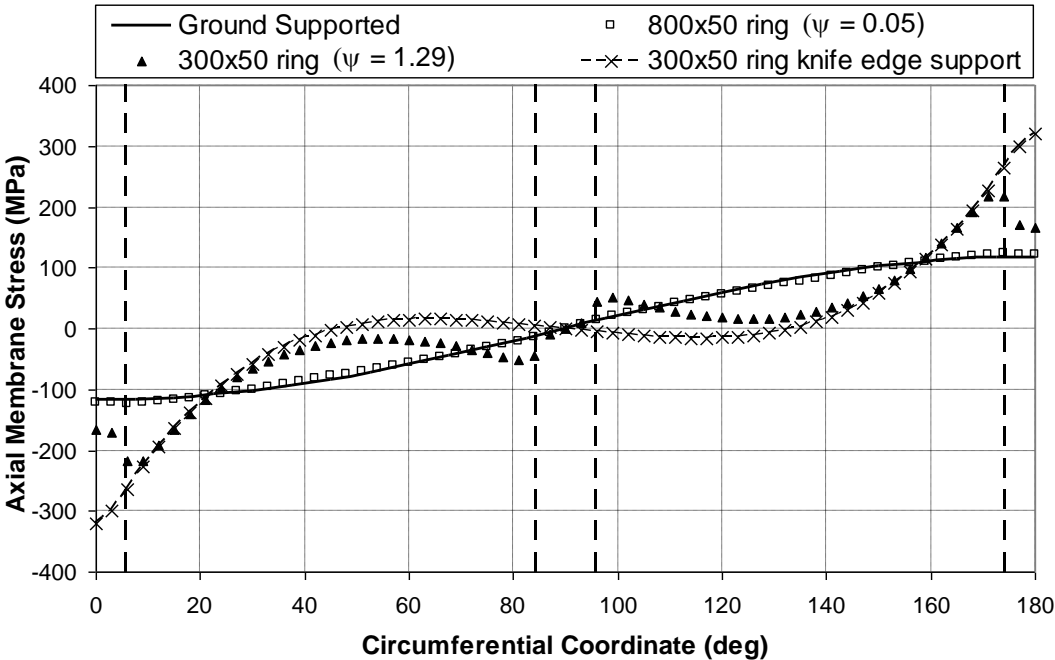


Figure 2.7 Variation of axial membrane stress along the circumference for cases with different beam geometries and support conditions

All analyses focused on the peak axial stress (σ_{max}) in the shell that occurs above supports. Based on 4320 separate finite element analyses, these stresses are

normalized by the reference stress ($\zeta = \sigma_{\max} / \sigma_{\text{ref}}$) and are plotted in Figures. 2.8, 2.9, 2.10 and 2.11 against the stiffness ratio ψ defined by Equation 2.37. The results for a knife edge support are given in Figure 2.8 while the ones for other support-width-to-radius ratios are given in Figures 2.9, 2.10, and 2.11. The first conclusion from the analysis results is that the stiffness ratio ψ clearly captures the trend of the data. The data points fall within a narrow band similar to the behavior presented in Figure 2.4.

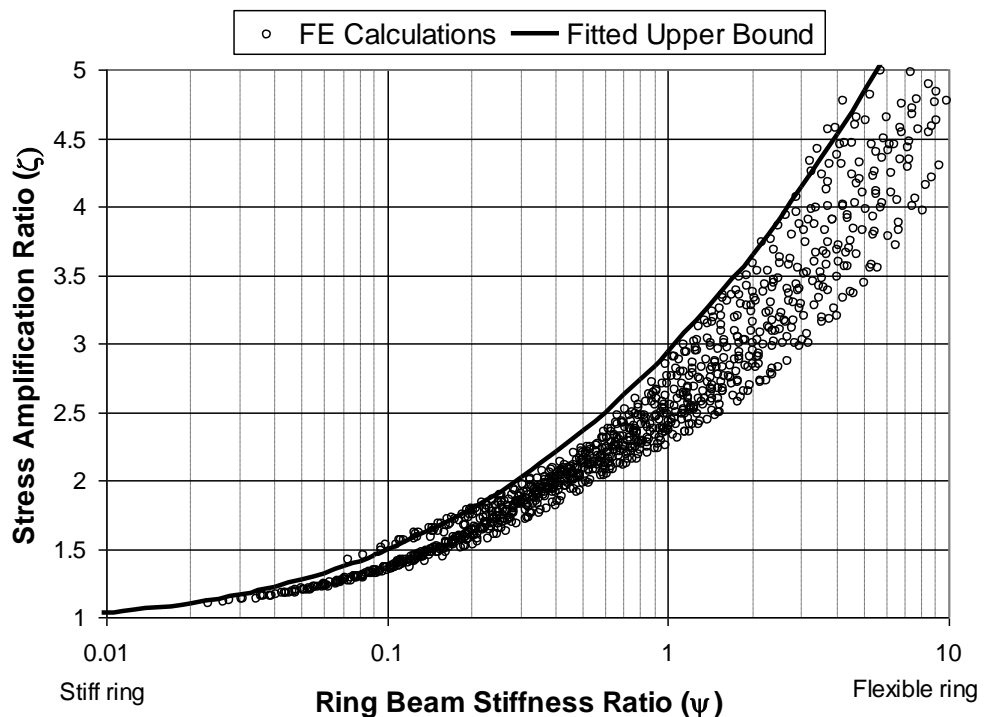


Figure 2.8 Relationship between ring beam stiffness ratio and stress amplification ratio for global bending (knife edge support)

The analysis results revealed that the stiffness ratio can be applied to silo shells under global shearing and bending actions. There are marked differences between the cases with different support conditions. The knife edge support condition produced much higher stress amplification ratios (ζ) when compared with the amplifications for a finite width support. This is an expected outcome as the smoothing action of the support described earlier and presented in Figure 2.7 is not present in the case of a

knife edge support. The following upper bound expressions were developed to represent the data.

$$\xi = 1 + 0.096 \left(1.5 + \log \left(\frac{\psi}{0.06} \right) \right)^3 \text{ for knife edge support} \quad (2.40)$$

$$\xi = 1.70 + 1.165 \ln(\psi + 0.55) \text{ for a support width-to-radius ratio of 0.05} \quad (2.41)$$

$$\xi = 1.33 + 1.20 \ln(\psi + 0.77) \text{ for a support width-to-radius ratio of 0.10} \quad (2.42)$$

$$\xi = 1.45 + 0.88 \ln(\psi + 0.6) \text{ for a support width-to-radius ratio of 0.20} \quad (2.43)$$

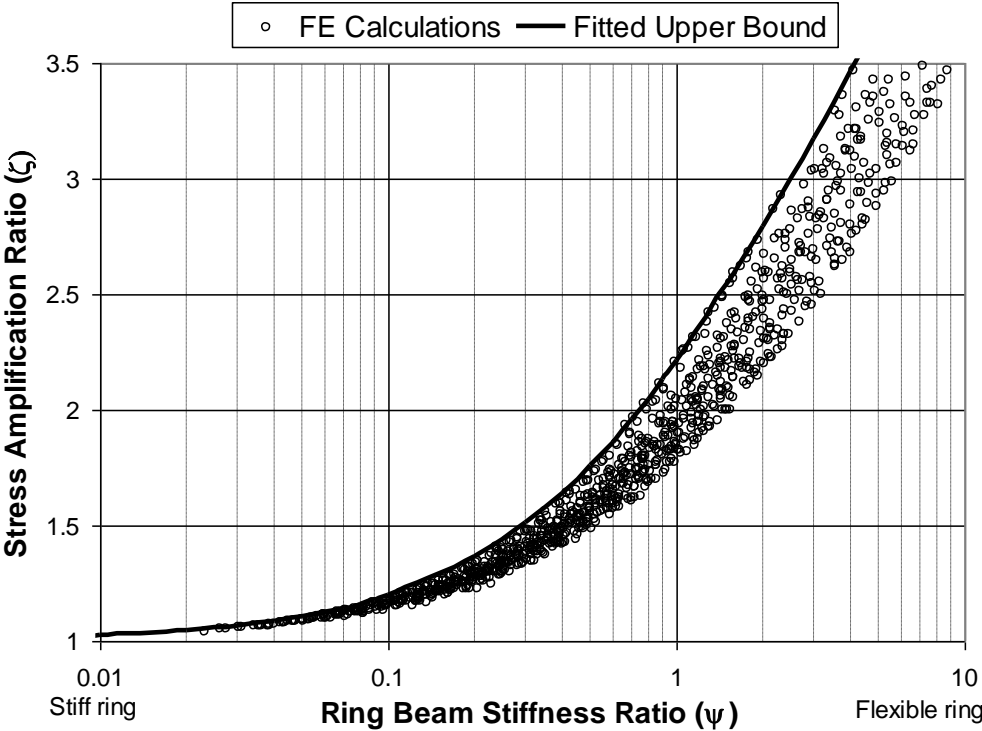


Figure 2.9 Relationship between ring beam stiffness ratio and stress amplification ratio for global bending (support width to radius ratio of 0.05)

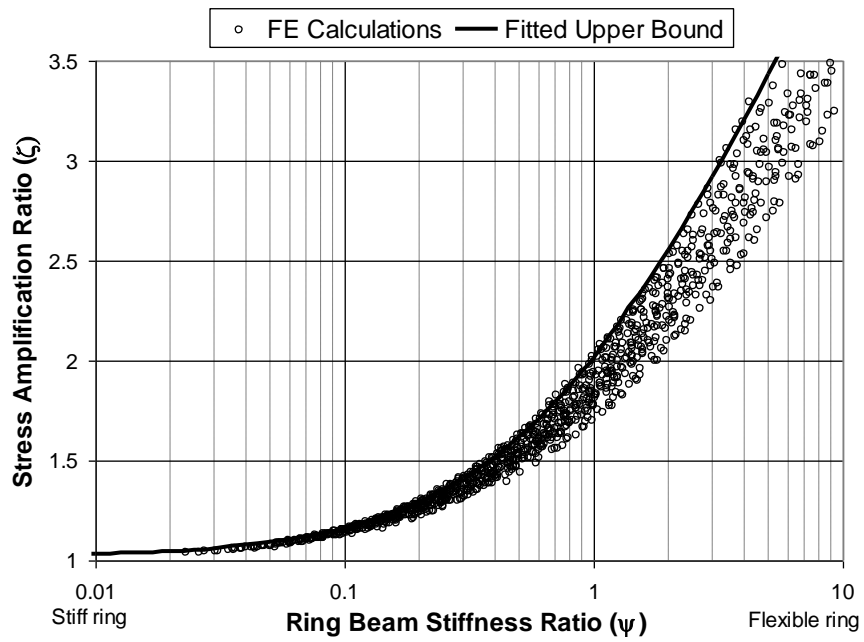


Figure 2.10 Relationship between ring beam stiffness ratio and stress amplification ratio for global bending (support width to radius ratio of 0.10)

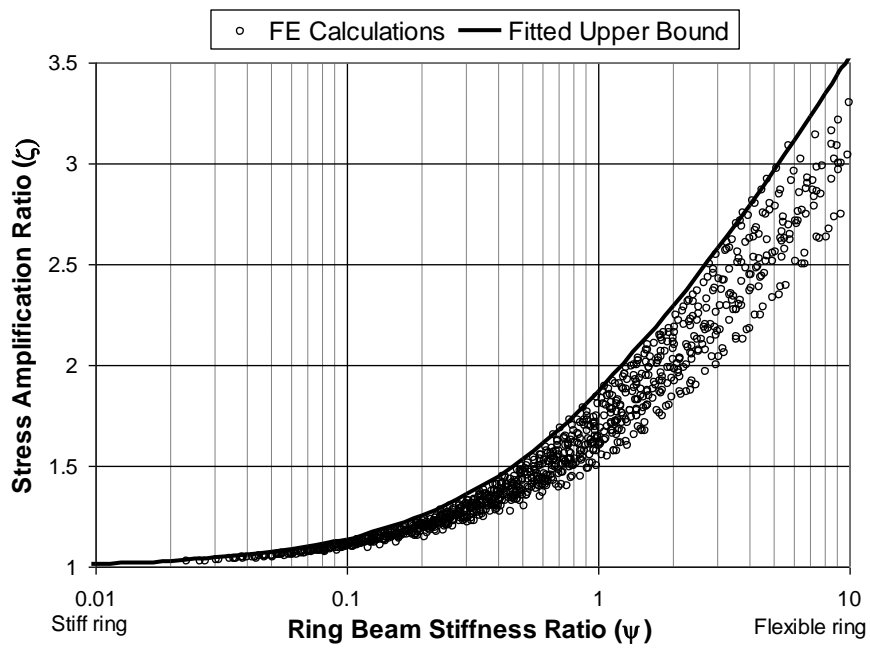


Figure 2.11 Relationship between ring beam stiffness ratio and stress amplification ratio for global bending (support width to radius ratio of 0.20)

The upper bound expressions for the finite width support (Equations 2.40 through 2.43) are compared with the upper bound expression (Equation 2.38) developed for a silo shell under axial line load in Figure 2.12. It is evident from this figure that the stress amplification ratio increases (ζ) as the support width-to-radius ratio decreases. The highest values of amplifications are reported for the knife edge support case as expected. There are marked differences between the behaviors reported for the axial line loading and loadings that create global bending. It should be mentioned that the expression (Equation 2.38) for axial line loading was developed based on a support width-to-radius ratio of 0.2. When this expression is compared with its counterpart (shell under global bending with support width-to-radius ratio of 0.2, i.e. Equation 2.43) differences are observed for the range $\psi < 6$. In general, the axial line loading produces higher stress amplifications when compared with a loading that causes global bending.

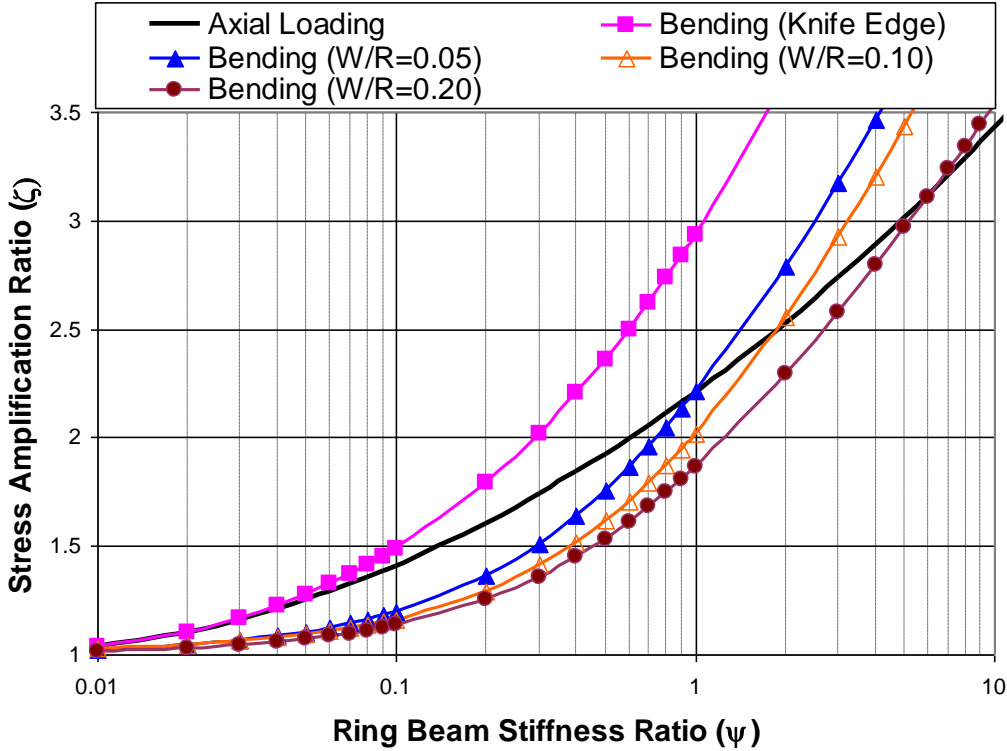


Figure 2.12 Comparison of responses for different support width-to-radius ratios

CHAPTER 3

ANALYSIS OF SILO SUPPORTING RING BEAMS RESTING ON DISCRETE SUPPORTS

3.1. Algebraic Closed-form Solution of Stress Resultants in the Ring Beam using Vlasov's Curved Beam Theory

The Eurocode EN 1993-4-1 (2007) only provides design equations for stress resultants produced in the isolated ring beam under uniform transverse loading. These stress resultants were derived by Rotter (1985) using equilibrium equations only. This study explores the extent to which a practical silo shell causes these stress resultants to be reduced when the ring beam has only practical stiffness.

The free body diagram of a closed section ring beam cross-section is indicated in Figure 3.1. By examination of this free body diagram, the forces acting in the two principal directions, the uniformly distributed vertical load (n_v) and the radial inward load (n_r), can be expressed as follows:

$$n_v = n_{xc} + n_{\phi h} \cos \beta \qquad n_r = n_{\phi h} \sin \beta \qquad (3.1)$$

where n_{xc} = the design value of compressive membrane stress resultant at the base of the cylinder; $n_{\phi h}$ = the design value of tensile membrane stress resultant at the top of the hopper; β = the hopper half angle.

As shown in Figure 3.1 the forces in the two principal directions act eccentrically with respect to the ring beam centroid (C). These forces can be decomposed into three basic loads on the ring beam shown in Figure 3.1 where the vertical and inward loads act through the centroid of the cross-section. The three basic loads are the transverse

distributed load (q_x), the circumferentially distributed torque (m_θ), and the concentrated torque at the supports (m_s) which can be expressed by the following relationships:

$$q_x = \frac{n_v(R-e_r)}{R} \quad m_\theta = \frac{n_v(R-e_r)}{R} e_r + \frac{n_r(R-e_r)}{R} e_x \quad m_s = Qe_s = 2n_v(R-e_r)\theta_0 e_s \quad (3.2)$$

where e_r = the radial eccentricity of the cylinder from the ring beam centroid; e_s = the radial eccentricity of the support from the ring beam centroid; e_x = the vertical eccentricity of the joint centre from the ring beam centroid; θ_0 = the circumferential angle in radians subtended by the half span of the ring beam ($\theta_0 = \pi/n$); n = the number of equally spaced discrete supports; Q = support force.

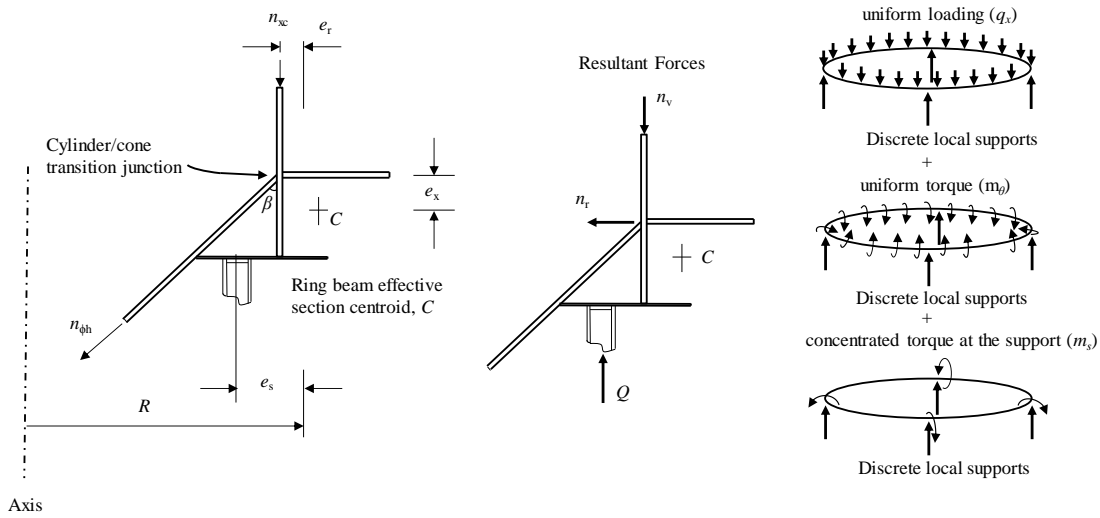


Figure 3.1 Simplified load-carrying mechanism model for the ring beam

The ring beam is analyzed for these three different load cases in turn.

3.1.1. Derivation of stress resultants – ring under transverse distributed load (q_x)

For the case where the only transverse distributed load (q_x) is concentrically applied to the ring (i.e. $q_r = q_\theta = m_r = m_\theta = m_x = 0$), the six basic equilibrium equations

which are given Equation 2.2 through 2.7 for the curved beam element in Figure 2.2 can be reduced to three differential relationships. One differential equation concerns bending of the ring in its own plane and can be uncoupled from the other two. The two-coupled differential equations of equilibrium can be expressed as:

$$\frac{1}{R} \left[\frac{\partial T_\theta}{\partial \theta} - M_r \right] = 0 \quad (3.3)$$

$$\frac{1}{R^2} \left[\frac{\partial^2 M_r}{\partial \theta^2} + \frac{\partial T_\theta}{\partial \theta} \right] = -q_x \quad (3.4)$$

Simultaneous solution of Equations 3.3 and 3.4 using the appropriate boundary conditions ($M_r(0)=M_r(2\theta_0)$, $T_\theta(0)=T_\theta(2\theta_0)=0$) reveal the following relationships:

$$M_r(\theta) = n_v R(R - e_r) [\theta_0 (\sin \theta + \cot \theta_0 \cos \theta) - 1] \quad (3.5)$$

$$T_\theta(\theta) = n_v R(R - e_r) [\theta_0 (\cot \theta_0 \sin \theta - \cos \theta + 1) - \theta] \quad (3.6)$$

3.1.2. Derivation of stress resultants – ring under circumferential distributed torque (m_θ)

In the same manner, the following two coupled differential equations are obtained for the case where only a circumferentially distributed torque (m_θ) is applied to the ring (i.e. $q_x = q_r = q_\theta = m_r = m_x = 0$):

$$\frac{1}{R} \left[\frac{\partial T_\theta}{\partial \theta} - M_r \right] = -m_\theta \quad (3.7)$$

$$\frac{1}{R^2} \left[\frac{\partial^2 M_r}{\partial \theta^2} + \frac{\partial T_\theta}{\partial \theta} \right] = 0 \quad (3.8)$$

Simultaneous solution of Equations 3.7 and 3.8 using the appropriate boundary conditions ($M_r(0)=M_r(2\theta_0)$, and $T_\theta(0)=T_\theta(2\theta_0)=0$) reveals the following relationships:

$$M_r(\theta) = (R - e_r)(n_v e_r + n_r e_x) \quad (3.9)$$

$$T_\theta(\theta) = 0 \quad (3.10)$$

3.1.3. Derivation of stress resultants – ring under concentrated torque at the supports (m_s)

The following coupled differential equations are obtained for the case where the concentrated torques (m_s) are applied at the supports of the ring (i.e. $q_x = q_r = q_\theta = m_x = m_r = m_\theta = 0$):

$$\frac{1}{R} \left[\frac{\partial T_\theta}{\partial \theta} - M_r \right] = 0 \quad (3.11)$$

$$\frac{1}{R^2} \left[\frac{\partial^2 M_r}{\partial \theta^2} + \frac{\partial T_\theta}{\partial \theta} \right] = 0 \quad (3.12)$$

Simultaneous solution of Equations 3.11 and 3.12 using the appropriate symmetry boundary conditions that considering the conditions of continuity ($M_r(0) = M_r(2\theta_0)$, $T_\theta(0) = 0$ and $T_\theta(2\theta_0) = m_s/2$) reveals the following relationships:

$$M_r(\theta) = -n_v e_s (R - e_r) \theta_0 (\sin \theta + \cot \theta_0 \cos \theta) \quad (3.13)$$

$$T_\theta(\theta) = n_v e_s (R - e_r) \theta_0 (\cos \theta - \cot \theta_0 \sin \theta) \quad (3.14)$$

Equations 3.5, 3.9 and 3.13 can be superposed to obtain the bending stress resultant and similarly Equations 3.6, 3.10 and 3.14 can be superposed to obtain the torsional stress resultant as follows:

$$M_r(\theta) = n_v (R - e_r) [(R - e_s) \theta_0 (\sin \theta + \cot \theta_0 \cos \theta) - R + e_r] + n_r e_x (R - e_r) \quad (3.15)$$

$$T_\theta(\theta) = n_v (R - e_r) [(R - e_s) \theta_0 (\cot \theta_0 \sin \theta - \cos \theta) + R(\theta_0 - \theta)] \quad (3.16)$$

Equations 3.15 and 3.16 are identical to those ones developed by Rotter (2001) and provided in the Eurocode EN 1993-4-1 (2007). One advantage of using the Vlasov's curved beam differential equations is that the transverse displacements of the beam can be obtained. The global force-deformation relationships for the transverse displacements were given in Equation 2.10 through 2.13.

The present study focuses on closed sections where the St. Venant's term dominates over the warping term. Therefore, the warping term is neglected in the calculations (i.e. $C_w \approx 0$). Combining Equations 2.12 and 2.13 reveals the following differential relationship:

$$\frac{\partial^3 u_x}{\partial \theta^3} + \frac{\partial u_x}{\partial \theta} = R^2 \left[\frac{T_\theta}{GJ} - \frac{1}{EI_r} \frac{dM_r}{d\theta} \right] \quad (3.17)$$

The resulting bending moment and torsional moment variations which are given in Equations 3.15 and 3.16 can be directly inserted into Equation 3.17 and solved using the appropriate boundary conditions ($u_x(0) = u_x(2\theta_0) = 0$, $u_x'(0) = u_x'(2\theta_0)$) to find the transverse displacements as:

$$u_x(\theta) = \frac{-n_v(R-e_r)R^2}{4EI_r GJ \sin^2(\theta_0)} \left\{ \begin{aligned} &EI_r R \theta (\theta - 2\theta_0) (1 - \cos 2\theta_0) - (EI_r + GJ)(R - e_s) \theta_0 [2\theta_0 + (\theta - 2\theta_0) \cos \theta - \theta \cos(\theta - 2\theta_0)] \\ &+ \theta_0 [\sin \theta - \sin(\theta - 2\theta_0) - \sin 2\theta_0] \times [EI_r (3R - e_s) + GJ(R - e_s)] \end{aligned} \right\} \quad (3.18)$$

3.2. Computational Verification of the Closed Form Solutions

Linear three dimensional finite element analysis was conducted to verify the accuracy of these equations for the stress resultants and displacements in the transverse direction. The commercial finite element program, ANSYS (2010), was used to perform the numerical analyses. The isolated ring beam analyzed here rests on $n = 4$ supports and has a cylinder radius of $R = 3000$ mm. A $500 \text{ mm} \times 500 \text{ mm}$ square hollow section with wall thickness of 50 mm was selected for the ring beam cross section. A constant uniform transverse loading (n_v) of 1.5 kN/mm was applied to the

ring beam. All eccentricity terms were neglected for simplicity. The ring beam was modelled using two-node beam elements (beam4) as shown Figure 3.2a. The modulus of elasticity was taken as 200 GPa and Poisson’s ratio as 0.30. The ring beam was assumed to rest on knife edge supports which were modelled by restraining only a single node at each support location.

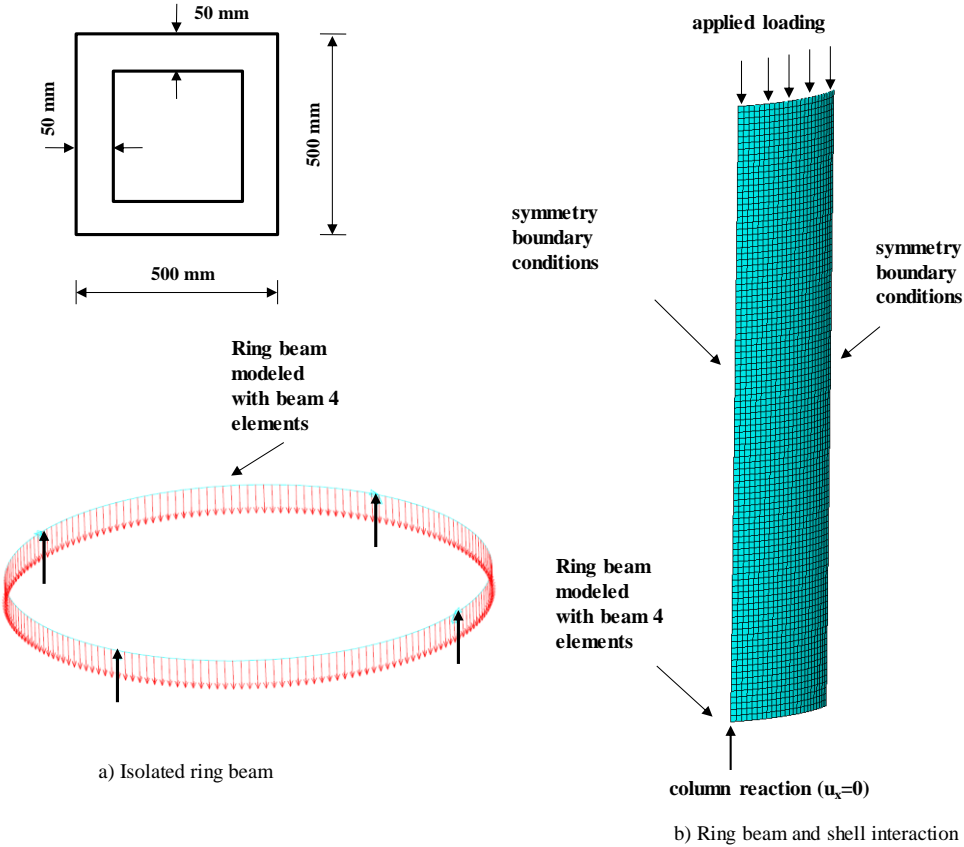


Figure 3.2 Finite-element modelling for the ring beam and cylindrical shell

The calculated variations of M_r , T_θ and u_x in the circumferential direction are shown in Figures 3.3, 3.4 and 3.5 respectively, together with the predictions of the closed form solutions (Equations 3.15, 3.16 and 3.18). When an isolated ring beam is considered, the comparisons show that the above equations provide very accurate solutions, with the largest differences being 0.078%, 0.002% and 0.024% for

maximum bending moment in the ring about a radial axis, torsional moment and transverse displacement respectively.

To investigate the behavior of a ring that interacts with the silo shell, silo structures with a ring beam were next considered with different shell thicknesses $t = 4$ and 10 mm and a constant height $H = 10000$ mm. The same support conditions and ring beam properties were used. A uniform axial load ($n_v = 1.5$ kN/mm) was applied to the top of the cylindrical shell around the full circumference. For a cylindrical shell resting on n equally spaced discrete supports, there are $2n$ planes of symmetry. The computational time was reduced by modelling only a segment covering an angle of θ/n , as shown in Figure 3.2b. Four-node shell elements (shell63), with a size of 100 mm in both the axial and circumferential directions, were employed to model the cylindrical shell. Symmetry boundary conditions were applied to the nodes on each symmetry plane. In practice, silo cylindrical shell walls are normally connected to other conical shells at the top and the bottom. These conical pieces effectively prevent out-of-round displacements of the cylinder at the two extremes. In this study, the restraining effect of the connected shells was modeled by restraining the displacements at these points. At the top both the radial and circumferential displacements and at the bottom only the radial displacements were restrained.

The variation of the stress resultants and displacement are shown in Figures. 3.3, 3.4 and 3.5 respectively. When the 4 mm thick shell was considered, the comparisons show that the above equations provide conservative solutions for the ring, with the largest differences being 18.2%, 14.7% and 14.8% for maximum bending moment about a radial axis, torsional moment and transverse displacement respectively. When the 10 mm thick shell was considered, the comparisons show that the above equations provide more conservative solutions for the ring, with the largest differences being 48.6%, 38.3% and 38.5% for maximum bending moment about a radial axis, torsional moment and transverse displacement respectively.

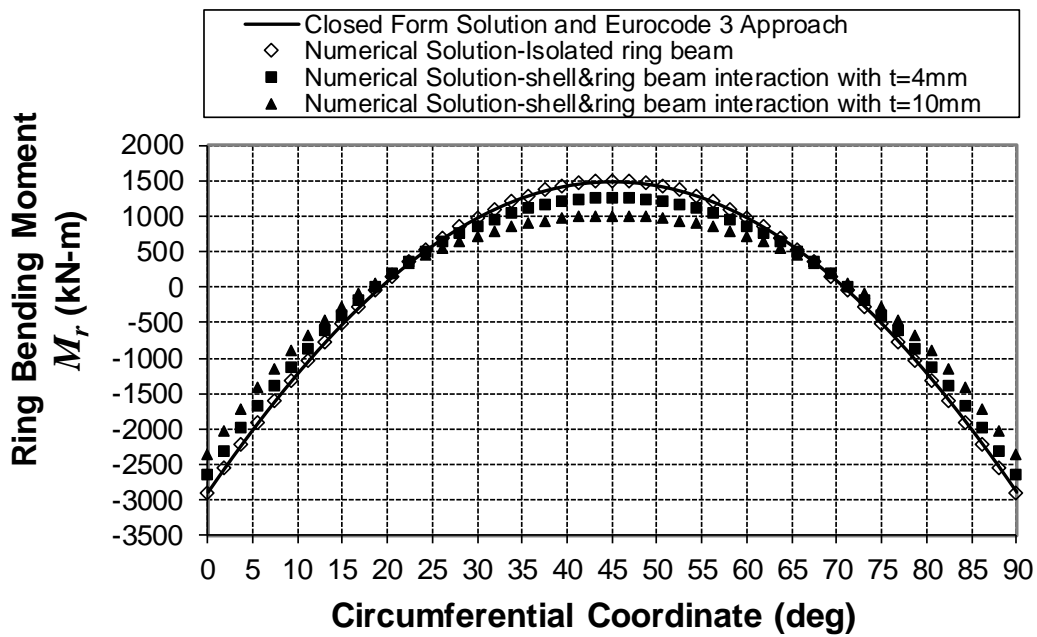


Figure 3.3 Comparison of closed form solution with numerical solutions for the ring beam bending moment (M_r)

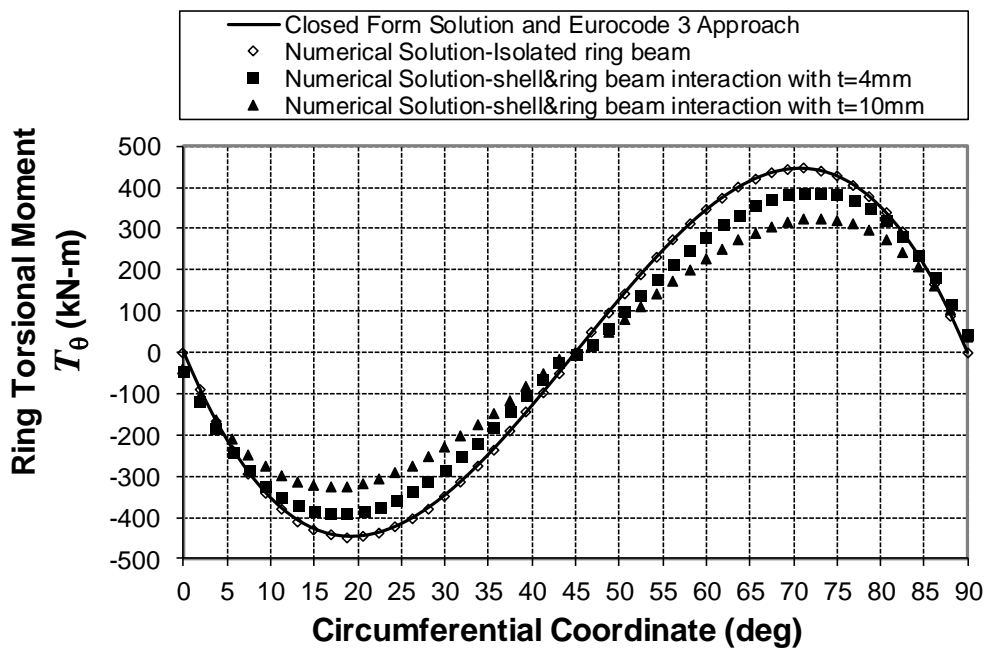


Figure 3.4 Comparison of closed form solution with numerical solution for the ring beam torsional moment (T_θ)

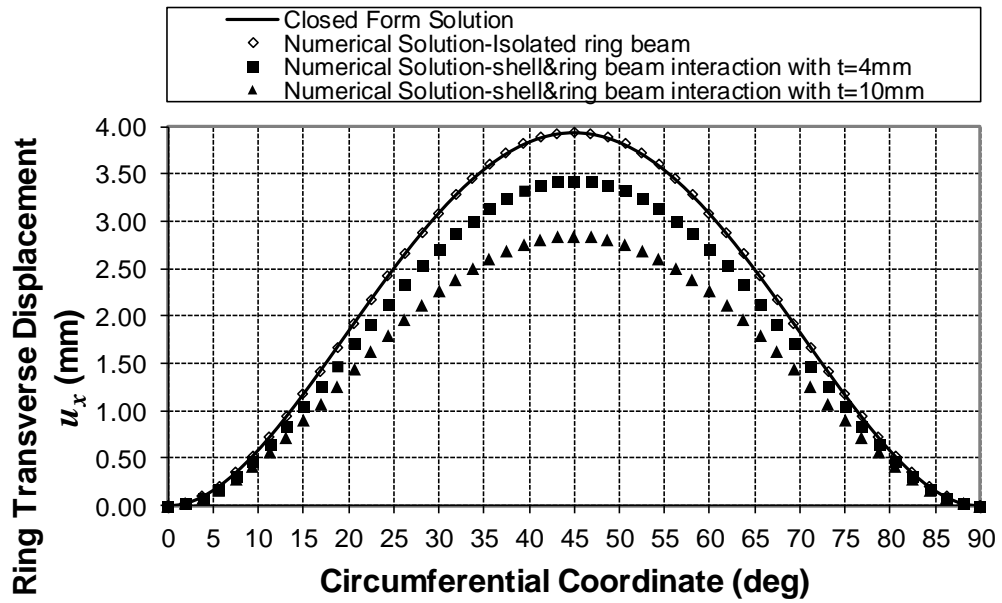


Figure 3.5 Comparison of closed form solution with numerical solutions for the ring beam transverse displacement (u_x)

3.3. Effect of Ring Beam Stiffness on Ring Beam Stress Resultants and Displacements

The interaction between the ring beam and the silo shell depends strongly on the stiffness of each component. Similarly, the redistribution of the support forces is directly related to the stiffness of the ring beam relative to the stiffness of the cylindrical shell. A ring beam stiffness ratio (ψ) was developed by Rotter (1985) and further developed and verified by Topkaya and Rotter (2011). Derivation of ring beam stiffness ratio was presented in Chapter 2. The relationship between the ring beam stress resultants and the ring beam stiffness ratio was explored in this section. Finite element parametric study was conducted to correlate the ring beam stiffness ratio with the ring beam stress resultants and displacements.

3.3.1. Computational assessment of the ring beam stiffness ratio

Finite element analyses were chiefly used to explore the variation of the bending moment in the radial direction, torsional moment and transverse displacement of the ring beam as a function of stiffness ratio in this study. The finite element models described earlier were adopted, with geometries defined as radius $R = 3000$ and 4500 mm, thickness $t = 4, 6, 8$ and 10 mm, shell heights of $6000, 8000, 10000, 15000$ and 18000 mm, with all cylindrical shells having the same number of supports $n = 4$, since this is the commonest arrangement in practice. A total of 40 combinations were adopted for the shell geometries with 30 different square hollow ring beam geometries resulting in 1200 analysis cases. For the ring beams wall heights of $400, 450, 500, 550,$ and 600 mm and wall thicknesses of $20, 30, 40, 50, 60,$ and 70 mm were considered. Different cross-section dimensions provide variations in the cross section properties.

In each analysis, the bending moment in the radial direction ($M_{r,max}$) at the support and at the mid-span, the maximum torsional moment ($T_{\theta,max}$) and the maximum displacement in the transverse direction ($u_{x,max}$) of the ring beam were recorded. A reference bending moment ($M_{r,ref}$) at the support and mid-span, reference torsional moment ($T_{\theta,ref}$) and reference transverse displacement ($u_{x,ref}$) were determined from the above closed form solutions. The normalised differences between the calculated and reference values $(M_{r,ref} - M_{r,max})/M_{r,ref}$, $(T_{\theta,ref} - T_{\theta,max})/T_{\theta,ref}$ and $(u_{x,ref} - u_{x,max})/u_{x,ref}$ are plotted in Figures 3.6, 3.7, 3.8 and 3.9 as a function of the stiffness ratio ψ respectively.

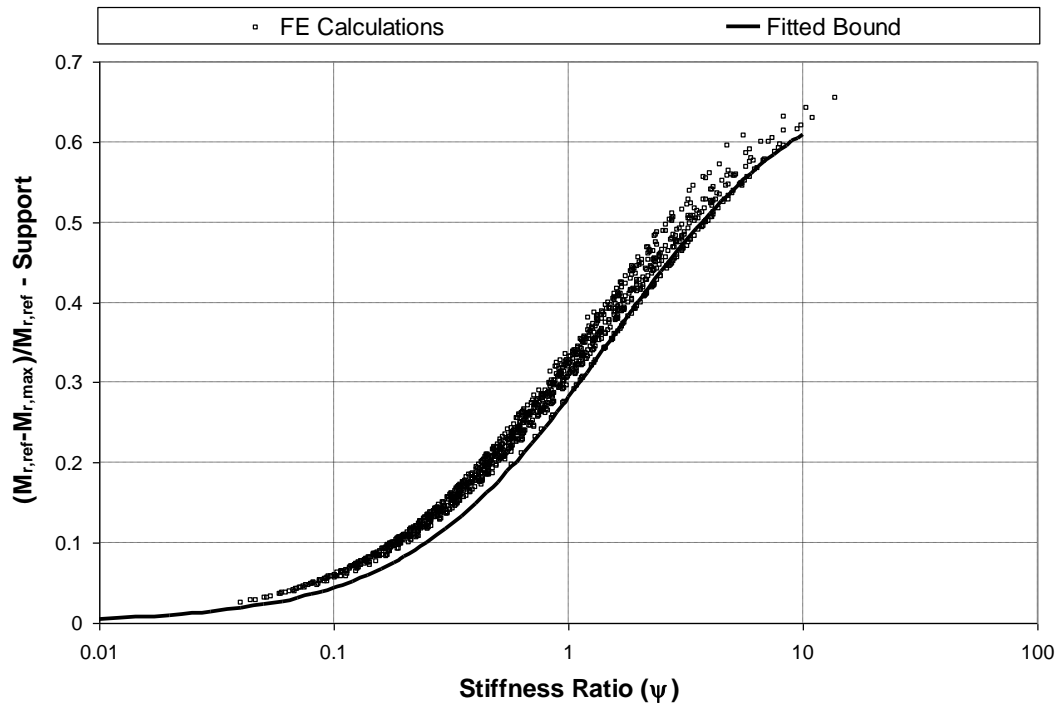


Figure 3.6 Assessment of the ring stiffness ratio (ψ) for the bending moment in the radial direction (support moment)

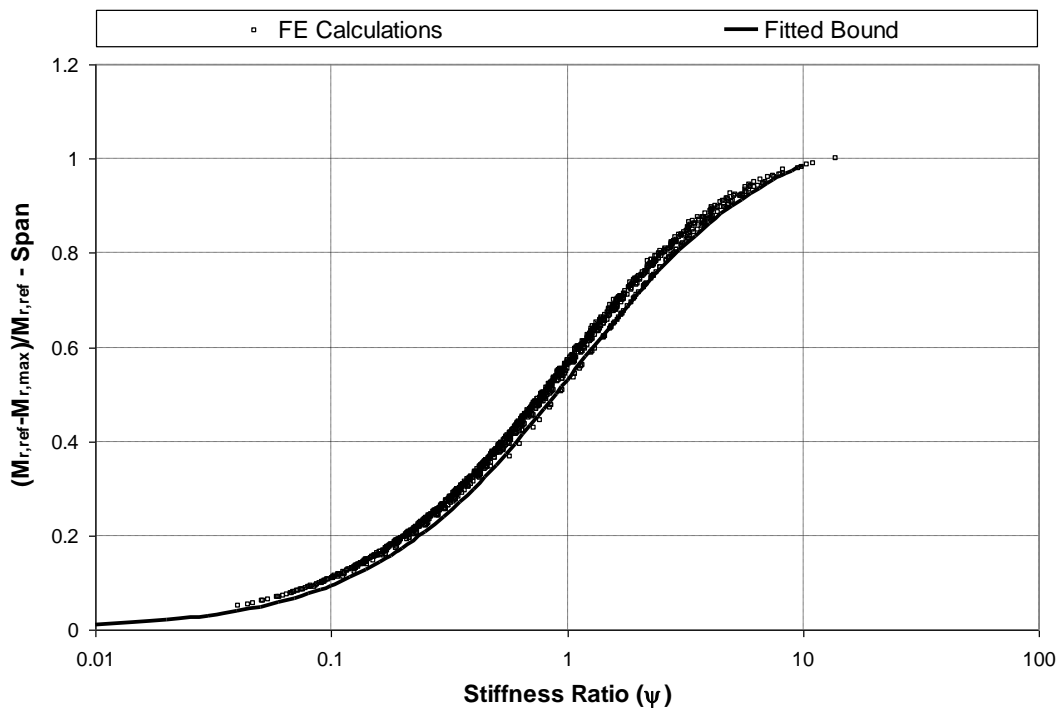


Figure 3.7 Assessment of the ring stiffness ratio (ψ) for the bending moment in the radial direction (span moment)

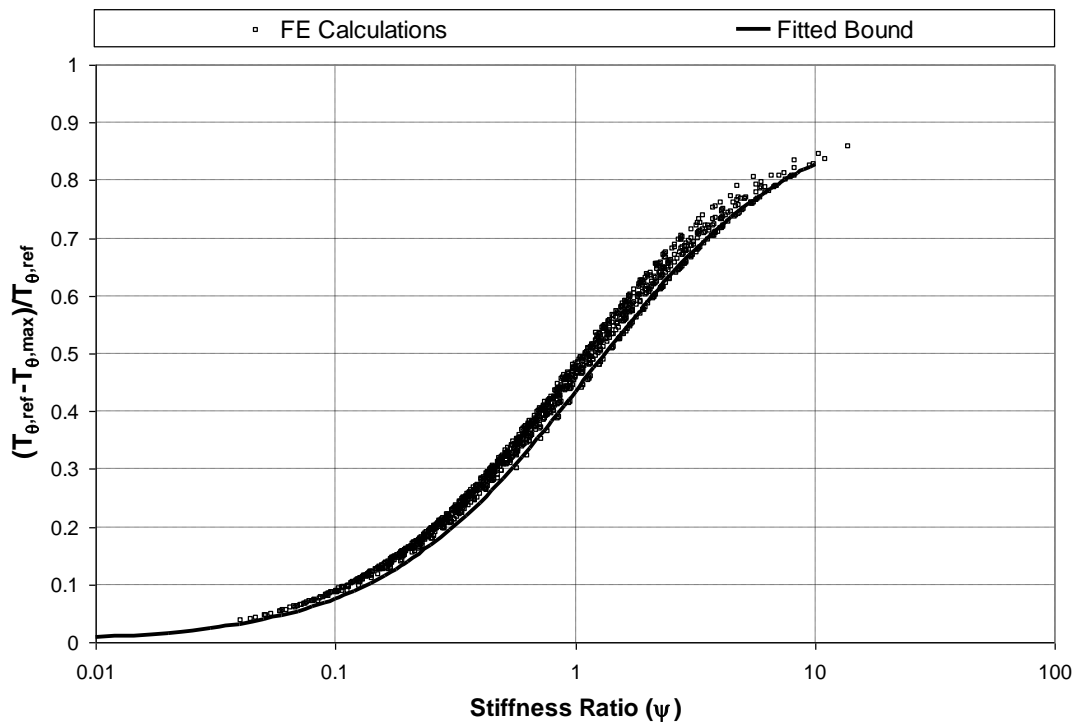


Figure 3.8 Assessment of the ring stiffness ratio (ψ) for the torsional moment

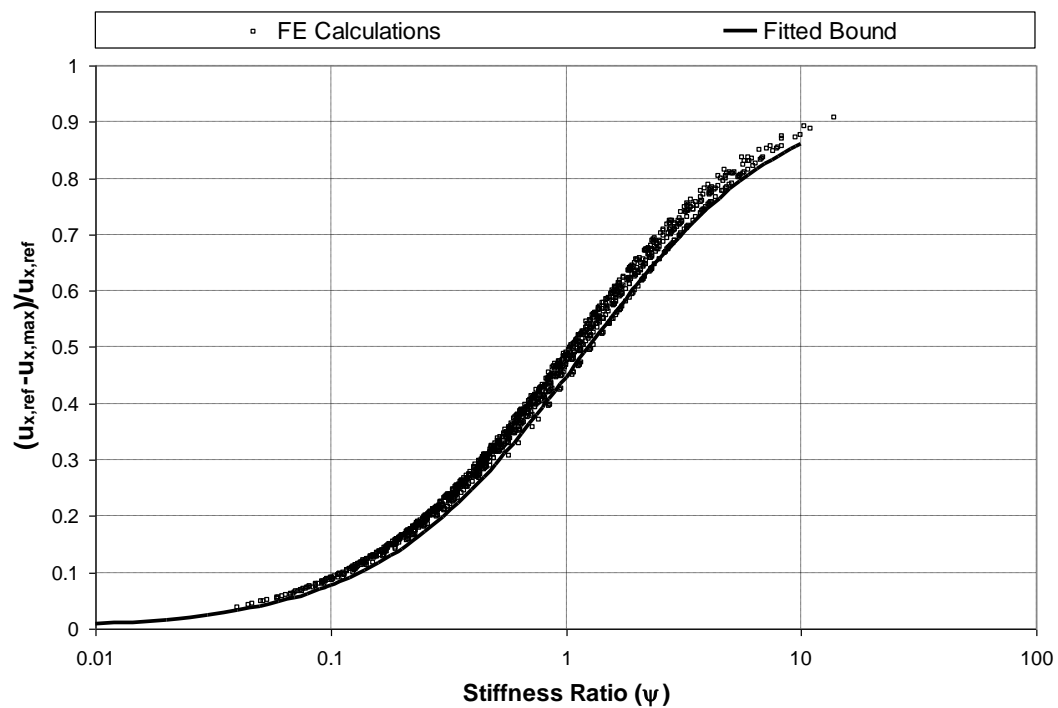


Figure 3.9 Assessment of the ring stiffness ratio (ψ) for the transverse displacement

The results indicate that the stiffness ratio (ψ) clearly captures the trend of the data. The data points for bending moment at the support and mid-span, torsional moment and transverse displacement each fall within a rather narrow band. The results show that the reduction below the isolated ring beam values caused by the shell structure can be directly related to the ring beam stiffness ratio. The reduction in mid-span bending moment is much more pronounced when compared with the support moment.

The following relationships provide conservative bounds which can be used at the design stage to find out the reduction in response quantities.

$$\frac{(M_{r,ref} - M_{r,max})}{M_{r,ref}} = \frac{0.7\psi}{1.49 + \psi} \quad \text{for support moment} \quad (3.19)$$

$$\frac{(M_{r,ref} - M_{r,max})}{M_{r,ref}} = \frac{1.09\psi}{1.06 + \psi} \quad \text{for span moment} \quad (3.20)$$

$$\frac{(T_{\theta,ref} - T_{\theta,max})}{T_{\theta,ref}} = \frac{0.92\psi}{1.124 + \psi} \quad \text{for torsional moment} \quad (3.21)$$

$$\frac{(u_{x,ref} - u_{x,max})}{u_{x,ref}} = \frac{0.96\psi}{1.15 + \psi} \quad \text{for transverse displacement} \quad (3.22)$$

CHAPTER 4

REQUIREMENTS FOR INTERMEDIATE RING STIFFENERS ON DISCRETELY SUPPORTED SHELLS

4.1. Behavior of Cylindrical Shells with Intermediate Ring Stiffeners

One alternative method of achieving uniform axial membrane stresses is to use an intermediate ring stiffener with a flexible ring beam as shown in Figure 4.1 (i.e. double ring arrangement of Figure 1.1f). Greiner (1983, 1984), Öry *et al.* (1984) and Öry and Reimerdes (1987) showed that an intermediate ring stiffener can be very effective in reducing the circumferential non-uniformity of axial stresses in the shell. Studies conducted by these researchers identified the variation of the axial membrane stress distributions up the height of the shell. It was shown that an intermediate ring stiffener can achieve a dramatic decrease in the peak axial membrane stress, producing a more uniform stress state above the intermediate ring. Recently Topkaya and Rotter (2014) showed that there is an *ideal location* for an intermediate ring stiffener, such that the axial membrane stress above this ring is circumferentially completely uniform. The ideal location is identified by the height H_I above the ring beam, defined as the vertical distance between the top of the ring beam and the centre of the intermediate ring stiffener as shown in Figure 4.1. This was determined analytically and is expressed in terms of basic geometric variables as follows (Topkaya and Rotter (2014)):

$$H_I = \sqrt{12(1+\nu)} \frac{R}{n} \quad (4.1)$$

For the case where $\nu = 0.3$, Equation 4.1 simplifies further into:

$$H_I = 3.95 \frac{R}{n} \approx \frac{4R}{n} \quad (4.2)$$

Equation 4.2 clearly indicates that the ideal ring location depends on only two geometric parameters: the radius R of the cylindrical shell and the harmonic number, which is closely related to the number of supports n . The height of the ideal ring is thus directly proportional to the radius, which identifies an aspect ratio for the lower section, and inversely proportional to the number of supports. It may be noted that each additional term of the harmonic series indicates an ideal height that is lower than this, so all terms are, in a sense, covered by this provision.

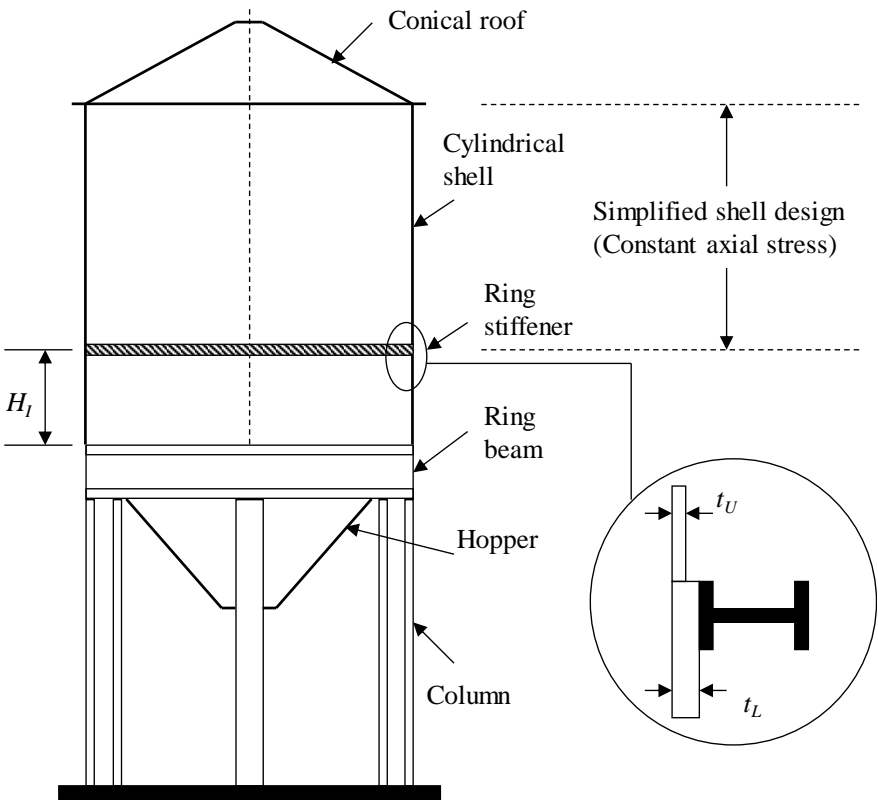


Figure 4.1 Typical circular planform silo

In cases where a shell with large radius rests on a few supports, the ideal location can be quite high and the option of placing the intermediate ring stiffener below the ideal height may provide a viable solution. A cylindrical shell with its axis vertical and supported on a single ring beam at the base (Figure 4.1) was analyzed using the finite element method by Topkaya and Rotter (2014) to study the effects of introducing

an intermediate stiffener at different heights. The steel silo structure analyzed had a cylinder radius of 3000 mm and a height of 10000 mm with a constant thickness of 6 mm. The cylinder had a ring beam at its lower boundary which rested on 4 equally spaced discrete stiff supports. The ring beam had an I-shaped cross section with a web height and thickness of 500 mm and 10 mm, respectively. The flange width and thickness of the ring beam were 200 mm and 15 mm respectively. The ring beam at the lower boundary of the shell was deliberately selected as of relatively low stiffness to ensure that a high stress amplification ratio ζ would be produced. The cylindrical shell was loaded uniformly from the top with a unit value of axial stress. Three cases were studied where the first case represents no intermediate ring, the second case represents an intermediate ring placed at half of the ideal height ($H_i/2$) and the third case represents an intermediate ring placed at the ideal height (H_i) (actually at $4R/n$, which is just above the strict ideal value). The axial membrane stresses calculated in the finite element analyses were normalized by the applied axial stress (=1.0).

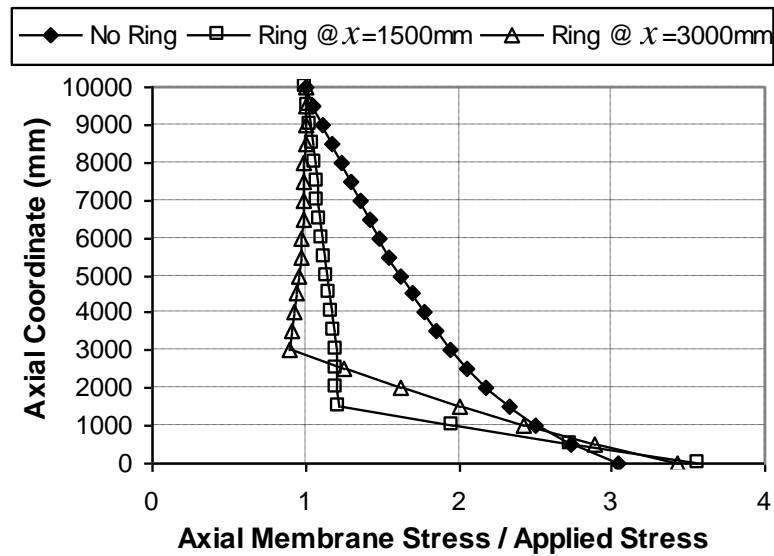


Figure 4.2 Variation of normalized axial membrane stress throughout the shell

The stress variations down the height on the generator above the support ($\theta=0$) are shown in Figure 4.2. For the case of a shell without an intermediate ring, the axial membrane stress immediately above the ring is just over 3 times the applied stress. On

this shell generator, the axial membrane stress progressively reduces from just above the ring to the top of the shell and the entire shell is involved in this redistribution. When the stiffener is placed at 1500 mm above the shell base ($H_I/2$), the normalized axial stress above the stiffener is reduced from 2.32 to 1.21, but when it is placed at 3000 mm (H_I) this stress is reduced from 1.95 to 0.89, which is a slight overcompensation, since the value 1.0 corresponds to a completely circumferentially uniform axial stress.

The circumferential variation of the normalized stresses is shown in Figures 4.3 through 4.5, where the pattern at 3 different levels is shown: at the base of the cylinder ($x=0$) (the top surface of the ring), at half of the ideal height ($x=1500$ mm) and at the ideal height ($x=3000$ mm). Naturally, the axial stresses vary around the circumference and the variation declines as the peak membrane stress is progressively redistributed. The intermediate stiffener at $x=1500$ mm forces the stresses at and above this level to be fairly uniform (Figure 4.4), with the normalized stress deviating from uniformity by only $\pm 20\%$ (between 1.2 and 0.8). The intermediate stiffener at $x=3000$ mm (Figure 4.5) also forces the stresses at this level to be fairly uniform, but actually overcompensates for the effect, causing a dip to 0.89 above the support and a rise to 1.07 away from it, producing a deviation from uniformity of around $\pm 10\%$.

When a stiffener is placed at the ideal height, it may arrest the circumferential non-uniformity of the axial stresses, rendering the zone above it uniformly stressed. Thus, an intermediate ring stiffener could be a viable design option to render the axial stresses above it quite uniform. The shell wall above such a stiffener can then be designed for simple uniform axial compression, requiring only a thin wall. The shell below this point would need to be thicker to resist local buckling, but this is a less demanding requirement because the shell wall thickness normally increases greatly towards the base and often has more buckling capacity than is necessary.

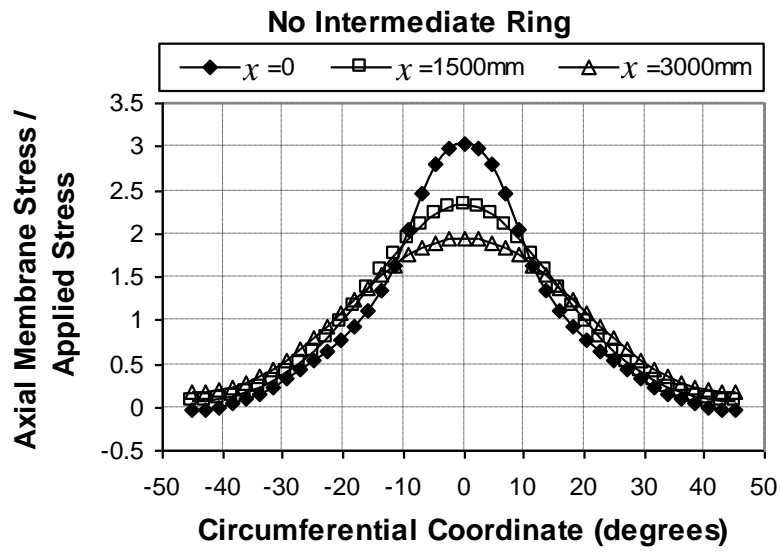


Figure 4.3 Normalized axial membrane stress at various levels: Variation around the circumference from the support to midspan: no intermediate ring

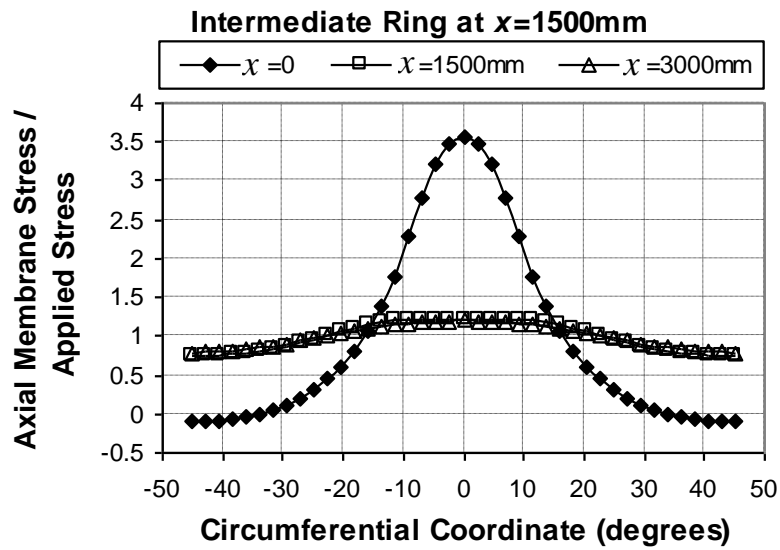


Figure 4.4 Normalized axial membrane stress at various levels: Variation around the circumference from the support to midspan: intermediate ring 1500 mm above the base ring

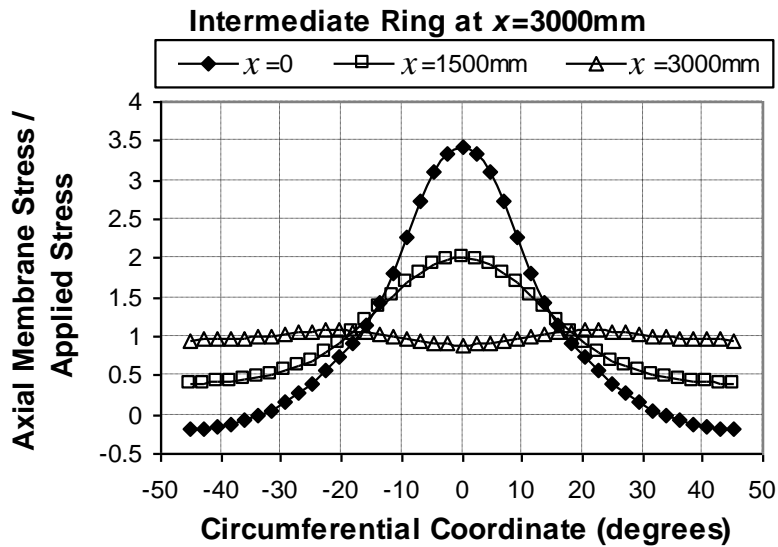


Figure 4.5 Normalized axial membrane stress at various levels: Variation around the circumference from the support to midspan: intermediate ring 3000 mm above the base ring

A ring at a lower location still has a significant effect on the circumferential variation of the axial stresses, but it does not render them uniform. As mentioned before, placing an intermediate ring stiffener below the ideal height can provide an economical solution for silos with a large radius and resting on a few supports.

The intermediate ring stiffener is expected to have sufficient strength and stiffness to fulfil its function properly. The key requirement for this intermediate ring stiffener is to prevent or significantly control the circumferential displacements of the cylindrical shell at that level. If the ring stiffener has inadequate stiffness, the circumferential uniformity of the axial stresses above it is not achieved. Furthermore, there is an interaction between the cylindrical shell and the ring stiffener which causes stress resultants to develop in the ring. These stress resultants could potentially cause failure of the ring stiffener either by yielding or by instability.

This study explores strength and stiffness requirements for intermediate ring stiffeners placed at or below the ideal location. A general shell and ring combination

is studied using the membrane theory of shells to identify the membrane shear forces induced in the shell by the ring. These forces are then considered as loads applied to the intermediate ring stiffener. Vlasov's curved beam theory (1961) is used to derive closed form expressions for the variation of the stress resultants around the circumference to obtain a suitable strength design criterion for the stiffener. A relative stiffness criterion for the ring is then devised by considering the ratio of the circumferential stiffness of the cylindrical shell to that of the intermediate ring. Using the same loads on the ring as for the strength determination, the circumferential displacements of the ring and the shell are derived. A simple algebraic expression is then developed to determine this relative stiffness. These analytical studies are then verified using a wide range of finite element analyses to identify suitable limiting values for use in practical design.

4.2. Stress and displacement transfer into intermediate ring stiffeners

Topkaya and Rotter (2014) determined the ideal location for an intermediate ring stiffener using the membrane theory of shells (Rotter (1987), Timoshenko and Woinowsky-Krieger (1959), Flügge (1973), Seide (1975), Ventsel and Krauthammer (2001)). The loading on intermediate ring stiffeners can be obtained by solving for the reactions on the shell produced by a stiffener infinitely stiff in its own plane.

All deformations, loading and stress resultants can be expressed in terms of a harmonic series around the circumference (Timoshenko and Woinowsky-Krieger (1959), Flügge (1973), Novozhilov (1959), Kraus (1967), Calladine (1983)) in order to solve the governing differential equations. In the case of discrete supports, the rapid decay in the effect of higher terms (Rotter (1990)) means that the fundamental harmonic term of the column support force is sufficient to study the requirements of the ring stiffener, so the support force can be represented by Equation 2.1.

The cylindrical shell is here separated into two parts: an upper shell and a lower shell with the intermediate ring at their junction, as shown in Figure 4.6, which also

indicates the chosen boundary conditions. The lower shell, of height H_L , is subjected to the fundamental harmonic of the column support. The upper shell is assumed to be unloaded on its upper boundary and restrained against circumferential displacements by a ring. Topkaya and Rotter (2014) demonstrated that the interface between the lower shell and upper shell will be free of both axial stress and axial displacements if an intermediate ring is placed at the ideal location. When the intermediate ring is placed below the ideal location some level of axial stress non-uniformity is present in the upper shell segment. In addition, the axial displacements no longer vanish, so the nonzero axial displacements can also be found at this interface.

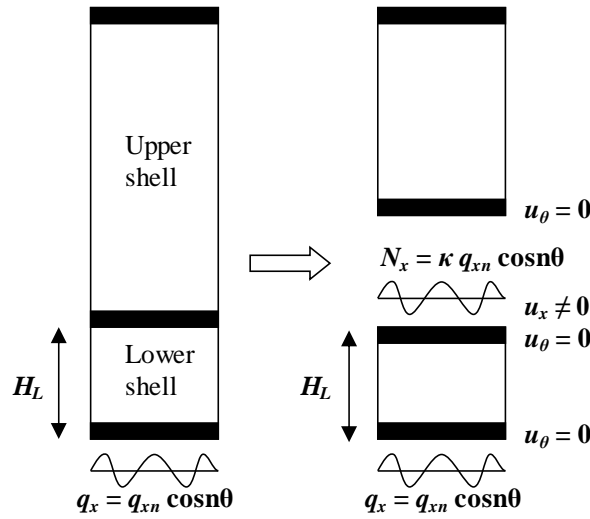


Figure 4.6 Boundary conditions used in closed-form solution

Considering the cylindrical shell element shown in Figure 4.7, the equilibrium equations are:

$$\frac{\partial N_x}{\partial x} + \frac{1}{R} \frac{\partial N_{x\theta}}{\partial \theta} + p_x = 0 \quad (4.3)$$

$$\frac{\partial N_{x\theta}}{\partial x} + \frac{1}{R} \frac{\partial N_\theta}{\partial \theta} + p_\theta = 0 \quad (4.4)$$

$$N_\theta + R p_n = 0 \quad (4.5)$$

where N_x , N_θ , $N_{x\theta}$ = axial, circumferential and shear membrane stress resultants respectively; and p_x , p_θ , p_n = external distributed pressures in the axial, circumferential and radial directions respectively.

The strain displacement and constitutive relationships can be written as:

$$\varepsilon_x = \frac{\partial u_x}{\partial x} = \frac{1}{Et}(N_x - \nu N_\theta) \quad (4.6)$$

$$\varepsilon_\theta = \frac{1}{R} \frac{\partial u_\theta}{\partial \theta} - \frac{u_r}{R} = \frac{1}{Et}(N_\theta - \nu N_x) \quad (4.7)$$

$$\gamma_{x\theta} = \frac{1}{R} \frac{\partial u_x}{\partial \theta} + \frac{\partial u_\theta}{\partial x} = \frac{1}{Gt} N_{x\theta} = \frac{2(1+\nu)}{Et} N_{x\theta} \quad (4.8)$$

where u_x , u_θ , u_r = displacements in the axial, circumferential and radial directions respectively; ε_x , ε_θ = strains in the axial and circumferential directions respectively; $\gamma_{x\theta}$ = shear strain; ν = Poisson's ratio; E = modulus of elasticity; G = shear modulus; and t = thickness of the shell.

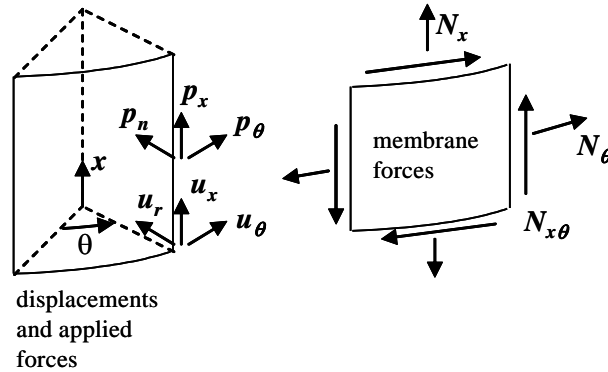


Figure 4.7 Loading, displacements and stress resultants in an element of the cylindrical shell

The circumferential membrane stress resultant is directly obtained from Equation 4.5 as:

$$N_\theta = -R p_n \quad (4.9)$$

In the lower shell, Equations 4.3 and 4.4 may be solved sequentially by integrating in the x direction to obtain:

$$N_{x\theta} = -\int \left(p_\theta + \frac{1}{R} \frac{\partial N_\theta}{\partial \theta} \right) dx + f_1(\theta) \quad (4.10)$$

$$N_x = -\int \left(p_x + \frac{1}{R} \frac{\partial N_{x\theta}}{\partial \theta} \right) dx + f_2(\theta) \quad (4.11)$$

where $f_1(\theta), f_2(\theta) =$ unknown functions of θ to be determined from two boundary conditions.

The general solution for the displacements of the shell may then be found as:

$$Et u_x = \int (N_x - \nu N_\theta) dx + f_3(\theta) \quad (4.12)$$

$$Et u_\theta = 2(1 + \nu) \int N_{x\theta} dx - \frac{Et}{R} \int \frac{\partial u_x}{\partial \theta} dx + f_4(\theta) \quad (4.13)$$

$$Et u_r = Et \frac{\partial u_\theta}{\partial \theta} - R(N_\theta - \nu N_x) \quad (4.14)$$

where $f_3(\theta), f_4(\theta) =$ additional functions to satisfy the boundary conditions on the edges $x = \text{constant}$.

where there is no surface loading on the shell ($p_x = p_\theta = p_n = 0$), Equations 4.9, 4.10 and 4.11 give:

$$N_\theta = 0 \quad (4.15)$$

$$N_{x\theta} = f_1(\theta) \quad (4.16)$$

$$N_x = -\frac{1}{R} \int \left(\frac{d}{d\theta} f_1(\theta) \right) dx + f_2(\theta) = -\frac{x}{R} \left(\frac{d}{d\theta} f_1(\theta) \right) + f_2(\theta) \quad (4.17)$$

At the base, $x = 0$, the axial membrane stress resultant is chosen as the fundamental harmonic of the discrete support, $N_x = -q_{xn} \cos n\theta$ (Equation 2.1), leading to:

$$f_2(\theta) = -q_{xn} \cos n\theta \quad (4.18)$$

When the ring is placed at the ideal location, the axial stress vanishes at this height ($N_x = 0$), but when the ring is placed below the ideal location non-uniform axial stresses will still be present. As shown in Figure 4.6, a certain proportion of the applied axial membrane stress resultant is assumed to be present at the interface. The ratio of the axial membrane stress resultant at the interface to the applied fundamental harmonic of the column support is here termed κ . Topkaya and Rotter (2014) explored the magnitudes of axial membrane stress resultants that remain at this interface using many linear finite element analyses. The location of the intermediate ring, shell radius, number of supports and shell thickness ratios ($g = t_U/t_L$ where t_U and t_L are the thicknesses of the upper and lower shells respectively) were considered as the primary variables. Figure 4.8 shows the variation of the ratio of axial membrane stress resultants for the case of $g = 0.5$. The following convenient lower and upper bound expressions can be developed to represent the data points:

$$\kappa = \frac{N_x}{q_{xn}} = 1 + g \left(\frac{H_L}{H_I} \right) - (1 + g) \left(\frac{H_L}{H_I} \right)^m \quad (4.19)$$

with

$$m = 0.5g(2.34 - g) \text{ for upper bound} \quad (4.20)$$

$$m = 0.4g(2.34 - g) \text{ for lower bound} \quad (4.21)$$

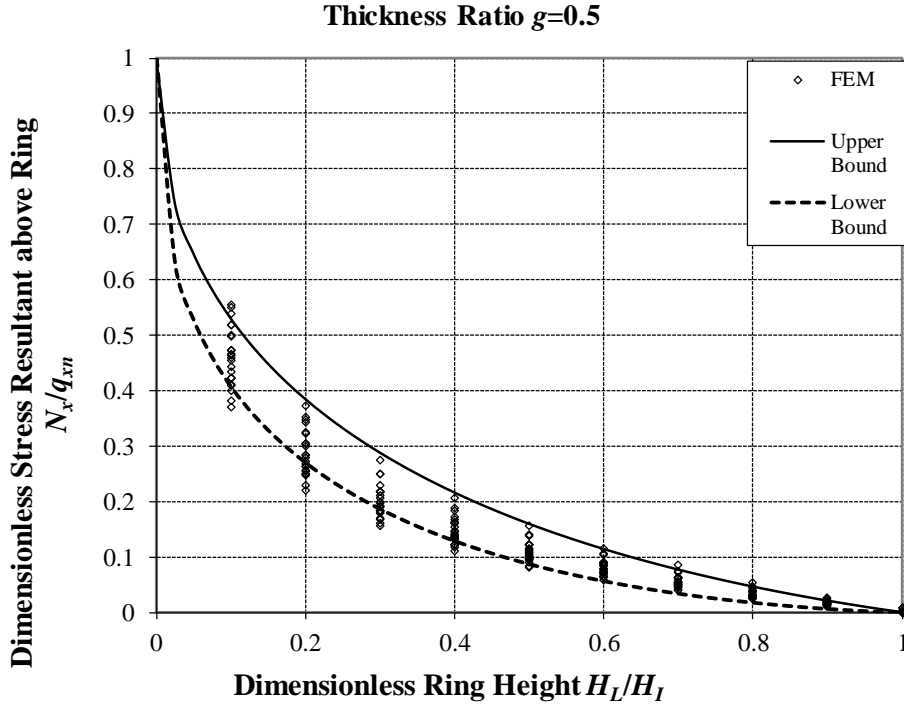


Figure 4.8 Variation of axial stress resultant for various intermediate ring heights with upper to lower shell thickness ratio $g = 0.5$

Considering an axial stress resultant $N_x = -\kappa q_{xn} \cos n\theta$ at the ring ($x = H_L$) leads to the following:

$$f_1(\theta) = -(1 - \kappa) \frac{R}{H_L n} q_{xn} \sin n\theta \quad (4.22)$$

Inserting Equations 4.12, 4.16 and 4.17 into Equation 4.13 yields the circumferential displacement as:

$$Et u_\theta = \frac{x^3}{6R^2} \left(\frac{d^2}{d\theta^2} f_1(\theta) \right) - \frac{x^2}{2R} \left(\frac{d}{d\theta} f_2(\theta) \right) + x \left[2(1 + \nu) f_1(\theta) - \frac{1}{R} \left(\frac{d}{d\theta} f_3(\theta) \right) \right] + f_4(\theta) \quad (4.23)$$

At $x = 0$ and $x = H_L$, the boundary condition of zero circumferential displacements, $u_\theta = 0$, yields the two results:

$$f_4(\theta) = 0 \quad \text{and} \quad f_3(\theta) = \left(\frac{(2 + \kappa)H_L}{6} + \frac{2(1 + \nu)(1 - \kappa)R^2}{H_L n^2} \right) q_{,xn} \cos n\theta \quad (4.24)$$

The axial displacements can be expressed in terms of the functions $f_1(\theta)$, $f_2(\theta)$ and $f_3(\theta)$ as:

$$Et u_x = -\frac{x^2}{2R} \left(\frac{d}{d\theta} f_1(\theta) \right) + x f_2(\theta) + f_3(\theta) \quad (4.25)$$

Inserting Equations 4.18, 4.22 and 4.24 into Equation 4.25 yields:

$$u_x = \frac{q_{,xn} \cos n\theta}{Et} \left[\frac{(1 - \kappa)x^2}{2H_L} - x + \frac{(2 + \kappa)H_L}{6} + \frac{2(1 + \nu)(1 - \kappa)R^2}{H_L n^2} \right] \quad (4.26)$$

When the intermediate ring is placed at the ideal height the axial displacements and axial stress resultants at the interface vanish. The condition of $\kappa = 0$ with $u_x = 0$ at $x = H_L = H_I$ leads to the ideal location of the intermediate ring stiffener, previously expressed in Equation 4.1.

In the solution presented above, rigid boundary conditions were assumed at the location of the intermediate ring. A finite shear membrane stress resultant $N_{x\theta}$ is produced when the intermediate ring prevents circumferential displacements u_θ at the interface. The reactions in the shell at this boundary can be treated as the loading exerted on the intermediate ring. Combining Equations 4.16 and 4.22 gives the following expression for the shear membrane stress resultant

$$N_{x\theta} = -(1 - \kappa) \frac{R}{H_L n} q_{,xn} \sin n\theta \quad (4.27)$$

Equation 4.27 shows that the intermediate ring is subjected to a sinusoidally varying circumferential line load in its own plane, whose magnitude is directly related to the discrete support force q_{xn} .

Similarly axial displacements are produced at the interface when the ring is placed below the ideal location. These axial displacements depend on the relative stiffness of the lower shell and the intermediate ring. In general, the shell segment is very stiff in its own plane. The out-of-plane stiffness of the intermediate ring is quite low compared with the axial stiffness of the shell, so it is reasonable to assume initially that the intermediate ring has a negligible effect on the axial displacements that are induced at the interface. The displacements obtained from the solution of the lower shell segment can then be directly applied to the intermediate ring stiffener. The displacements at the interface ($x = H_L$) can be found from Equation 4.26 as:

$$u_x = \left[\frac{12(1+\nu)(1-\kappa)R^2 - H_L^2 n^2 (1+2\kappa)}{6EtH_L n^2} \right] q_{xn} \cos n\theta \quad (4.28)$$

Equation 4.28 indicates that the intermediate ring experiences cosinusoidally varying out-of-plane deformations whose magnitude is directly related to the discrete support force q_{xn} . The effect of the out-of-plane stiffness of the intermediate ring on these displacements will be explored below.

4.3. Algebraic Closed-form Solution for the Stress Resultants in the Intermediate Ring Stiffener – Strength Criterion

4.3.1. Derivation of stress resultants – In plane behavior

The Vlasov curved beam differential equations (Vlasov (1961), Heins (1975)) were used to study the response of the intermediate ring stiffener. In-plane and out-of-plane behaviors were treated separately. In general, the behavior of a curved beam is governed by a series of differential equations. The equilibrium equations were first

derived for the curved beam element shown in Figure 2.2, where three orthogonal internal forces and three internal moments develop at each cross-section. The six basic equilibrium equations were expressed in Equation 2.2 through 2.7. The six basic equilibrium equations can be reduced to three differential relationships. The differential equation for bending of the ring in its own plane can be uncoupled from the other two. For the case where the only loading is q_θ (i.e. $q_r = q_x = m_r = m_\theta = m_x = 0$), the two coupled differential equations of equilibrium can be expressed as:

$$\frac{1}{R} \left[\frac{\partial T_\theta}{\partial \theta} - M_r \right] = 0 \quad (4.29)$$

$$\frac{1}{R^2} \left[\frac{\partial^2 M_r}{\partial \theta^2} + \frac{\partial T_\theta}{\partial \theta} \right] = 0 \quad (4.30)$$

The uncoupled differential equation can be expressed as follows:

$$\frac{1}{R^2} \left[\frac{\partial^3 M_x}{\partial \theta^3} + \frac{\partial M_x}{\partial \theta} \right] + q_\theta = 0 \quad (4.31)$$

Direct solution of Equation 2.5 and simultaneous solution of Equations 4.29 and 4.30 reveal the following relationships for in-plane loading:

$$M_r(\theta) = 0 \quad T_\theta(\theta) = 0 \quad Q_x(\theta) = 0 \quad (4.32)$$

These relationships indicate that the torsional moment in the ring, the bending moment in the radial direction and the transverse shear force vanish for the simple loading case of q_θ alone.

The shear membrane stress resultant expressed in Equation 4.27 can be adopted for the loading on the intermediate ring (i.e. $q_\theta = N_{x\theta}$) leading to the following relationships by solving Equation 4.31:

$$M_x(\theta) = M_{x,\max} \cos n\theta \quad M_{x,\max} = (1 - \kappa) \frac{q_{xn}}{H_L} \frac{R^3}{n^2(n^2 - 1)} \quad (4.33)$$

Inserting Equation 4.33 into Equation 2.6 reveals the radial shear force Q_r :

$$Q_r(\theta) = Q_{r,\max} \sin n\theta \quad Q_{r,\max} = (1 - \kappa) \frac{q_{xn}}{H_L} \frac{R^2}{n(n^2 - 1)} \quad (4.34)$$

Inserting Equation 4.34 into Equation 2.2 reveals the circumferential tension Q_θ :

$$Q_\theta(\theta) = Q_{\theta,\max} \cos n\theta \quad Q_{\theta,\max} = -(1 - \kappa) \frac{q_{xn}}{H_L} \frac{R^2}{(n^2 - 1)} \quad (4.35)$$

Equations 4.33, 4.34 and 4.35 indicate that the intermediate ring stiffener is subjected to circumferential and shear forces in the plane of the ring and bending about the axis transverse to the plane of the ring. The intermediate ring is at ideal location for the case where $H_L = H_I$ and $\kappa \rightarrow 0$.

4.3.2. Derivation of stress resultants – Out-of-plane behavior

The depth of a typical intermediate ring stiffener is small when compared with the typical radii of silo shell. Therefore, it is meaningful and convenient to neglect any offset that would be produced by the geometric centroid of the intermediate ring stiffener and the axis of the silo shell. The complexity of the offset of a practical ring makes the analysis significantly more complicated so this has been omitted for the sake of simplicity needed in practical design calculations. The out-of-plane displacements of the intermediate ring are here treated as equal to the axial displacements of the lower shell at the interface. There is a complex interaction between the shell and the intermediate ring stiffener. The amount of rotations ϕ around a circumferential axis that take place at the location of the intermediate ring stiffener must be known in

advance to fully extract the stress resultants. Preliminary finite element analysis revealed that it would be conservative to neglect these rotations (i.e. $\phi = 0$). Because these rotations are not known in advance or obtained as a part of the solution, the individual contributions of uniform torsion and warping torsion to the torsional moment in the ring cannot be determined.

Inserting Equation 4.28 into Equation 2.12 and considering $\phi = 0$, the following relationship can be derived for bending moment in the ring about a radial axis M_r :

$$M_r(\theta) = M_{r,\max} \cos n\theta \quad M_{r,\max} = \frac{I_r \left[12(1+\nu)(1-\kappa)R^2 - H_L^2 n^2 (1+2\kappa) \right]}{6H_L R^2 t} q_{xn} \quad (4.36)$$

Inserting Equation 4.36 into Equation 2.7 and considering $m_\theta = 0$, reveals the torsional moment in the ring T_θ :

$$T_\theta(\theta) = T_{\theta,\max} \sin n\theta \quad T_{\theta,\max} = \frac{I_r \left[12(1+\nu)(1-\kappa)R^2 - H_L^2 n^2 (1+2\kappa) \right]}{6H_L n R^2 t} q_{xn} \quad (4.37)$$

Inserting Equations 4.36 and 4.37 into Equation 2.5 reveals the shear force in the ring in the transverse direction Q_x :

$$Q_x(\theta) = Q_{x,\max} \sin n\theta \quad Q_{x,\max} = \frac{-I_r (n^2 - 1) \left[12(1+\nu)(1-\kappa)R^2 - H_L^2 n^2 (1+2\kappa) \right]}{6H_L n R^3 t} q_{xn} \quad (4.38)$$

Equations 4.36, 4.37 and 4.38 indicate that the intermediate ring stiffener is subjected to transverse shear forces, bending about a radial axis and torsional moments due to the imposed displacements by the axially stiff lower shell segment. Equations 4.36, 4.37 and 4.38 result in $M_r(\theta) = 0$, $T_\theta(\theta) = 0$, $Q_x(\theta) = 0$ for the case of $H_L = H_t$ and $\kappa \rightarrow 0$.

4.4. Assessment of stress resultants

When the intermediate ring is placed at the ideal location the only stress resultants are M_x , Q_r and Q_θ . Equations 4.33, 4.34 and 4.35 indicate that the maximum in-plane bending moment and circumferential force occur at the same location. The shear stress resultant is at its maximum at locations where the other stress resultants vanish. Placing an intermediate ring below the ideal height produces the additional stress resultants M_r , T_θ and Q_x . The maximum out-of-plane bending moment occurs at same locations where the in-plane bending moment and circumferential force are also at their maxima. Therefore, the strength requirement for the intermediate ring demands a check of the cross-section under the combined actions of circumferential force, out-of-plane bending and in-plane bending. To obtain conservative estimates of these stress resultants, the lower bound expression (Equation 4.21) should be used for the ratio of axial membrane stress resultants κ . Alternatively, $\kappa = 0$ can be directly used in design.

It is evident that the magnitudes of the out-of-plane stress resultants are controlled by the deformation of the lower part of the shell, so a ring with higher stiffness against out-of-plane deformation will develop higher associated stress resultants. An examination of Equations 4.36, 4.37 and 4.38 shows that this is indeed the case, so the stress resultants in the ring are directly proportional to its second moment of area about a radial axis (I_r). A normal design calculation would lead to the ring size (related to I_r) as an outcome, but in this case the stress resultants depend on I_r . It is evident that a ring that is flexible for out-of-plane bending will develop much smaller associated bending moments. In practice, it is therefore more efficient to use either flat annular plate stiffeners or I-sections with the web horizontal to give a high in-plane stiffness and a low out-of-plane stiffness (Figure 4.1). Considering typical ratios of the strong axis to weak axis elastic section moduli of rolled I sections, it is here recommended that the ratio of out-of-plane moment to in-plane moment should be limited to 10% ($M_r/M_x < 0.1$). Neglecting the contribution of κ (i.e. $\kappa = 0$), the section can be selected

by using the following expression for the second moment of area about the radial axis (I_r):

$$I_r < \frac{R^3 t}{20(1 + \nu)n^2(n^2 - 1) \left(1 - \left(\frac{H_L}{H_I} \right)^2 \right)} \quad (4.39)$$

Having restricted the out-of-plane bending moment using Equation 4.39, the intermediate ring can be designed to resist out-of-plane moments of only 10% of the maximum in-plane bending moment. Equation 4.36 can be used where a more accurate estimate of the out-of-plane moment is needed.

4.5. Computational verification of the Closed-form equations

Linear three dimensional finite element analyses were conducted to verify the accuracy of these equations. The commercial finite element program, ANSYS v12.1 (2010), was used to perform the numerical analysis. Since a cylinder resting on n equally spaced discrete supports has $2n$ planes of symmetry, the computational time was reduced by modelling only a segment covering the angle π/n , as shown in Figure 4.9a. Four-node shell elements (shell63) with a size of 100 mm in both the axial and circumferential directions were employed to model the cylindrical shell. The intermediate ring stiffener was modelled using two-node beam elements (beam4). The modulus of elasticity was taken as 200 GPa and Poisson's ratio as 0.30.

Symmetry boundary conditions were applied to the nodes on each symmetry plane. In practice, silo cylindrical shell walls are normally connected to other conical shells at the top and the bottom as shown in Figure 4.1. These conical pieces effectively prevent out-of-round displacements of the cylinder at the two extremes. In this study, the restraining effect of the connected shells was modelled by restraining the displacements at these points. At the top and bottom, both the radial u_r and circumferential u_θ displacements were restrained.

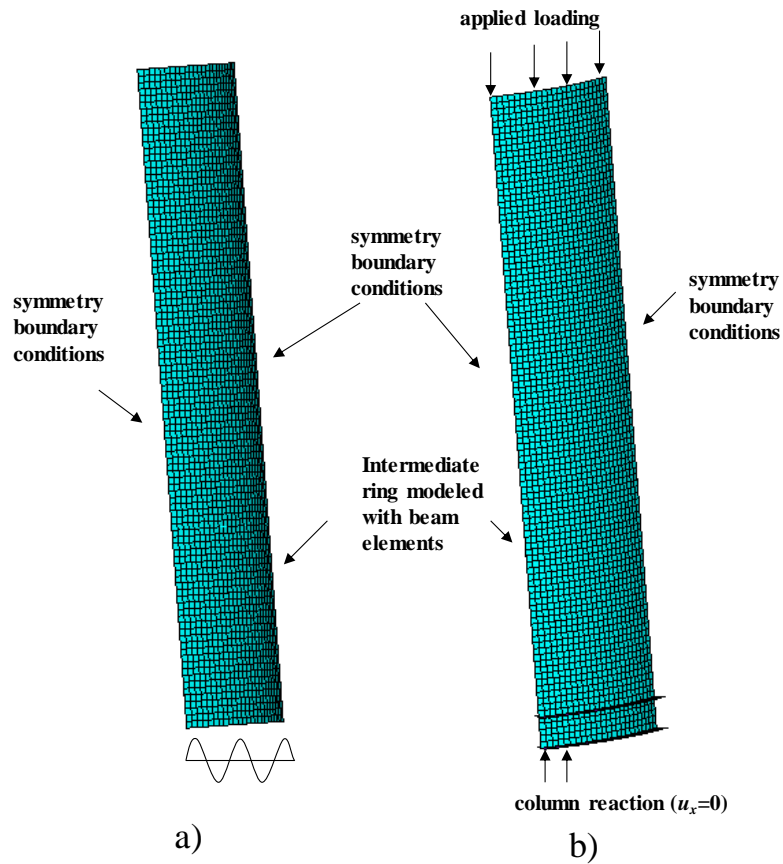


Figure 4.9 Finite-element mesh for the cylindrical shell and I-section ring beam

The cylinder base was subjected to loading in harmonic 4 (Equation 2.1), corresponding to the number of equally spaced discrete supports. The top edge was axially free, though radially and circumferentially restrained, so the axial stresses there were zero. Because the loading is purely harmonic, axial displacements need not be restrained at either boundary.

4.5.1. Case1: Intermediate ring at the ideal height

The silo structure analyzed here had a cylinder radius of 3000 mm and a height of 10000 mm with a constant thickness of 6 mm. An intermediate ring stiffener was placed at the ideal height (Equation 4.1) and it was modeled using stiff beam elements. The loading at the bottom of the shell was chosen to give a maximum axial membrane

stress of 1.0 GPa above the support. The calculated variations of M_x , Q_r , and Q_θ around the circumference are shown in Figures 4.10, 4.11, and 4.12 respectively, together with the predictions of the closed form solutions (Equations 4.33, 4.34, and 4.35) for the case of $H_L = H_I$ and $\kappa \rightarrow 0$. The comparisons show that the above equations provide acceptably accurate solutions, with the largest differences being 0.48%, 0.77%, and 3% for maximum bending moment, shear force and circumferential force respectively.

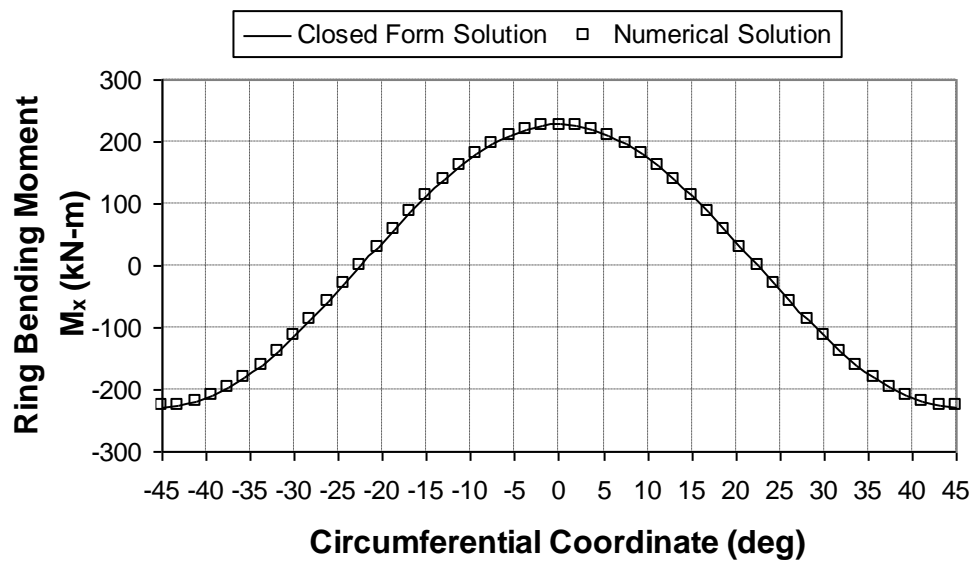


Figure 4.10 Comparison of closed form solution with numerical solution for ring bending moment

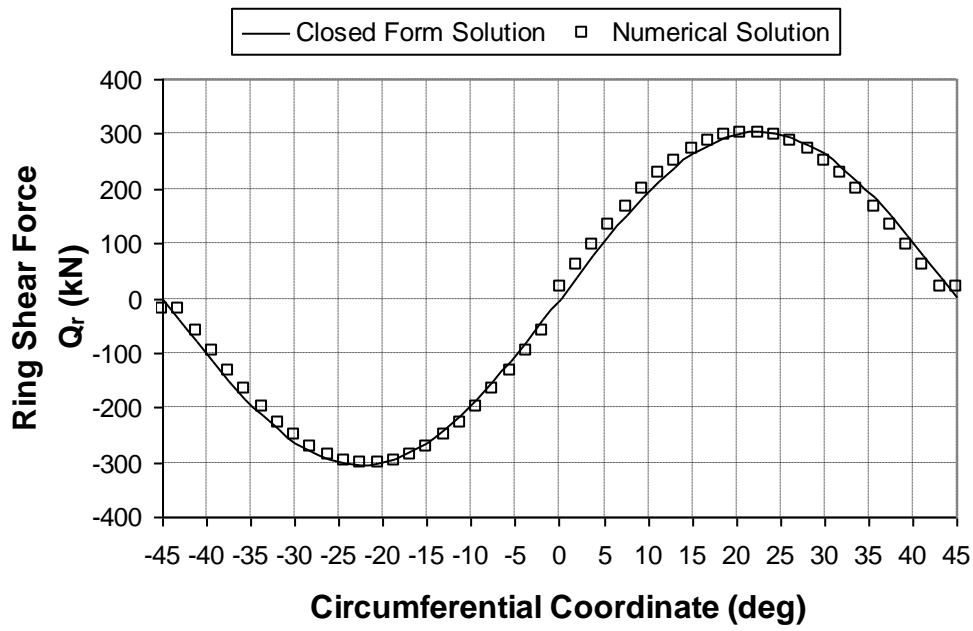


Figure 4.11 Comparison of closed form solution with numerical solution for ring shear force

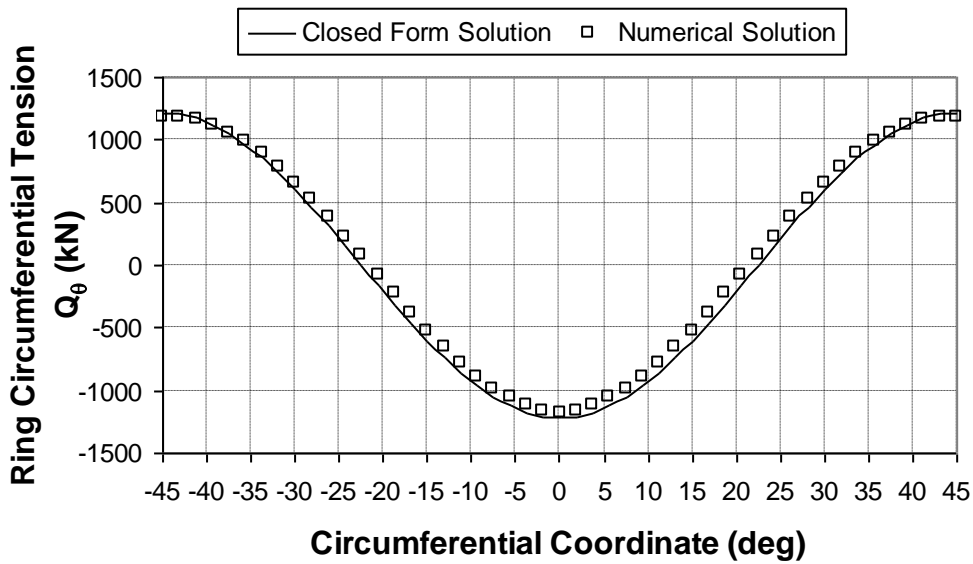


Figure 4.12 Comparison of closed form solution with numerical solution for ring circumferential tension

4.5.2. Case2: Intermediate ring below the ideal height

The silo structure analyzed here had a cylinder radius of 3000 mm and a height of 10000 mm. The lower and upper shell thicknesses were 6 mm and 3 mm respectively. The intermediate ring was placed at half of the ideal height ($H/2$). The loading at the bottom of the shell was chosen to give a maximum axial membrane stress of 100 MPa above the support. Two cases were considered to evaluate the assumption behind the derivation of internal forces and moments that reflect out-of-plane behavior. The simple assumption was made that the intermediate ring is very flexible compared to the in-plane stiffness of the shell. As a consequence, the displacements of the shell could be imposed as displacements of the intermediate ring. In cases where the out-of-plane stiffness of the intermediate ring is high, the contribution of its stiffness to the deformation of the shell is very significant. Intermediate rings with two different values of out-of-plane bending stiffness, but the same in-plane stiffness were studied. The first case involved a flexible ring, where the out-of-plane second moment of area is defined by the upper limit given in Equation 4.39. The second case involved a stiff ring, where the out-of-plane stiffness was made 10 times the upper limit of Equation 4.39. Annular plate stiffeners were considered in the verification study and the uniform torsional constant (K_T) was considered to be equal to four times the out-of-plane second moment of area.

The calculated variations of M_x , Q_r , Q_θ , M_r , T_θ and Q_x around the circumference, together with the predictions of the closed form solutions (Equations 4.33, 4.34, 4.35, 4.36, 4.37 and 4.38) for the flexible and stiff intermediate rings are shown in Figures 4.13 and 4.14 respectively. The lower bound expression (Equation 4.21) was used in closed form solutions. The comparisons show that the above equations provide acceptably accurate solutions for the flexible intermediate ring case, with the largest differences being 4.8%, 5.1%, 4.8%, 18.2%, 20.2% and 18.4%, for maximum M_x , Q_r , Q_θ , M_r , T_θ and Q_x respectively. The predictions are less accurate for the stiff intermediate ring where large differences were found for the stress resultants caused by out-of-plane deformation of the ring. The largest differences here were 11.3%,

11.7%, 10.9%, 37.3%, 37.6% and 37.7%, for maximum M_x , Q_r , Q_θ , M_r , T_θ and Q_x respectively. It should be noted that all the predictions given by the above equations were greater than the values found in the finite element analysis, so these equations give safe over-estimates and are conservative.

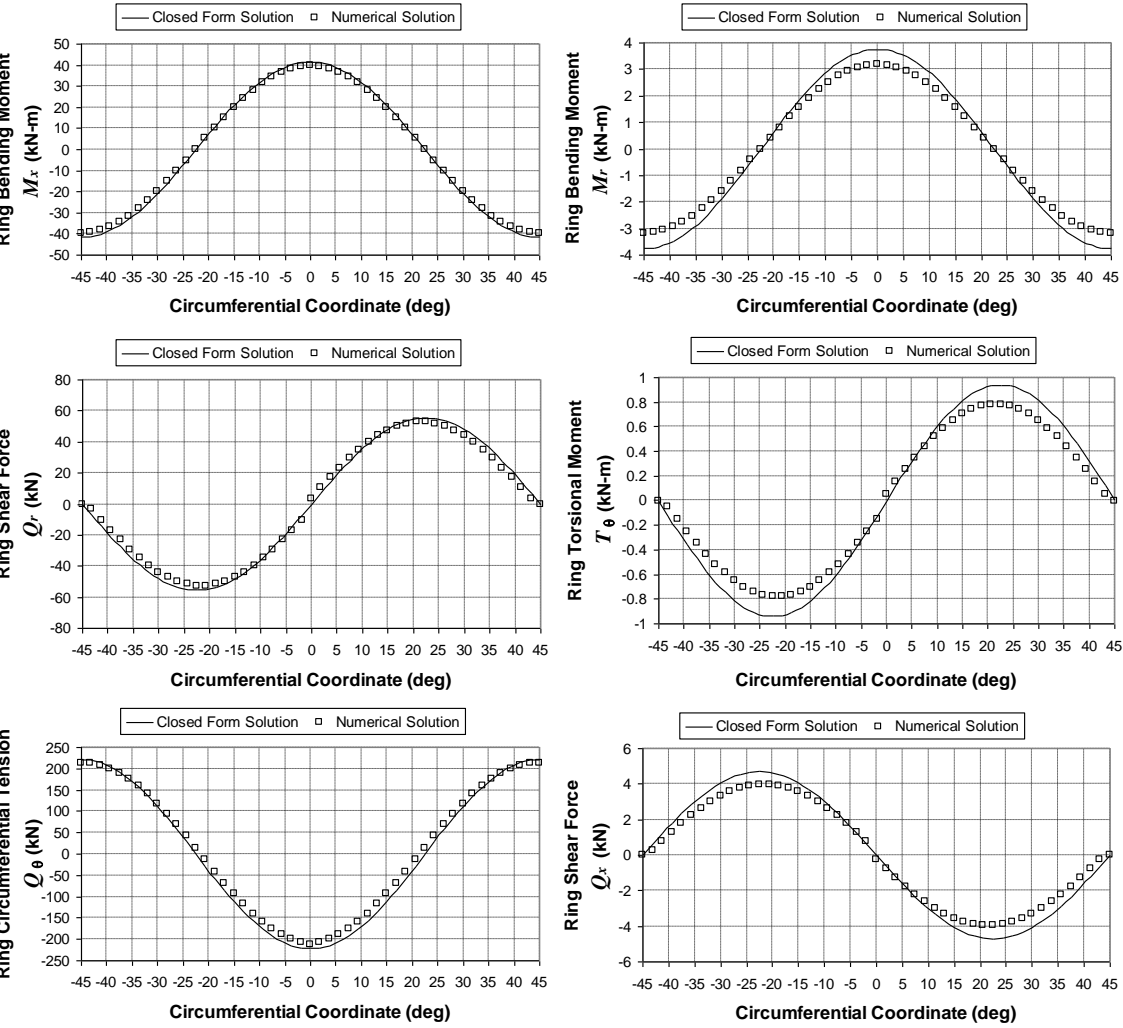


Figure 4.13 Comparison of closed form solution with numerical solution for a flexible intermediate ring

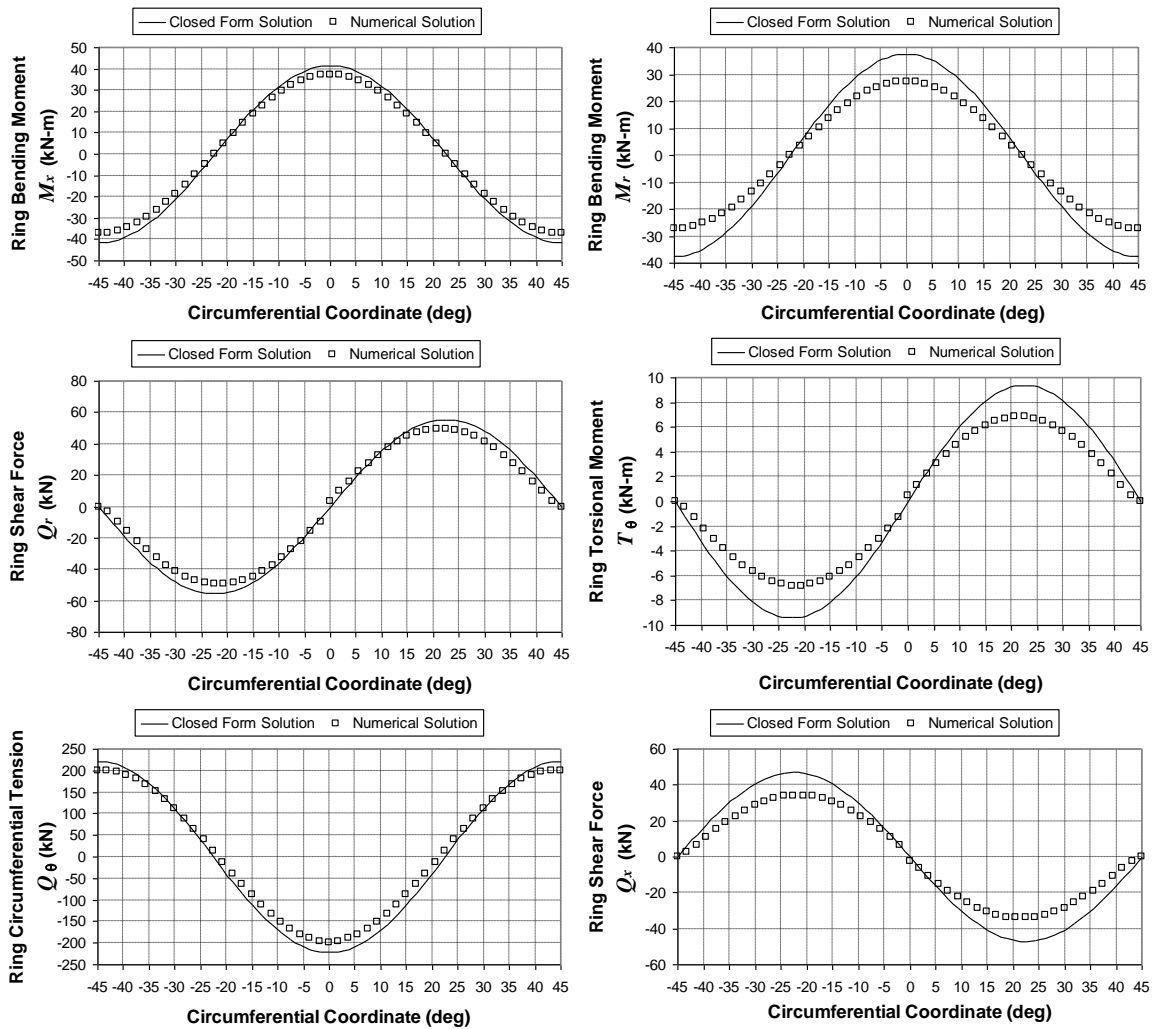


Figure 4.14 Comparison of closed form solution with numerical solution for a stiff intermediate ring

The reasons for the large differences found for the stiff intermediate ring were explored by examining the variation of axial displacements on the generator above the support ($\theta = 0$). This is shown in Figure 4.15 where the intermediate ring location is shown by a dashed line. The axial displacement at the ring was reduced from 0.29 mm to 0.25 mm by the stiff ring. Since the above formulation ignores the restraining effect of the ring on axial displacements at the ring level, the predictions are conservative for stiffer rings.

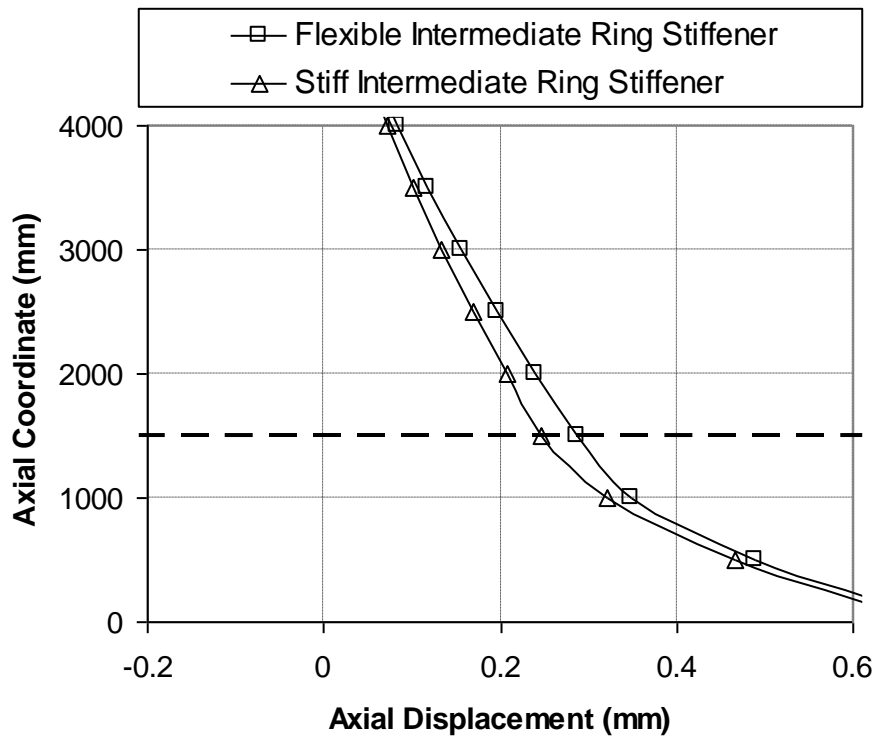


Figure 4.15 Variation of axial displacements throughout the shell

The proposal given in Equation 4.39 was substantiated by examining the calculated bending moments both in-plane and out-of-plane. For the two cases, the maximum in-plane values were 39.7 kNm and 37.3 kNm for the flexible and stiff rings respectively, whilst the maximum out-of-plane values were 3.2 kNm and 27.4 kNm respectively. It is clear from these maxima that the limit given in Equation 4.39 provides a convenient upper bound on the out-of-plane bending moment. The ratio of out-of-plane to in-plane bending moment was only 8% for the flexible ring, but rose to 73% for the stiff ring. This high moment in the stiff ring makes it very clear that a good design for an intermediate ring should be very flexible for out-of-plane deformations, as suggested above.

4.6. Computational assessment of the dominant harmonic

4.6.1. Case1: Intermediate ring at the ideal height

A practical silo shell usually rests on a discretely supported ring beam as shown in Figure 4.1. The interaction between the ring beam and the silo shell is complex and the stresses produced at the bottom of the silo wall are directly related to the relative stiffnesses of the shell and ring beam (Topkaya and Rotter (2011)). A similar finite element model to that described above was made of a silo consisting of a ring beam and shell combination with the geometry: $R = 4500$ mm, $t = 6$ mm, $n = 4$, shell height $H = 10000$ mm, beam depth $d = 1000$ mm, beam flange width $w = 600$ mm, beam flange thickness $T = 30$ mm, and beam web thickness $t_w = 20$ mm. This ring was deliberately chosen to be far too flexible to meet the required stiffness criterion obtained by Topkaya and Rotter (2011). The ring was modeled using four-node shell elements as shown in Figure 4.9b. In this model, the shell was loaded by a circumferentially uniform axial line load of magnitude P_u at its top. The ring beam was supported on discrete pads, with a circumferential width-to-radius ratio of 0.2, following the assumption of Teng and Rotter (1992). Figure 4.16 shows the circumferential variation of the axial membrane stress resultant at the bottom of the shell wall. The peak value, here termed the stress amplification ratio ζ , is seen to be 2.39, but the ratio of the local axial membrane stress resultant N_x to the applied stress resultant P_u varies around the circumference between 2.39 and 0.055. If the ring beam were stiff enough, this ratio should not vary significantly, but should be close to unity. The observed non-uniformity of the axial membrane stress resultant occurs because the ring beam is rather flexible, as intended by the choice made above.

Three curves are shown in Figure 4.16. The result of the finite element analysis is shown with diamond symbols: its mean value is naturally 1.0, corresponding to the applied load P_u , and there is a distinct local rise close to the support at the circumferential coordinate of zero. If this pattern of stress resultants is to be safely

modeled using only the sum of a uniform value and a dominant harmonic cosine term, then the result could be calibrated either to the stress over the support (peak value 2.39) or to the lowest value at midspan between supports (min value 0.055). The two possible simple models are shown in Figure 4.16 as the “support match” and “midspan match” treatments. However, for a safe design, it is desirable that the unsymmetrical component of this membrane stress resultant should be evaluated to be as large as possible, so the calibration of the sum of these two components is best done using the support match value.

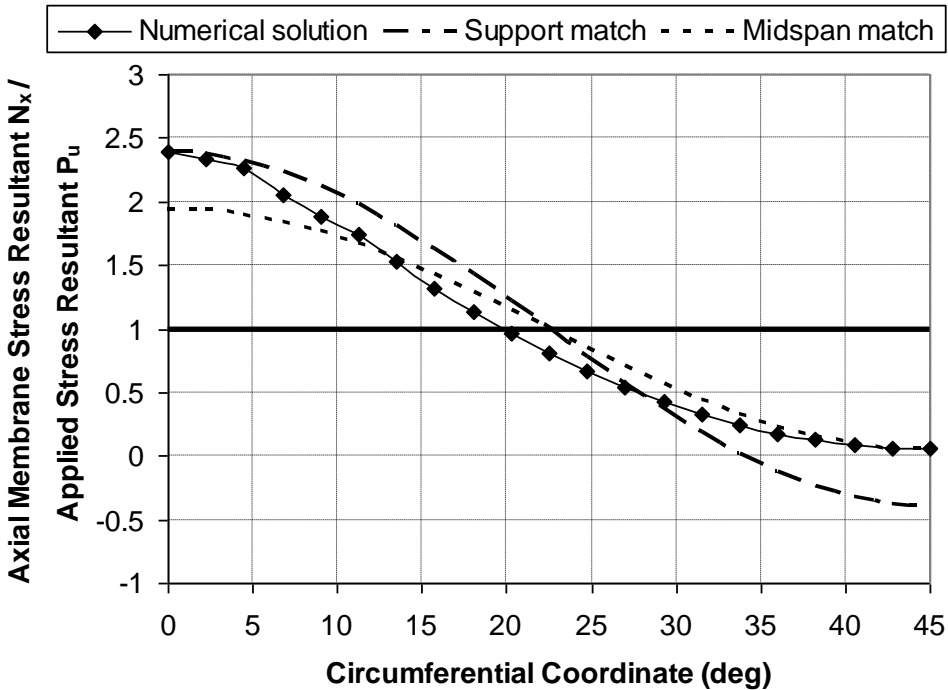


Figure 4.16 Variation of axial membrane stress resultant at the bottom of the shell

The result of this discussion is that a simple approximation to the stress pattern in Figure 4.16 is found from the stress amplification ratio ζ as

$$q_{xn} = (\zeta - 1)P_u \tag{4.40}$$

This first approach was evaluated using a finite element parametric study. The finite element model given in Figure 4.9b was adopted for all cases. Shells with dimensions $R = 3000$ and 4500 mm, $t = 3$ and 4.5 mm, $n = 3, 4$ and 6 , all with height = $10\,000$ mm were assessed. This led to a total of 12 possible shell geometries; for each, 10 different ring beam dimensions were assessed, resulting in 120 analysis cases. Beam depths of 1000, 1500, 2000, 2500 and 3000 mm, with flange widths of 600 and 1000 mm were calculated. The flange and web thicknesses were retained constant at 30 and 20 mm respectively. From each analysis the stress amplification ratio ζ , the maximum stress resultants in the intermediate ring stiffener (maximum bending moment $M_{x,max}$ and maximum circumferential force $Q_{\theta,max}$) were collected. For each case, two corresponding values for q_{xn} were backfigured from the predictions of Equations 4.33 and 4.35 for the case where $H_L = H_I$ and $\kappa \rightarrow 0$ independently, resulting in two coefficients: one for bending moment and the other for circumferential force in the intermediate ring. The results presented in Figure 4.17 for the extracted coefficient q_{xn} indicate that the proposed model provides quite satisfactory estimates of this coefficient when the bending moment is used. The data points mostly fall on a straight line, but where the results depart significantly from this simple concept, the proposed model over-predicts the value of q_{xn} resulting in safer designs. The straight line of Equation 4.40 is shown as the heavy line in Figure 4.17, which indicates that the simple conservative deduction used in Figure 4.16 provides a close approximation where the stress amplification ratio ζ lies below about 2, but is increasingly conservative when this ratio is larger, corresponding to very flexible ring beams that produce to higher local peak stresses in the shell above the support.

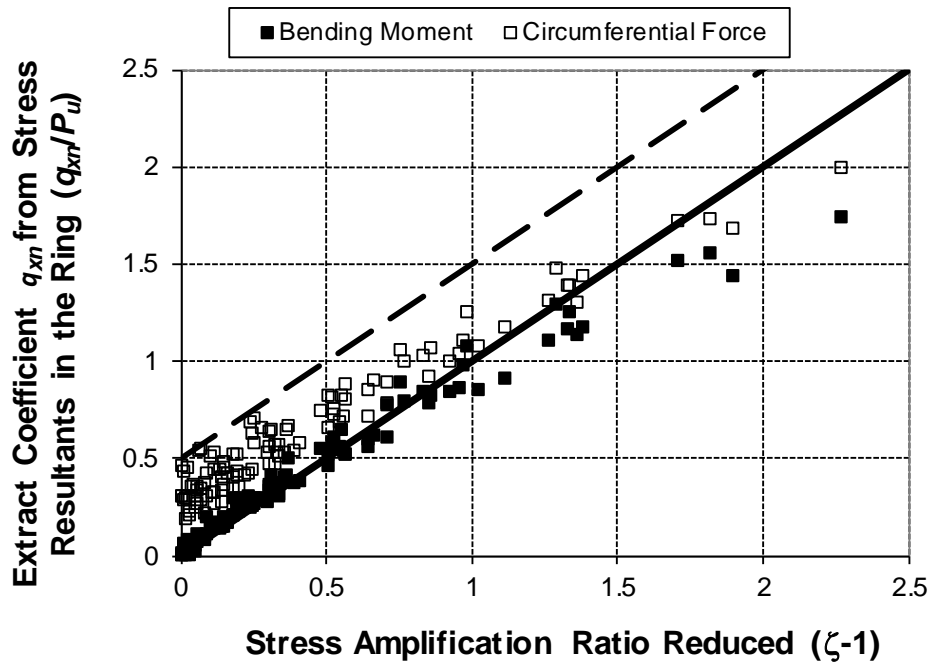


Figure 4.17 Verification of the proposed model for the Fourier coefficient (q_{xn})

This proposed model provides less accurate predictions when the coefficient q_{xn} is derived using the circumferential force as a measure, backfigured from Equation 4.35 for the case where $H_L = H_I$ and $\kappa \rightarrow 0$. The coefficients implied by the finite element analysis are generally higher than those indicated in the proposed model because part of this arises because the membrane theory treatment has ignored the restraint of Poisson expansion under uniform axial compression that induces a small additional circumferential force in the intermediate ring. To make some allowance for this effect, a conservative bound shown as dashed lines in Figure 4.17 can be adopted when assessing the circumferential force that may develop in the intermediate ring as follows:

$$q_{xn} = (\zeta - 0.5)P_u \quad \text{for circumferential force} \quad (4.41)$$

4.6.2. Case2: Intermediate ring below the ideal height

The applicability of Equations 4.40 and 4.41 to cases where the intermediate ring lies below the ideal height was explored through a parametric study. A similar finite element model to that described above was made of a silo consisting of a ring beam and shell combination. The base ring beam was modelled using four-node shell elements as shown in Figure 4.9b. The top of the shell was loaded by a circumferentially uniform axial line load of magnitude P_u . Shells of height 10 000 mm with dimensions $R = 3000$ and 4500 mm, $t_L = 6$ mm and $t_U = 3$ mm, $n = 3$ and 4 , $H_L/H_I = 0.5, 0.6, 0.7, 0.8$ and 0.9 were calculated, leading to a total of 20 possible shell geometries. For each shell geometry, 10 different ring beam dimensions were used, resulting in 200 analysis cases. Beam depths of 1000, 1500, 2000, 2500 and 3000 mm were adopted, with flange widths of either 600 or 1000 mm. The flange and web thicknesses were retained constant at 30 and 20 mm respectively. Intermediate rings with high in-plane stiffness were considered. The out-of-plane stiffness of the rings were determined using Equation 4.39. From each analysis the stress amplification ratio ζ , the maximum stress resultants in the intermediate ring stiffener (maximum bending moment $M_{x,max}$ and maximum circumferential force $Q_{\theta,max}$) were collected. For each case, two corresponding values for q_{xn} were backfigured from the predictions of Equations 4.33 and 4.35 independently, resulting in two coefficients: one for bending moment and the other for the circumferential tensile force in the intermediate ring.

The results are presented in Figures 4.18 and 4.19 for the extracted coefficient q_{xn} and indicate that the proposed models can be safely used for shells with an intermediate ring placed below the ideal height. The other stress resultants were also examined. The results indicate that Equation 4.40 can be safely used for Q_r , M_r , T_θ and Q_x . The maximum out-of-plane bending moment always remained below 10% of the calculated maximum in-plane bending moment.

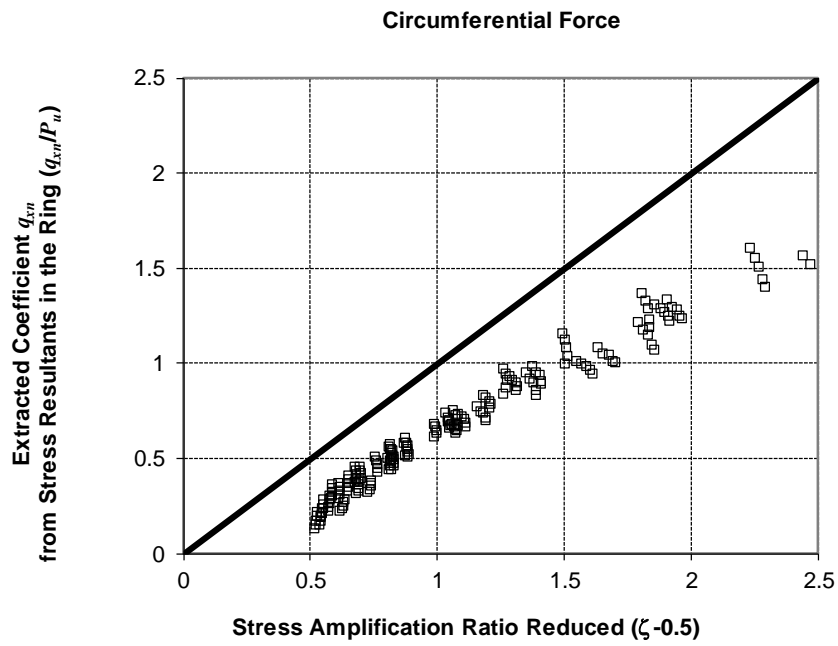


Figure 4.18 Verification of the proposed model for the Fourier coefficient (q_{xn}) (circumferential force)

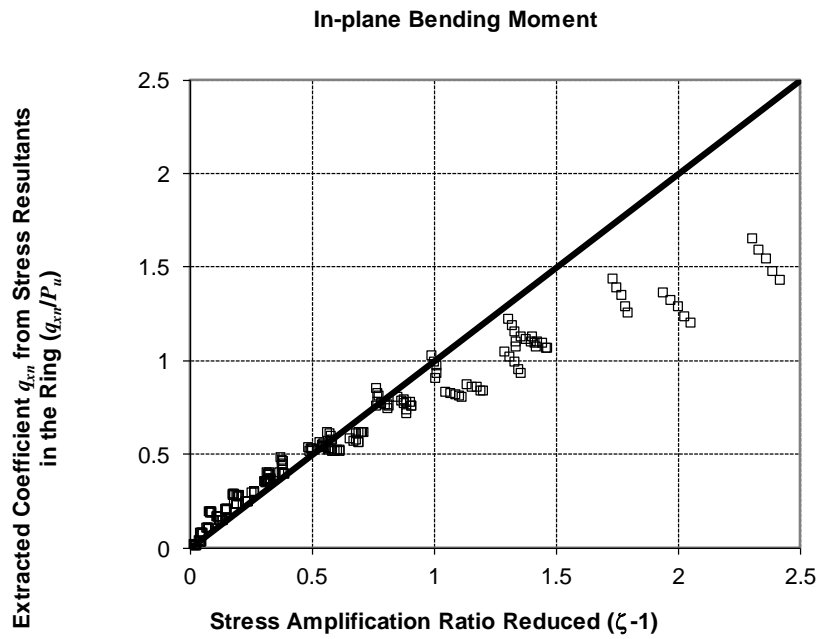


Figure 4.19 Verification of the proposed model for the Fourier coefficient (q_{xn}) (In-plane bending moment)

This method of finding the stress resultants in an intermediate ring requires the stress amplification ratio ζ to be obtained first. This factor can be conveniently found using a simple hand calculation. The stress amplification ratio ζ is related to the relative stiffness of the shell to the ring beam at the base of the shell (Figure 1.2). This relative stiffness is expressed as the ring beam stiffness ratio ψ , as originally devised by Rotter (1985) but improved and verified by Topkaya and Rotter (2011). The relationship between the stress amplification ratio (ζ) and the ring beam stiffness ratio (ψ) has been demonstrated by Topkaya and Rotter (2011) through extensive finite element analyses. The evaluations of the stress amplification ratios (ζ) arising from different ring beam stiffness ratios (ψ) presented by Topkaya and Rotter (2011) shown in Figure 2.4, where over 1000 analyses are plotted. For design purposes, it is desirable that an upper bound on the stress amplification ratio is used, since this leads to conservative designs. A convenient upper bound has been developed using the data of Figure 2.4. This upper bound was defined by Equation 2.38 and it can be used to give a simple safe estimate of the stress amplification ratio of a given shell/ring beam geometry. This equation is applicable for ring beam stiffness ratios (ψ) greater than 0.0038. For lower values ($\psi < 0.0038$) $\zeta = 1$ should be adopted.

4.7. Stiffness Criterion for the Intermediate Ring Stiffener

The intermediate ring stiffener must have adequate stiffness to fulfil its function properly. A stiffness criterion was obtained comparing the relative stiffnesses of the intermediate ring and the shell for rings.

The intermediate ring stiffness ratio (χ) was expressed as:

$$\chi = \frac{K_{shell}}{K_{stiffener}} = \frac{N_{x\theta}/u_{\theta,shell}}{q_{\theta}/u_{\theta,stiffener}} = \frac{u_{\theta,stiffener}}{u_{\theta,shell}} \quad (4.42)$$

where $K_{stiffener}$, K_{shell} = circumferential stiffnesses of the ring stiffener and shell respectively; $u_{\theta,stiffener}$, $u_{\theta,shell}$ = circumferential displacements of the ring stiffener and

shell respectively. The loading condition of Equation 4.27 was adopted by neglecting the contribution of κ to compute the stiffnesses.

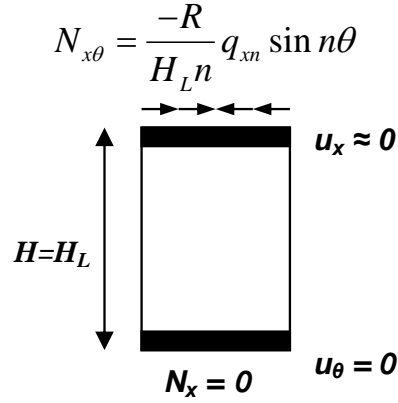


Figure 4.20 Boundary conditions used for closed form solution of shell stiffness

For the loading and boundary conditions given in Figure 4.20 the following can be derived using Equations 4.9 and 4.10:

$$N_\theta = 0 \quad N_{x\theta} = f_1(\theta) = \frac{-R}{H_L n} q_{xn} \sin n\theta \quad (4.43)$$

Imposing the boundary conditions $N_x = 0$ and $u_\theta = 0$ at $x = 0$ reveals:

$$f_2(\theta) = 0 \quad f_4(\theta) = 0 \quad (4.44)$$

At $x = H_L$, the boundary condition of nearly zero axial displacement ($u_x \approx 0$) yields:

$$f_3(\theta) = \frac{-H_L}{2} q_{xn} \cos n\theta \quad (4.45)$$

Using Equation 4.23 the circumferential displacement of the shell at the interface can be found as:

$$u_{\theta(\text{shell})} = \frac{-[H_L^2 n^2 + 6(1+\nu)R^2]}{3EtRn} q_{xn} \sin n\theta \quad (4.46)$$

The circumferential displacements of the intermediate ring stiffener under the same loading condition (i.e. $q_\theta = N_{x\theta}$) can be obtained by solving Vlasov's curved beam differential equations. Considering $\kappa = 0$ and inserting Equation 4.33 into Equation 2.11 yields the radial displacement of the ring:

$$u_r(\theta) = \frac{-R^5}{H_L EI_x n^2 (n^2 - 1)^2} q_{xn} \cos n\theta \quad (4.47)$$

Inserting Equations 4.35 and 4.47 into Equation 2.10 and solving the differential equation leads to the circumferential displacements of the intermediate ring stiffener as:

$$u_{\theta(\text{stiffener})} = \frac{-R^3 (AR^2 + I_x n^4 - I_x n^2)}{H_L AEI_x n^3 (n^2 - 1)^2} q_{xn} \sin n\theta \quad (4.48)$$

Finally the intermediate ring stiffness ratio χ can be expressed as:

$$\chi = \frac{3R^4 t (AR^2 + I_x n^4 - I_x n^2)}{AI_x n^2 (n^2 - 1)^2 H_L [H_L^2 n^2 + 6(1+\nu)R^2]} \quad (4.49)$$

Equation 4.49 indicates that the geometrical parameters that influence the intermediate ring stiffness ratio are the radius of the shell and ring stiffener R , the thickness of the shell t , the area and second moment of area normal to the plane of the intermediate ring stiffener A and I_x , and the number of supports n .

A finite element parametric study was conducted to obtain a practical limit for the intermediate ring stiffness ratio χ . Pursuant to this goal, combinations of shells and

intermediate ring stiffeners were analyzed under the fundamental harmonic of the column support. The finite element models all had a height $H = 10000$ mm, with geometries defined as radius $R = 3000$ and 4500 mm, thickness $t_L = 6$ mm, $t_u = 3$ and 6 mm, number of supports $n = 3$ and 4 , $H_L/H_I = 0.5, 0.7$ and 0.9 . A total of 24 combinations were adopted for the shell geometries with 20 different intermediate ring stiffener dimensions, resulting in 480 analysis cases. A reference axial membrane stress resultant ($N_{x,ref}$) was calculated by using idealized rigid boundary conditions at the intermediate ring location. In each analysis, the axial membrane stress resultant in the shell above the intermediate ring stiffener (N_x) was recorded. The difference between the axial membrane stress resultants ($N_x - N_{x,ref}$) was calculated and normalized relative to the maximum applied stress at the bottom. Normalized values of the stress resultants found in the finite element analyses are plotted in Figure 4.21 as a function of the stiffness ratio χ . The results indicate that when the stiffness ratio is lower than about 0.2, the peak axial membrane stress resultant above the intermediate stiffener drops to below 6% of the applied value. Therefore, it is recommended here that the limit of $\chi < 0.2$ for intermediate rings.

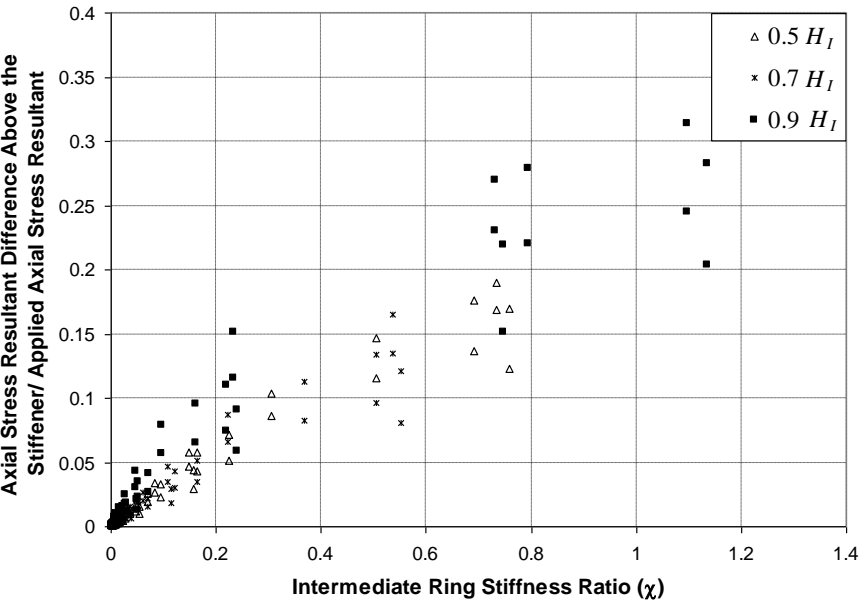


Figure 4.21 Assessment of an appropriate value for the intermediate ring stiffness ratio χ

CHAPTER 5

SUMMARY AND CONCLUSIONS

5.1. Summary

This thesis reports findings of a three part analytical and numerical study on silo supporting ring beams and intermediate ring stiffeners.

The first study has been undertaken to investigate the applicability of the stiffness criterion to cylindrical shells under global shear and bending. Pursuant to this goal extensive finite element analyses were conducted where different ring beam and cylindrical shell combinations are subjected global shearing and bending actions.

The second study explores the ring beam stress resultants when closed section ring beams of lower stiffness and practical dimensions are used. A complementary finite element parametric study was conducted to investigate variation of the values of stress resultants and displacements caused by the connection of the ring to the stiff shell. The effects of the ring beam stiffness ratio on the stress resultants and transverse displacement were also investigated.

The third study investigates a combination of a ring beam and an intermediate ring stiffener for large silos. Design requirements for intermediate ring stiffeners placed at or below the ideal location are explored. Pursuant to this goal, the cylindrical shell below the intermediate ring stiffener was analyzed using the membrane theory of shells and the reactions produced by the stiffener on the shell were identified. Furthermore, the displacements imposed by the shell on the intermediate ring stiffener were obtained. These force and displacement boundary conditions were then applied to the intermediate ring stiffener to derive closed form expressions for the variation of the stress resultants around the circumference to obtain a strength design criterion for

the stiffener. A relative stiffness criterion for the ring is then devised by considering the ratio of the circumferential stiffness of the cylindrical shell to that of the intermediate ring. These analytical studies were then compared with complementary finite element analyses to verify closed-form design equations for ring stiffeners.

5.2. Conclusions

5.2.1. Conclusions about Application of Ring Beam Stiffness Criterion for Discretely Supported Shells under Global Shear and Bending

The applicability of the stiffness criterion proposed by Rotter (1985) to a silo shell resting on a discretely supported ring beam and subjected to global shear and bending was studied herein. A total of 4320 three dimensional finite element analyses were conducted to evaluate the stiffness ratio. The geometry of the silo shell, ring beam and the support conditions were considered as the prime variables.

The results indicate that the stiffness criterion proposed by Rotter (1985) can be conveniently extended to cases where the silo shell resting on a discretely supported ring beam is subjected to global shear and bending. Upper bound expressions were developed to represent the data produced by finite element analysis and these expressions can be readily adopted by the design standards. The support conditions were found to significantly influence the response. The knife edge support condition results in much higher stress amplifications over the support making the ring beam less effective. On the other hand, a finite width supports having support width-to-radius ratios that range between 0.05 and 0.2 were found to reduce the level of stress amplification considerably when compared with the knife edge support case.

5.2.2. Conclusions about Analysis of Silo Supporting Ring Beams Resting on Discrete Supports

Closed form design equations obtained from Vlasov's curved beam theory were compared with numerical results. The comparisons show that these equations provide acceptably accurate solutions when the isolated ring beam is considered. On the other hand, when the ring beam and shell interaction is considered, the values obtained from finite element calculations diverge from those of the closed form solutions. As the thickness of the shell gets thicker, the difference between the closed form solution and the numerical calculations increases. The design of a ring beam as an isolated curved beam is conservative, since it neglects the contribution of the attached shell and hopper.

A complementary finite element parametric study was also conducted to investigate variation of the values of stress resultants and displacements caused by the connection of the ring to the stiff shell. These variations were plotted as a function of stiffness ratio (ψ). The results indicate that the reduction from the isolated ring beam values can be directly and accurately related to the ring beam to shell stiffness ratio. When the ring beam is quite flexible, the reduction in the stress resultants and displacement from the values for an isolated ring beam becomes very large. Future research should concentrate on determining displacements and stresses in the ring when open section ring beams are used.

5.2.3. Conclusions about Requirements for Intermediate Ring Stiffeners on Discretely Supported Shells

The results demonstrate that the intermediate ring is only subject to in-plane forces and bending moments when intermediate ring stiffener is placed at ideal location. However, the closed form expressions reveal that the intermediate ring stiffener is subjected to out-of-plane internal forces and bending moments in addition to the in-plane stress resultants when the ring is placed below the ideal height. The developed

expressions were compared with numerical solutions and a good agreement has been demonstrated.

The closed form solutions indicate that the out-of-plane internal forces and bending moments depend on the out-of-plane bending stiffness of the ring. For economical designs, it is proposed that the out-of-plane bending moment should be kept below 10% of the in-plane bending moment. A simple criterion to permit a quick fulfilment of this requirement was developed and verified.

A stiffness criterion has been developed, based on the relative stiffnesses of the ring stiffener and the cylindrical shell under the harmonic force transfer between the shell and the stiffener. The resulting intermediate ring stiffness ratio (χ) depends on the geometrical properties of both the shell and the stiffener. A complementary finite element parametric study was conducted to determine practical limits for the intermediate ring stiffness ratio. The results indicate that ratios below about $\chi < 0.2$ provide a satisfactorily uniform axial membrane stress distribution above the intermediate ring stiffener, so this limit is recommended for practical design. Future research should concentrate on exploring the effect of a stepped-wall varying thickness in the shell above the ring.

REFERENCES

ANSYS, Version 12.1 On-Line User's manual, 2010.

Calladine, C.R., *Theory of shell structures*. Cambridge University Press, U.K., 1983.

Doerich C., Rotter J.M., Behavior of cylindrical steel shells supported on local brackets J. Struct Eng, ASCE, 134 (8), pp. 1269-1277, 2008.

Doerich, C., Vanlaere, W., Lagae, G., Rotter, J.M., "Stability of column-supported steel cylinders with engaged columns" Proceedings of the International Association for Shell and Spatial Structures (IASS) Symposium, Valencia, Evolution and Trends in Design, Analysis and Construction of Shell and Spatial Structures, 2009.

ECCS "Stability of Steel Shells: European Design Recommendations: Fifth Edition 2008", Eds J.M. Rotter and H. Schmidt, Publication P125, European Convention for Constructional Steelwork, Brussels, 384 pp, 2008.

Ellinas C. P., Batista R. C., and Croll J. G. A., Overall buckling of stringer stiffened cylinders, Proc. Instn Civ. Engrs, Part 2, vol.71, 479-512, 1981.

EN 1993-1-6, "Eurocode 3: Design of Steel Structures – Part 1-6: Strength and Stability of Shell Structures", CEN, Brussels, 2007.

EN 1993-4-1, "Eurocode 3: Design of Steel Structures, Part 4.1: Silos", European Committee for Standardization, Brussels, Belgium, 2007.

Flügge, W., *Stresses in Shells*, Springer-Verlag, Berlin, 1973.

Gaylord, E.H. and Gaylord, C.N., *Design of Steel Bins for Storage of Bulk Solids*, Prentice Hall, Englewood Cliffs, 1984.

Gillie, M., Holst, J.M.F.G., Structural behaviour of silos supported on discrete, eccentric brackets, *Journal of Constructional Steel Research* Vol. 59(7), 887-910, 2003.

Gillie, M., Holst, J.M.F.G., Münch, M. and Rotter, J.M. Behaviour of silos supported on discrete brackets, *International Journal of Structural Stability and Dynamics*, Vol. 2(1), 45-62, 2002.

Gould, P. L., Ravichandran, R.V. and Sridharan, S. "A local-global FE model for nonlinear analysis of column-supported shells of revolution", *Thin-Walled Structures*, 31, 25-37, 1998.

Gould, P. L., Sen, S. K., Wang, R. S. C., Suryoutomo, H. and Lowrey, R. D. "Column Supported Cylindrical-Conical Tanks", *J Struct. Div., ASCE*, 102 (ST2), 429-447, 1976.

Gould, P.L. and Sen, S.K. "Column moments in eccentrically supported tanks", *J Struct. Div., ASCE*, 100 (ST3) 2165-9, 1974.

Greiner, R. and Guggenberger, W., "Buckling Behaviour of Axially Loaded Steel Cylinders on Local Supports - with and without Internal Pressure", *Thin Walled Structures*, Vol. 31, pp 159-167, 1998.

Greiner, R., "Zur Ingenieurmässigen Berechnung und Konstruktion zylindrischer behälter aus Stahl unter allgemeiner Belastung", (Analysis and Construction of Cylindrical Steel Cylinders under non axisymmetric Loading). *Proc. "Wissenschaft und Praxis"*, Vol. 31 FHS Biberach/Riss, Stahlbau Seminar, 51pp, 1983.

Greiner, R., “Zur Laengskrafteinleitung in stehende zylindrische Behaelter aus Stahl”, *Stahlbau*, 53(7), 210-215, 1984.

Guggenberger, W., Greiner, R. and Rotter, J.M. “Cylindrical shells above local supports”, in *Buckling of Thin Metal Shells*, eds J.G. Teng & J.M. Rotter, Spon, London, pp 88-128, 2004.

Guggenberger, W., Greiner, R. and Rotter, J.M., “The Behaviour of Locally-Supported Cylindrical Shells: Unstiffened Shells”, *J. Constr. Steel Res.*, 56(2) 175-197, 2000.

Heins, C.P., *Bending and torsional design in structural members*. Lexington Books, Lexington, Massachusetts, 1975.

Holst J.M.F.G., Rotter J.M., Gillie M., Münch M., Failure Criteria for Shells on Local Brackets. In: Drew H.R., Pellegrino S. (eds) *New Approaches to Structural Mechanics, Shells and Biological Structures*. Solid Mechanics and Its Applications, vol 104, 315–327, Springer, Dordrecht, 2002.

Jansseune A., Corte W.D., and Belis J., Optimal stiffening configuration for locally supported cylindrical silos: Engaged columns, *Journal of Constructional Steel Research*, Vol. 119, 17-29, 2016.

Jansseune, A., De Corte, W. and Belis, Elastic Failure of Locally Supported Silos with U-shaped Longitudinal Stiffeners, *KSCE Journal of Civil Engineering*, 19(4), 1041-1049, 2015.

Jansseune, A., De Corte, W., Belis, J “Imperfection sensitivity of locally supported cylindrical silos subjected to uniform axial compression” *International Journal of Solids and Structures*, Vol. 96, pp 92-109, 2016.

Jansseune, A., De Corte, W., Van Impe, R., “Column-supported silos: Elasto-plastic failure” *Thin Walled Structures*, Vol. 73, pp 158-173, 2013.

Jansseune, A., De Corte, W., Vanlaere, W., Van Impe, R. “Influence of the cylinder height on the elasto-plastic failure of locally supported cylinders” *Steel and Composite Structures*, Vol. 12, No. 4, pp 291-302, 2012.

Kildegard, A. “Bending of a Cylindrical Shell subject to Axial Loading”, 2nd Symp. *Theory of Thin Shells*, IUTAM, Springer, Berlin, 301-315, 1969.

Kraus, H., *Thin Elastic Shells*, Wiley and Sons, New York, 1967.

Novozhilov, V.V., *The theory of thin shells*. Noordhoff, Groningen, Netherlands, 1959.

Öry, H. and Reimerdes, H.G., “Stresses in and Stability of Thin Walled Shells under Non-ideal Load Distribution”, *Proc. Int. Colloq. Stability Plate & Shell Structs*, Gent, ECCS, 555-561, 1987.

Öry, H., Reimerdes, H.G., Tritsch, W., “Beitrag zur bemessung der schalen von metallsilos” *Stahlbau*, 53(8), 243-248, 1984.

Pippard, A.J.S. and Baker, J.F., *The Analysis of Engineering Structures*, Edward Arnold, London, 1957.

Rotter, J.M. “Buckling of cylindrical shells under axial compression”, in *Buckling of Thin Metal Shells*, eds J.G. Teng & J.M. Rotter, Spon, London, pp 42-87, 2004.

Rotter, J.M., “Analysis and Design of Ringbeams”, in *Design of Steel Bins for Storage of Bulk Solids*, ed J.M. Rotter, *University of Sydney*, 164-183, 1985.

Rotter, J.M., “Bending Theory of Shells for Bins and Silos”, *Trans. Mech. Engrg*, IEAust, ME12 (3) 147-159, 1987.

Rotter, J.M., “Elastic Behaviour of Isolated Column-Supported Ringbeams”, *Journal of Constructional Steel Research*, 4(4), 235-252, 1984.

Rotter, J.M., “Guide for the Economic Design of Circular Metal Silos”, Spon, London, 2001.

Rotter, J.M., “Membrane Theory of Shells for Bins and Silos”, *Transactions of Mechanical Engineering, Institution of Engineers, Australia*, Vol. ME12 No.3 September, pp 135-147, 1987.

Rotter, J.M., “Structural Design of Light Gauge Silo Hoppers”, *Journal of Structural Engineering, ASCE*, 116(7), 1907-1922, 1990.

Rotter, J.M., “The Analysis of Steel Bins Subject to Eccentric Discharge”, Proc., Second International Conference on Bulk Materials Storage Handling and Transportation, Institution of Engineers, Australia, Wollongong, pp 264-271, 1986.

Rotter, J.M., Cai, M. and Holst, J.M.F.G., “Buckling of thin cylindrical shells under locally elevated axial compression stresses”, *Journal of Pressure Vessel Technology*, 133 (1) 011204-1 to 11, 2011.

Safarian, S.S. and Harris, E.C., *Design and Construction of Silos and Bunkers*, Van Nostrand Reinhold, New York, 1985.

Samuelson L.Å., Practical Analysis Methods for Design of Circular Cylinders with Longitudinal Stiffeners and Subjected to Axial Compression. In: Ramm E. (eds) *Buckling of Shells*. Springer, Berlin, Heidelberg, 1982.

Seide, P., *Small Elastic Deformations of Thin Elastic Shells*, Noordhoff, Leyden, Holland, 1975.

Sonat, C., Topkaya, C., Rotter, J.M., “Buckling of cylindrical metal shells on discretely supported ring beams.” *Thin-Walled Structures*, 93, 22-35, 2015.

Teng, J.G., Rotter, J.M., “Linear bifurcation of perfect column-supported cylinders: Support modelling and boundary conditions.” *Thin-Walled Structures*, 14(3) 241-263, 1992.

Timoshenko, S.P. and Gere, J.M. “Theory of Elastic Stability”, 2nd edn, McGraw-Hill, New York, 1961.

Timoshenko, S.P. and Woinowsky-Krieger, S., *Theory of Plates and Shells*, McGraw-Hill, New York, 1959.

Topkaya, C., Rotter, J.M., “Ideal location of intermediate ring stiffeners on discretely supported cylindrical shells”, *ASCE Journal of Engineering Mechanics*, 140(4), pp. 1-10, 2014.

Topkaya, C., Rotter, J.M., “Ring beam stiffness criterion for column supported metal silos”, *ASCE Journal of Engineering Mechanics*, 137(12) 846-853, 2011.

Trahair, N.S., Abel, A., Ansourian, P., Irvine, H.M. and Rotter, J.M., “Structural Design of Steel Bins for Bulk Solids”, *Australian Institute of Steel Construction*, Sydney, 1983.

Vanlaere W., Doerich, C., Lagae G., and Van Impe R., Steel cylinders on local supports with rigid stiffeners, Proceedings of the International Association for Shell and Spatial Structures (IASS) Symposium, Valencia, 2009.

Vanlaere W., Van Impe R., and Lagae G., and Thomas M., Effect of varying the size of flatbar stiffeners on the buckling behaviour of thin cylinders on local supports, *Structural Engineering and Mechanics*, Vol. 19(2), pp. 217-230, 2005.

Vanlaere W., Van Impe R., and Lagae G., Buckling of Stringer Stiffened Cylinders on Local Supports, IABSE Symposium, pp. 33-38(6), Budapest 2006.

Vanlaere W., Sonck D., Callewaert D., Van Impe R., and Lagae G., The Buckling Behaviour of Steel Cylinders with Engaged Columns, National Congress on Theoretical and Applied Mechanics, 8th, Proceedings. p. 413-41, 2009.

Ventsel, E. and Krauthammer, T., *Thin plates and shells: theory, analysis and applications*. Marcel Dekker, NY, 2001.

Vlasov, V.Z., General theory of shells and its applications in engineering. NASA Technical Translation, TTF-99, Washington, D.C, 1964.

Vlasov, V.Z., *Thin-walled elastic beams*. National Science Foundation, Washington, D.C., 1961.

Wozniak, R.S., *Steel Tanks*, Structural Engineering Handbook, 2nd edn, Section 23, Eds. E.H. and C.N. Gaylord, McGraw-Hill, New York, 1979.

Zhao Y., Yu J., and Ye J., Structural Behavior of Column-Supported Steel Silos with Engaged Columns, *Engineering Mechanics*, Vol.23, 63-69, 2006.

CURRICULUM VITAE

PERSONAL INFORMATION

Surname, Name: Özer ZEYBEK
Nationality: Turkish (TC)
Date and Place of Birth: 28 November 1984, Fethiye
Marital Status: Married
Phone: +90 555 414 51 91
email: ozeybek@metu.edu.tr

EDUCATION

Degree	Institution	Year of Graduation
MS	DEU Civil Engineering	2011
BS	DPU Civil Engineering	2006

WORK EXPERIENCE

Year	Place	Enrollment
2011-	Middle East Technical University	Research Assistant
2009 - 2011	Mugla Sıtkı Kocman University	Research Assistant
2008 - 2009	Modül Yapı Denetim	Civil Engineer

FOREIGN LANGUAGES

Advanced English

PUBLICATIONS

1. International Journal Papers:

- a) Zeybek Ö., Topkaya C, Rotter J. M., “Strength and Stiffness Requirements for Intermediate Ring Stiffeners on Discretely Supported Cylindrical Shells”, Thin-Walled Structures, 96, 64-74, 2015.
- b) Zeybek Ö., Topkaya C, Rotter J. M., “Requirements for Intermediate Ring Stiffeners Placed Below the Ideal Location on Discretely Supported Shells”, Thin-Walled Structures, 115, 21-33, 2017.

c) Topkaya C, Zeybek Ö., “Application of ring beam stiffness criterion for discretely supported shells under global shear and bending”, Advances in Structural Engineering, Special Issue for Professor Rotter, 2018 (accepted).

2. National Journal Papers:

a) Kural M. E., Zeybek Ö., “Merkezi Çelik Çaprazla Teşkil Edilmiş Çok Katlı Çelik Yapıların İkinci Mertebe Analizi”, İstanbul Ticaret Üniversitesi Fen Bilimleri Dergisi, Cilt 10, Sayı:20, sf.1-14, İstanbul, 2011.

b) Kural M. E., Zeybek Ö., Seçer M., “Çelik Yapı Sistemlerinde İkinci Mertebe Analiz Yöntemlerinin İncelenmesi”, Dokuz Eylül Üniversitesi Fen ve Mühendislik Dergisi, Cilt 13, Sayı:2, sf. 75-87, İzmir, Mayıs 2012.

3. International Conference Papers:

a) Zeybek, Ö., Topkaya, C., Rotter, J.M., “Design criteria for intermediate ring stiffeners for discretely supported cylindrical shells”, 8th International Conference on Advances in Steel Structures ICASS, Lisbon, Portugal, 2015.

b) Zeybek, Ö., Topkaya, C., Rotter, J.M., “Design Requirements for Intermediate Ring Stiffeners on Discretely Supported Cylindrical Steel Shells”, The International Colloquium on Stability and Ductility of Steel Structures - SDSS 2016, Timisoara, Romania, 2016.

c) Zeybek, Ö., Topkaya, C., “Design of Ring Beams for Discretely Supported Cylindrical Steel Silos Based on Eurocode 3 Approach” 12th International Congress on Advances in Civil Engineering-ACE 2016, İstanbul, 2016.

d) Zeybek, Ö., Topkaya, C., Rotter, J.M., “Analysis of Silo Supporting Ring Beams Resting on Discrete Supports”, The 8th European Conference on Steel and Composite Structures-Eurosteel 2017, Copenhagen, Denmark, 2017.

e) Zeybek, Ö., Topkaya, C., Rotter, J.M., “Design of Intermediate Ring Stiffeners for Column-Supported Cylindrical Steel Shells”, 9th Hellenic National Conference of Steel Structures, Larisa (Greece) 5-7 October 2017.

f) Zeybek, Ö., Topkaya, C., Rotter, J.M., “Analysis of Ring Beams for Discretely Supported Cylindrical Silos”, 9th Hellenic National Conference of Steel Structures, Larisa (Greece) 5-7 October 2017.

4. National Conference Papers:

a) Zeybek Ö., Seçer M., Kural M. E., “Düzlem Çelik Çerçevelerin İkinci Mertebe Analiz Yöntemlerinin İncelenmesi”, 4. Çelik Yapılar Sempozyumu, sf. 213-222, İstanbul, 24-26 Ekim 2011.

b) Birgöl, R., Yılmaz, N., Saygılı, A., Zeybek, Ö., Kahyaoğlu, M.R., Aktan, E. “Muğla Üniversitesi İnşaat Mühendisliği Bölümü lisans eğitimi programı güncelleme çalışması”, İnşaat Mühendisliği Eğitimi 2. Sempozyumu, sf. 201-210, Muğla, 23-24 Eylül 2011.

c) Zeybek Ö., Topkaya C., “Silindirik Metal Silolardaki Halka Kirişlerin Eurocode 3’e Göre Tasarımı” 6. Çelik Yapılar Sempozyumu, sf. 197-206, Eskişehir, 15-17 Ekim 2015.